공학박사학위논문

마이크로 액체 금속 패턴을 위한 액체 금속 패터닝 시스템

Resolution Enhancement of Liquid Metal Patterns via Mechanical Deformation and Phase Change Mediated Transfer

2018 년 8 월

서울대학교 대학원

기계항공공학부

김 도 윤

Ph.D. Dissertation of Mechanical Engineering

Resolution Enhancement of Liquid Metal Patterns via Mechanical Deformation and Phase Change Mediated Transfer

마이크로 액체 금속 패턴을 위한 액체 금속 패터닝 시스템

August 2018

Graduate School of
Seoul National University
Mechanical Engineering Major

Doyoon Kim

Resolution Enhancement of Liquid Metal Patterns via Mechanical Deformation and Phase Change Mediated Transfer

Doyoon Kim

Submitting a Ph.D. Dissertation of Public Administration

August 2018

Graduate School of

Seoul National University

Mechanical Engineering **Major**

Doyoon Kim

Confirming the Ph.D. Dissertation written by

Doyoon Kim

August 2018

Chair _____(Seal)

Vice Chair _____(Seal)

Examiner _____(Seal)

Examiner _____(Seal)

Examiner _____(Seal)

Abstract

Resolution Enhancement of Liquid Metal Patterns via Mechanical Deformation and Phase Change Mediated Transfer

Doyoon Kim

Department of Mechanical and Aerospace Engineering

Graduate School of

Seoul National University

Recently, eutectic gallium indium (EGaIn) has been actively investigated towards stretchable and wearable electronic devices with the aid of high fluidity, high electrical conductivity and low toxicity. However, high surface tension along with spontaneous oxidation makes it difficult to realize fine patterning below ~10 μm, thus physical molding into an elastomeric mold is thought to be a unique solution. Here, we present a novel manufacturing technique that enables EGaIn patterns of single-digit micrometer width without using a guide mold for the first time. First, a custom direct printing setup is constructed with a laser displacement sensor, a 3-axis motorized stage, and an electronic pressure regulator to enable continuous and uniform printing of EGaIn by feedback control of the distance between the dispensing needle and the substrate. With the custom direct printing setup, a 120 μm wide linear pattern is printed

on a Ecoflex™, platinum catalyzed silicone elastomer. To enable a single-digit micrometer pattern, the initial printed line is stretched, frozen with deionized (DI) water, and then transferred to an unstretched Ecoflex substrate. Upon gentle heating after the pick-and-place of the EGaIn line frozen with DI water, only the stretched EGaIn line is left on the new Ecoflex substrate. The aforementioned pick-and-place transfer of the stretched EGaIn frozen with DI water is cascaded multiple times until a target width is reached. With the proposed idea, a 2 μm wide linear pattern, 60-fold reduction with respect to the initial dimension, is obtained. For practical applications, strain and pressure sensors are demonstrated with width-reduced EGaIn patterns.

Keywords **: Eutectic gallium indium (EGaIn), Liquid metal printing, Stretchable substrate, Phase change mediated pick-n-place transfer, Liquid metal sensor**

Student Number **: 2011-20686**

TABLE OF CONTENTS

LIST OF FIGURES

LIST OF TABLES

LIST OF SYMBOLS

θ_s	static contact angle
θ_a	advancing contact angle
θ_r	receding contact angle
E_r	pinning force
γ	surface tension
h_0	gap distance between a dispensing needle and a substrate
ID	inner diameter of dispensing needle
n	number of phase change mediated transfer
h	measured height with a laser displacement sensor
w	EGaIn pattern width
S	cross-sectional area of EGaIn
R	resistance
ρ	resistivity
l	EGaIn pattern length

Acronym and abbreviations

PDMS Polydimethylsiloxane

Ecoflex Ecoflex 0030

EGaIn eutectic gallium indium

PAA Polyacrylic acid

Chapter 1. Introduction

1.1 Overview

With the advent of wearable electronics, structurally compliant devices that are flexible, foldable, or even stretchable have been under development in academia and industries. One of the most common approaches is based on solid-state nanomaterials [1-19] or engineered thin films [20-24] incorporated with flexible polymeric materials. Discrete solid-state nanomaterials such as carbon blacks, [11,12] carbon nanotubes, [13-15] graphenes, [16-18] carbon nanofibers, [19] or metallic nanowires [1-10] constructing percolation networks of many individual elements tend to suffer from irreversible conductivity recovery upon relaxation from a large strain or experience hysteresis during repeated cyclic operations. On the other hand, top-down fabricated continuous thin-film conductors such as buckled semiconductor [20,21] or ceramic [22] nanoribbons and metallic planar meanders [23,24] exhibit improved strain range up to 300 % [24] with the help of wavy structures that make brittle inorganic materials flexible. However, they still have limited operation windows and cannot withstand excessive strains beyond 500 %.

Liquid metals are promising candidates that can offer exceptional stretchability while maintaining electrical functionality once they are continuously printed onto or

embedded in stretchable materials. [25-34] In fact, liquid metals are known to be the best when both stretchability and conductivity are considered. [33] Since the stretchability of liquid metals easily surpasses that of most flexible materials including Ecoflex™ and Dragon Skin™ and is practically infinite, [33] liquid metals are best suited for applications not yet explored in hyper elastic regimes. Recently, gallium-based alloys such as eutectic gallium indium (EGaIn) have been of great interest due to their low toxicity and reactivity compared to mercury. Various methods such as stencil lithography, [25] direct writing, [26] direct laser patterning, [27] imprint lithography, [28,35] microfluidic injection, [36] and microcontact printing [37] have been utilized to pattern EGaIn onto or within substrates. In common, patterning resolutions of most techniques are approximately several tens of micrometers in width partly due to the high surface tension of the EGaIn. To date, single-digit micrometer lateral resolutions, ~2 μm, have only been demonstrated by the imprint lithography. [28,35] The imprint lithography, however, requires lithographically fabricated polydimethylsiloxane (PDMS) molds that significantly increase in the overall processing time and practically limits further improvements in the patterning resolution.

To improve the patterning resolution beyond the characteristic dimension of tools and setups, lithographically controlled wetting [38,39] and auxiliary solvent-based-sublimation aided nanostructring [40] have been reported with soluble materials. Although those works are impressive, they cannot be applied to liquid metals. In another study [41], the width of EGaIn has been reduced down to ~10 μm by stretching EGaIn patterns on or in viscoelastic materials. Although this approach is interesting,

the uniformity in stretched EGaIn patterns is limited due to the manual stretching and stretched EGaIn patterns are difficult to be separated from viscoelastic materials.

In this paper, we propose a new patterning method and transferring method for EGaIn, which offers a single-digit micrometer lateral resolution without using lithographically prepared PDMS (Sylgard-184) molds. Our two concept ideas to reduce the liquid metal width are simple. First, as conceptually shown in **Figure 1.1**, linear EGaIn patterns are directly printed on a stretchable substrate, stretched to reduce the width. After frozen under the frozen point of EGaIn, the stretched and phase changed EGaIn patterns is simply picked up with a researched transfer method and placed onto a new stretchable substrate. These sequential processes are repeated until the target EGaIn pattern width is acquired. As shown in **Figure 1.2**, we also reduce EGaIn pattern width using the natural contraction of materials. As like **Figure 1.1**, linear EGaIn patterns are directly printed on a substrate that can maintain the pattern shape. After covering all patterned area with PAA (Polyacrylic acid), PAA brick placed inside the oven. The setup is heated to contract the PAA and the EGaIn pattern imprinted inside the PAA is also contracted. After removing the PAA, only reduced width liquid metal pattern is on the substrate.

The patterning method proposed herein is exclusively applicable to highly stretchable conductors, such as liquid metals, without using an adhesive. Furthermore, it can potentially offer sub-micrometer lateral resolution once high-end manipulators and *in-situ* process monitoring are integrated.

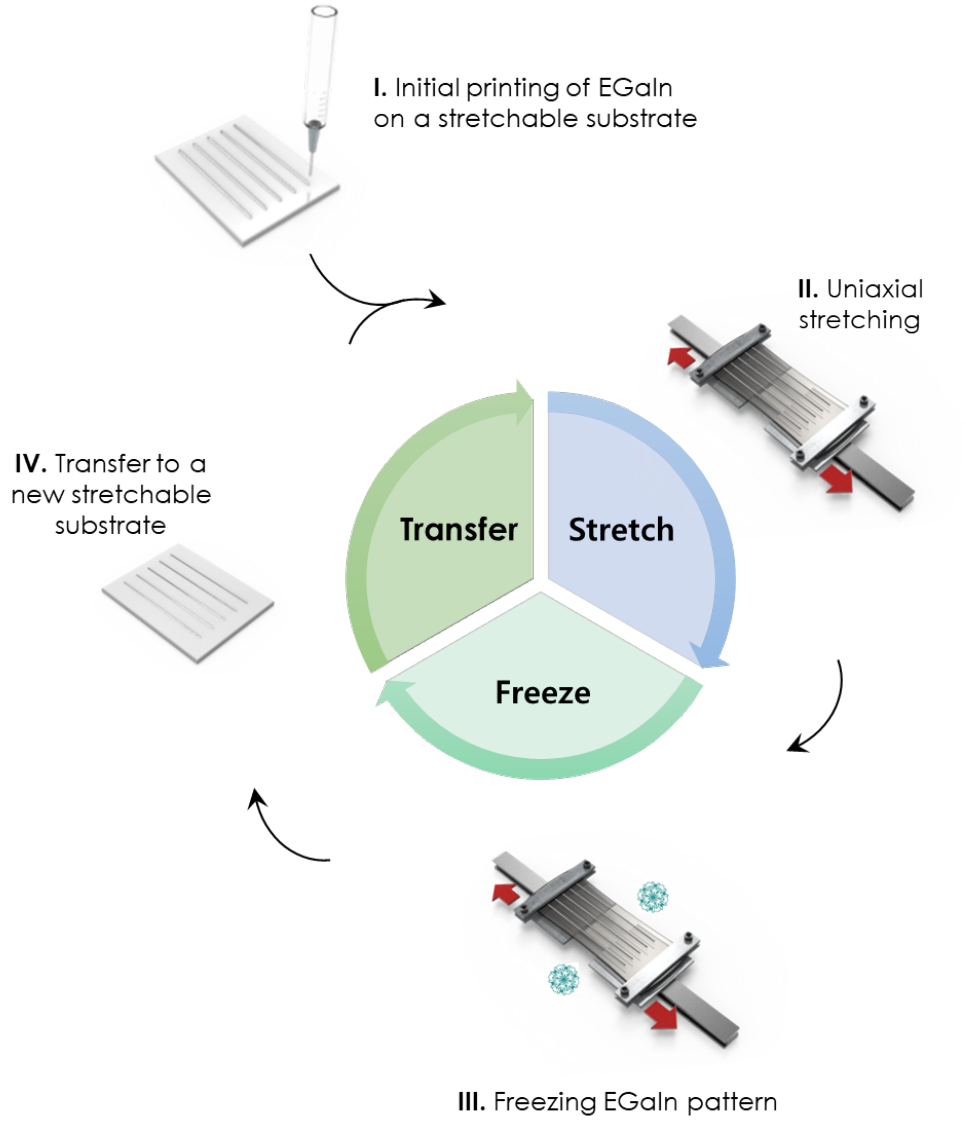

Figure 1.1. First concept idea to pattern narrow EGaIn.

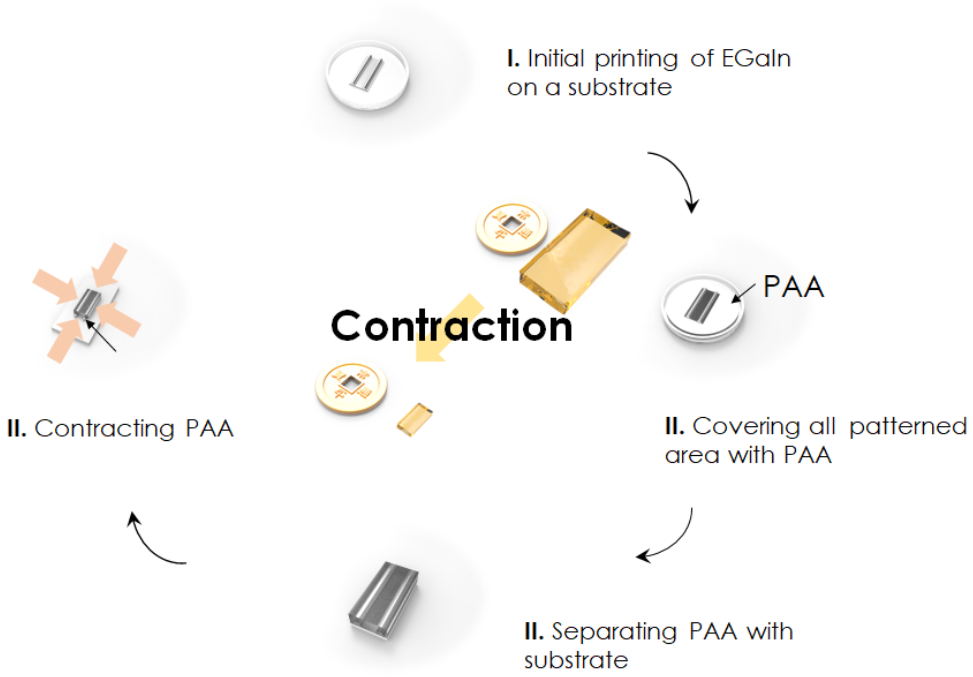

Figure 1.2. Second concept idea to pattern narrow EGaIn.

1.2 Motivation

As shown in **Table 1.1**, liquid metal is the metal that can exist in liquid state at room temperature because of its low melting point [42, 49]. Despite its superior conductivity, low resistivity [43] and low viscosity [44], toxicity of liquid metal has delayed the research. However, recently Ga based liquid alloy has been spotlighted because of its stability and low toxicity. Using the Ga based liquid alloy, we can easily pattern Ga based liquid metal on to the substrate because of its low melting point and Ga oxide film [45]. In addition, after encapsulation, Ga based liquid metal can maintain the electrical connection under the extreme external force condition. With this advantage, Ga based liquid metal has become a promising candidate to make a flexible device.

Apparently, as shown in **Figure 1.3** and **Table 1.2**, there are many methods that can consist the electrical wire inside the flexible device, like deterministic geometries and random composite. Deterministic geometries [46-50] are methods that use a thin metal film. This method has good electrical conductivity and good rigidity; however, deformation limit is decided by its structure. It is also possible to make a stretchable device with the random composite method [8, 51-59]. By percolated conductive particle inside the substrate, it can maintain the electrical conductivity. This method, represented by carbon nanotubes (CNT) can strain over 500%, but have low electrical conductivity than any other candidates. The liquid metals, material that used in this research, are easy to deform with substrate because of its liquid state. Although this

material still has the problem with the encapsulation, however, it has an excellent superior conductivity and has the possibility to stretch than any other materials. For these reasons, we do research about liquid metal in this paper.

Table 1.1 Characteristics of various liquid metals. [43,60,61]

	Mercury	**Gallium**	**Galinstan**	**EGaIn**	**Rubidium**
Melting point (℃)	-38.3	29.8	10.7	15.5	39.3
Boiling point (℃)	256.7	2402	>1300	2000	688
Density (g/cm^3)	13.53	5.91	6.44	6.25	1.532
Viscosity (10^{-3}Kg/m ·s)	1,526	1.969	2.09	1.99	-
Surface tension (N/m)	0.48	0.75	0.71	0.6	84.7
Thermal conductivity (W/m·K)	8.30	30.5	25.4	26.4	58.2
Electric resistivity (μΩ·cm)	96.1	27.2	30.3	29.44	12.8
Attributes	Toxic	Low toxicity	Low toxicity	Low toxicity	Highly reactive

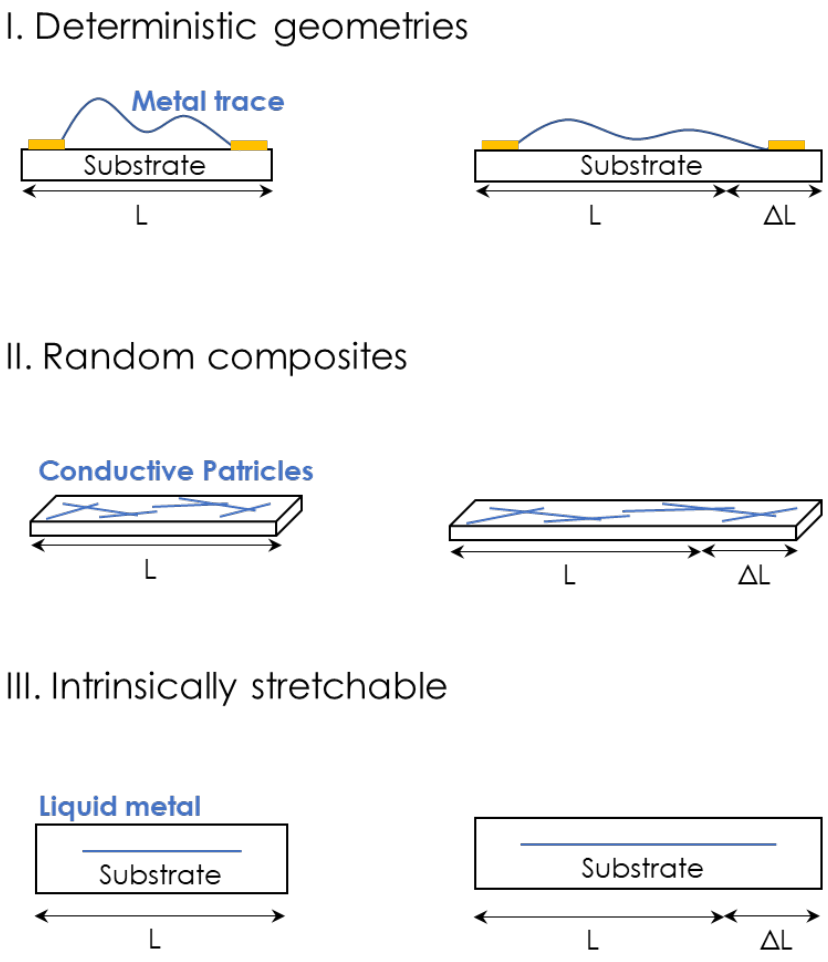

Figure 1.3. Strategies for making stretchable electronics [33].

Table 1.2. Characteristics of each strategies [33].

	Deterministic geometries	**Random composite**	**Random composite**	**Liquid metals**
Material	Au film	CNT in elastomer	Ag nanowire	EGaIn
Strain Limit	20 % wavy, 300% serpentine	500 %	250 %	Unlimited
Electrical conductivity (S cm^{-1})	4 x 10^5	6 (@134% strain)	6.3 × 10^4	3 x 10^4
Limitations	Must be thin	Dispersion & percolation	Dispersion & percolation	Encapsulation

1.3 Literature Review

There are several patterning techniques that enables to pattern liquid metal (EGaIn).

Imprinting [28, 35] - This imprinting method based on a lithographically prepared mold to shape the liquid metal pattern. To make a pattern, the flat surface covered with liquid metal, stamped with the prepared mold, and for more attraction between the mold and the liquid metal, the mold is rolled by a roller. After rolling, the liquid metal pattern wetted inside the mold and removed extra liquid metal from the substrate. This embedded liquid metal is encapsulated by the elastomer after patterning. In this paper, researchers suggested the novel technique to pattern liquid metal with ~2 μm. However, this method cannot guarantee the connection of the liquid metal after wetting and hard to make a long ang complex structure.

Direct writing [26] – Direct writing is the method that directly injects the liquid metal onto the substrate with dispensing needle. In this research, 2-axial motorized stages, the syringe pump, and the dispensing needle consist the hardware of the system. With this direct writing system, researcher success to pattern 40 μm liquid metal pattern on the sliding glass. In addition, with this result, they analyzed the stable region to pattern liquid metal. However, this method cannot afford uniform liquid metal pattern because of its hardware limit.

Direct laser patterning [27] – Direct laser patterning is the method that pattern liquid metal by cutting the layer with a CO_2 laser cutter. Before cutting sequence, the

layer structure made of polymer and flat liquid metal is prepared. After cutting this layer structure with the CO_2 laser cutter, only the planned liquid metal pattern remained. This method is a simple and applicable method to industries; however, it needs sophisticated control of laser movement, and pattern resolution also depends on the spot size of laser sensor. Moreover, liquid metal can be evaporated or exploded by the laser cutter during the patterning.

Microfluidic injection [36] – Microfluidic injection is the most common liquid metal patterning method. As like a title of the pattern method, this method injects liquid metal using a dispensing needle at the lithographically prepared channel. This method has an excellent possibility to make a multilayer channel, and easy to inject. Comparing with the direct writing method, this method does not need the injection strategy. However, this method must need the lithographically prepared channel and cannot pattern liquid metal under 50 μm, because of adhesion between the liquid metal and the channel.

With these patterning techniques, there is hundreds of research that demonstrates sensors of liquid metals. Representatively, Pressure sensor, tunable fluidic antenna, strain gauge sensor, positioning sensor, capacitance sensor [12, 62 – 77] has been developed. In addition, recently, there is research to make an electrical component with liquid metal, like memory resistor [78], switch [79], diode [80] and capacitor [81].

1.4 Objectives of Present Study

The goal of this dissertation is to research the novel technique to pattern liquid metal. To establish our aforementioned concept idea, the customized direct system is designed. In addition, stretch, transfer and contraction strategy are researched to control liquid metal. From the research, ~2 μm liquid metal pattern is obtained, and from the result, strain and tactile sensor are demonstrated.

In chapter 2, candidate substrates examined by its contact angle and pinning force. Next, the customized direct printing system is built with distance and pressure feedback system. In addition, dispensing needle is protected by paraffin coating from the liquid metal to pattern uniform shape. With this system, straight-forward EGaIn pattern obtained.

In chapter 3, stretch and transfer strategy are explained. In this section, we do research about stretching liquid metal uniformly and transferring liquid metal onto another substrate with no harm.

In chapter 4, phase change mediated pick-n-place transfer is explained in detail.

In chapter 5, pattern result with phase change mediated transfer is shown with image and graph.

In chapter 6, another patterning method is introduced. In this section, a pre-printed liquid metal pattern is prepared and cover all printed area with PAA. After heating material, liquid metal width is reduced by contracting of PAA.

In chapter 7, strain and tactile sensors are constructed with new connection method. These sensors are tested with the external strain or pressure and result is analyzed in this chapter.

Finally, the conclusions are summarized in chapter 8.

Chapter 2. Advanced direct writing with stretchable substrate

2.1 Stretchable substrate for direct EGaIn printing

2.1.1 Substrate characteristics

One of the key elements in our proposed method is a highly compliant substrate where EGaIn can be directly printed and reliably stretched. In previous liquid metal patterning works, [25-29, 34-37] PDMS is typically used as a target substrate considering its native adhesion to gallium oxide which spontaneously forms when the EGaIn is exposed to air and moldability to make microchannels where the EGaIn is injected afterwards. Compared to other substrates, PDMS, however, exhibits relatively high elastic modulus that ranges from 300 to 900 kPa at 10 % curing agent concentration [82] and low maximum elongation of ~200 % [21, 65, 83]. Thus, it is not well suited for the proposed approach. Towards our goal, it is recommended to choose a substrate with higher stretchability and better adhesion with EGaIn. Considering the stretchability as a primary requirement first, Ecoflex 0030, a platinum catalyzed silicone rubber, referred to as “Ecoflex” hereafter is chosen. Ecoflex is known to have a maximum elongation of ~900 % [65] and elastic modulus of ~60 kPa [84].

2.1.2 Pinning force with contact angle

To check the adhesion of EGaIn to Ecoflex, the contact angle of EGaIn on Ecoflex is measured. Contact angle measurement is also repeated with PDMS (10% curing agent concentration) and Slide glass for comparison. **Figure 2.1** shows the measured contact angle between EGaIn and various substrates including Ecoflex, PDMS and slide glass. The static contact angle is measured by capturing a single EGaIn droplet with a digital microscope. As shown in **Figure 2.2**, The captured droplet image is converted from RGB to grayscale to be analyzed with the Image J plug-in, LB-ADSA [85-87]. **Figure 2.3** shows measured contact angles on Ecoflex, PDMS, and slide glass where twenty measurements are repeated for each substrate. From the analyzed process, the measured static contact angle of the EGaIn on Ecoflex, 129.5 ± 4.0°, is smaller than that on PDMS, 143.6 ± 4.0°.

It seems that EGaIn is much stable and have excellent adhesion with substrate because of analyzed static contact angle; however, in the condition of the rough surface or chemically special status, we must consider the pinning force with contact angle hysteresis. Aforementioned, EGaIn produces thin Ga oxide film [88] in the air condition. Due to the presence of this gallium oxide skin, we need to consider the contact angle hysteresis by measuring dynamic contact angles (advancing and receding contact angles). As shown in **Figure 2.4**, receding and advancing contact angles are measured by taking EGaIn droplet images under suction or injection by the 25G dispensing needle and analyzed its contact angle by Image J plug-in. The measured

advancing (θ_a) and receding contact angle (θ_r) of the EGaIn on Ecoflex are $\theta_a = 134.8 \pm 4.0°$ and $\theta_r = 10 \pm 5.0°$ and that on PDMS are $\theta_a = 158.3 \pm 4.0°$ and $\theta_r = 10 \pm 4.0°$. From measured dynamic contact angles, the pinning force between the EGaIn and the substrate can be directly calculated by uncompensated Young's force [26, 89].

$$E_r = \gamma (\cos\theta_r - \cos\theta_a) \quad (1)$$

where $\gamma = 0.6\ \mathrm{N}/m$ is the surface tension of EGaIn. As shown in **Figure 2.5**, the calculated pinning forces are ~1.022 N/m for Ecoflex and ~1.152 N/m for PDMS, respectively. Since the pinning forces of the EGaIn on Ecoflex or PDMS is higher than the cohesion of EGaIn (0.5 N/m) [26], it helps to maintain the shape of printed EGaIn patterns and also helps their adhesion to the substrate upon stretching.

Table 2.1 shows the overall characteristics of three representative substrates for EGaIn printing in this section. This show that the Ecoflex is better suited for the proposed phase change mediated transfer than other substrates due to better adhesion to EGaIn, lower Young's modulus, and higher elongation rate.

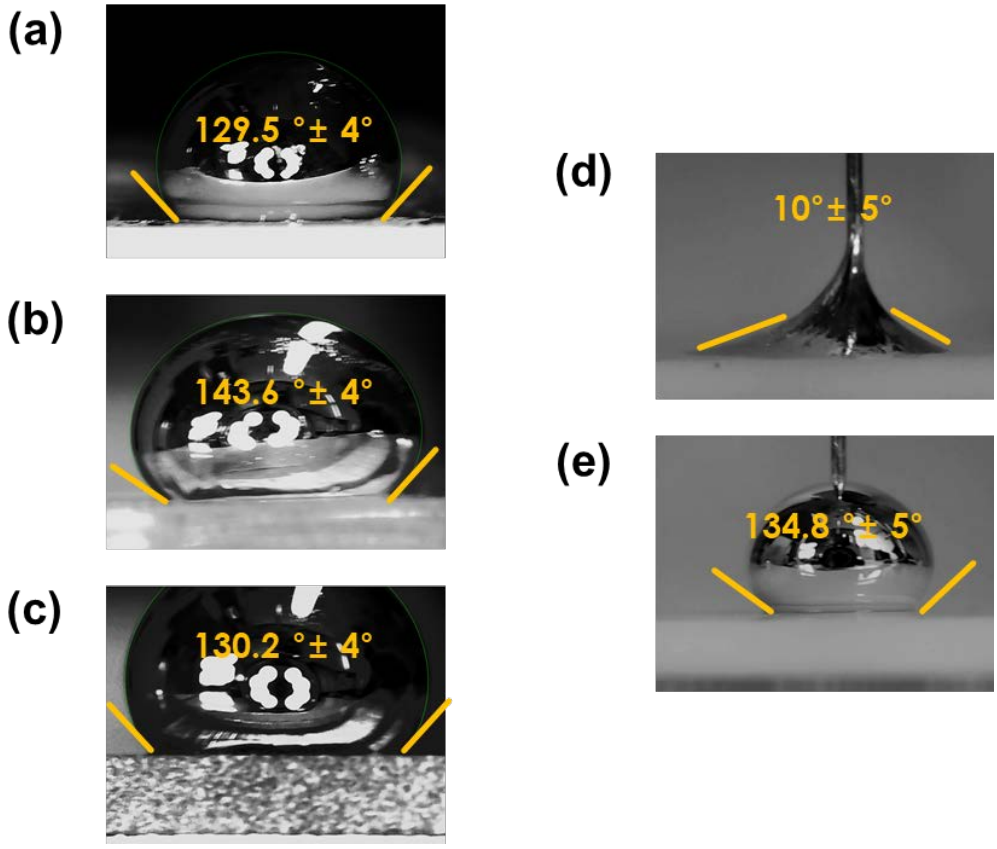

Figure 2.1. Static contact angle between EGaIn and (a) Ecoflex, (b) PDMS, (c) Slide glass**.** (d) Receding contact angle of EGaIn on Ecoflex. (e) Advancing contact angle of EGaIn on Ecoflex.

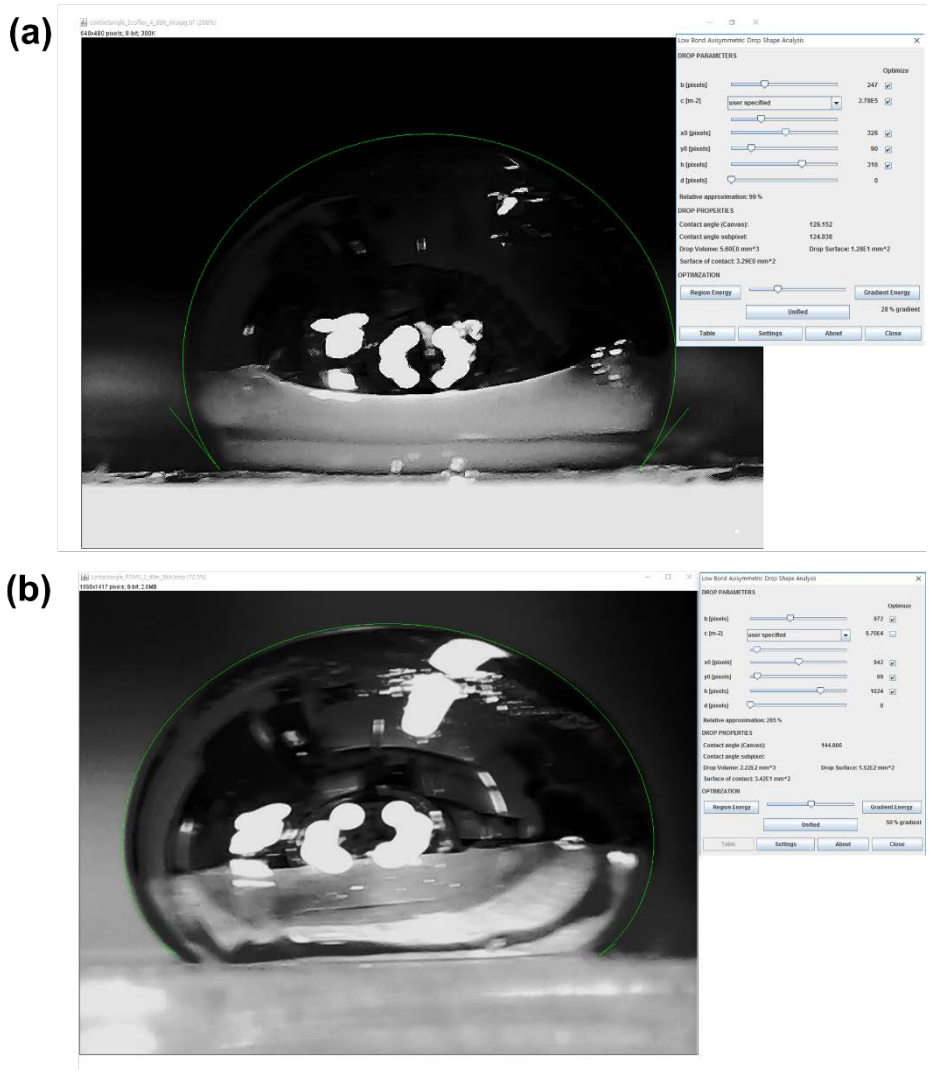

Figure 2.2. Analyze droplet contact angle on the Ecoflex (a) and PDMS (b) with the Image J plug-in LB-ADSA.

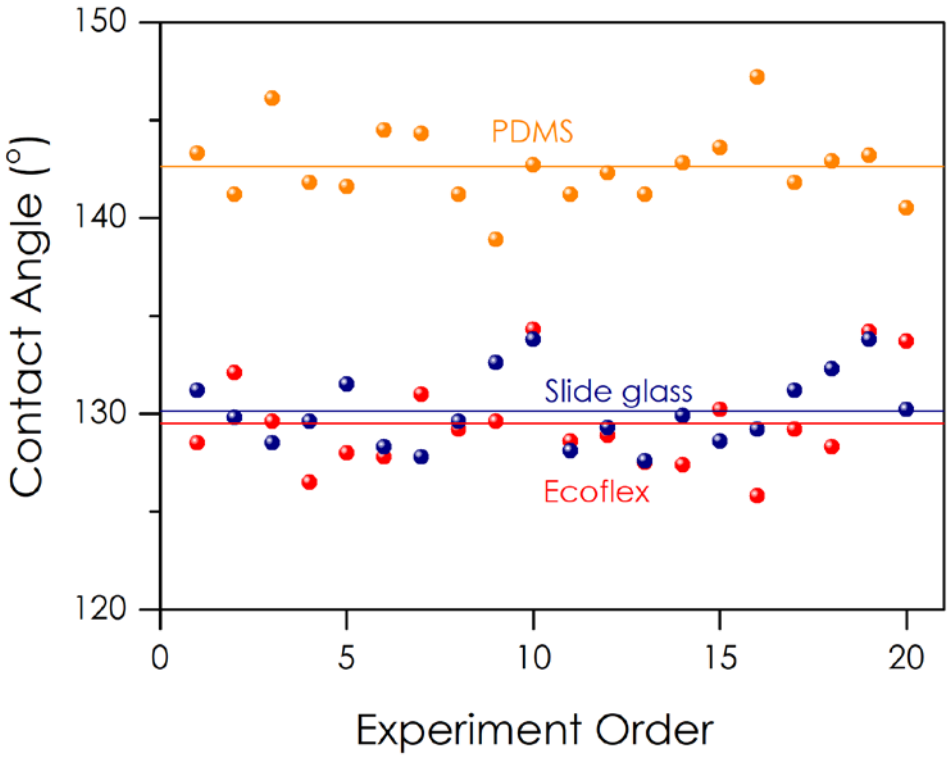

Figure 2.3. Measured static contact angles on each substrate.

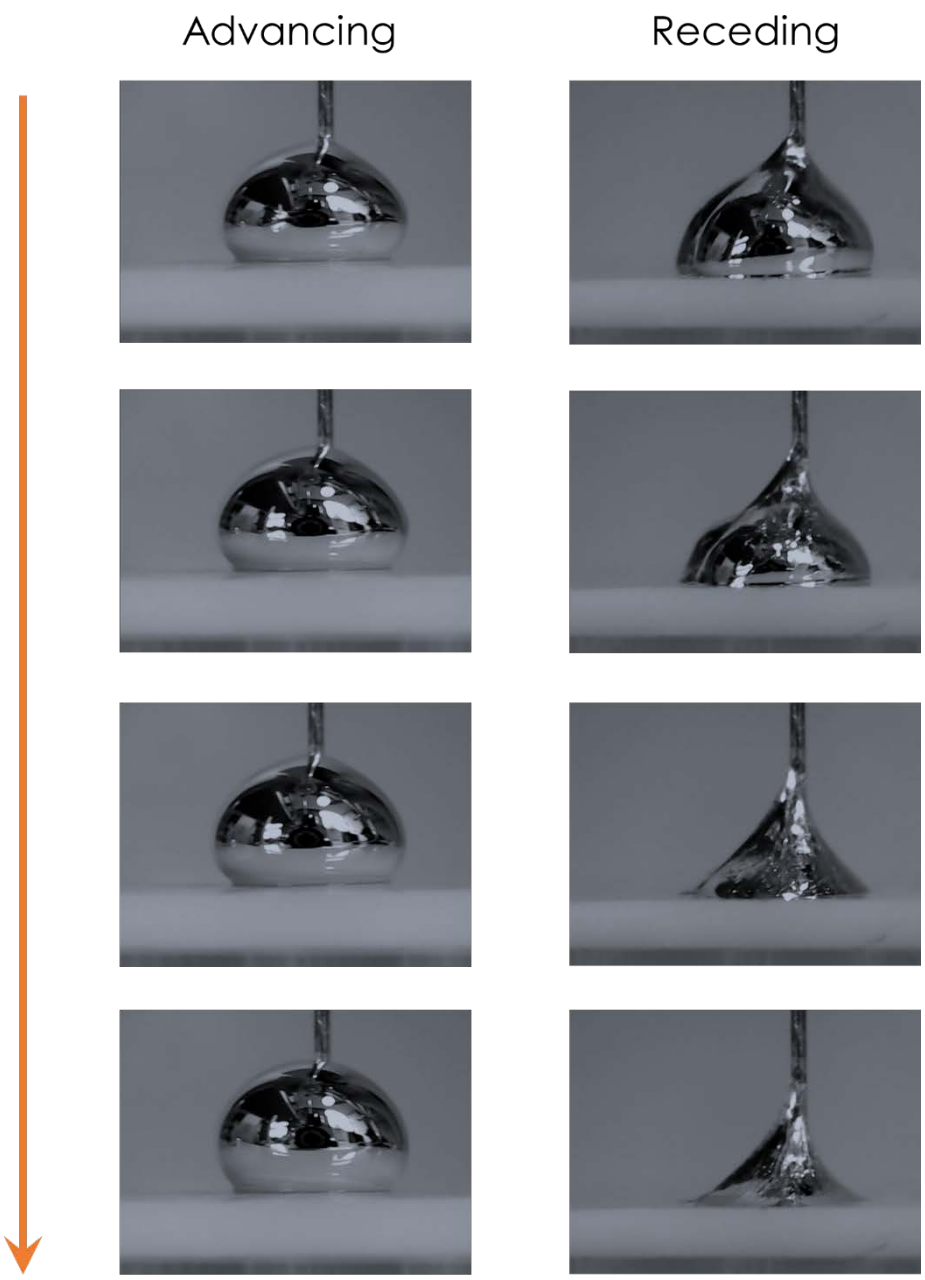

Figure 2.4. Measuring process of advancing and receding contact angles.

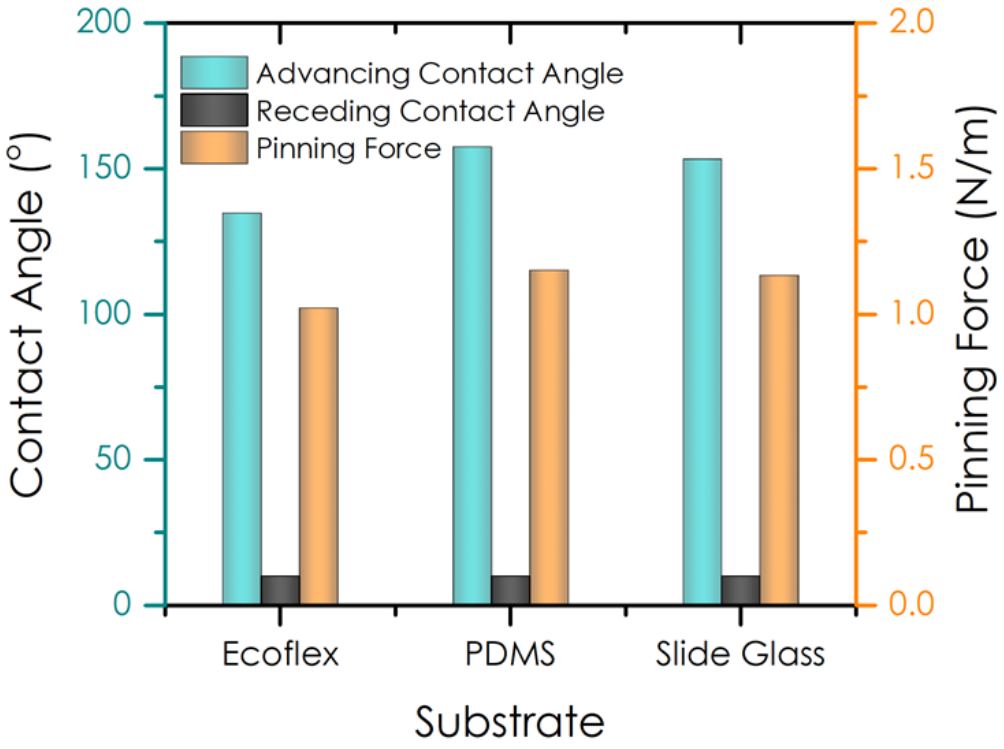

Figure 2.5. Averaged dynamic contact angles from 20 measurements and calculated pinning force by uncompensated Young's force for each substrate.

Table 2.1. Characteristics of representative substrates.

	Ecoflex	PDMS	Slide glass
Elongation (%) [26, 65, 83]	900	200	0
Tensile strength (MPa)	1.38	2.24	40
Static contact angle (˚)	129.5 ± 3	143.6 ± 4	130.2 ± 4
Advancing contact angle (˚)	134.8 ± 5	158.3 ± 4	151.3 ± 5
Receding contact angle (˚)	10 ± 5	10 ± 4	10 ± 5
Young's modulus (kPa)	60 [84]	360~879 [82]	7×10^{7} [82]

2.2 Direct EGaIn printing with the needle-substrate distance feedback control

2.2.1 Technical problem between previous direct printing system and concept idea

In previous direct EGaIn printing setups [26,33,90,91], the hardware of the printing system had just consisted of 2-axial motorized stages and syringe pump. The vertical position of the dispensing needle was fixed so that the needle – substrate distance was subject to change if the substrate was uneven or inclined. This uncertainty potentially varying the needle-substrate distance tends to result in non-uniform EGaIn patterns that are irregular or even broken occasionally. Two other possible sources of non-uniform EGaIn patterns are pressure fluctuation caused by the pulsating syringe pump and wetting of the oxidized EGaIn around the dispensing needle. If EGaIn patterns are used as printed, non-uniformity may be a relatively minor problem. However, if printed EGaIn patterns are transferred to another substrate, especially multiple times as the phase change mediated transfer with proposed stretching, more defects occur as the transfer time increases. This is due to the fact that stretching the Ecoflex substrate (process shown in **Figure 1.1**) with irregularly patterned EGaIn generally induces defects. To address aforementioned issues, a custom direct EGaIn printing setup with the needle-substrate distance feedback and precision pressure regulators is designed and constructed. As a separate effort, proper coating materials

and methods for the dispensing needle are investigated to promote the dewetting of the oxidized EGaIn from the dispensing needle.

2.2.2 Necessity to control the distance between needle and substrate

Aforementioned we explain that the rough substrate surface causes the ununiform EGaIn pattern. In the direct printing system most of the silicon-based elastomer made by mixing base and curing agent. This mixing process of the silicon-based elastomer causes the height of the substrate become irregular. Using spin coating device may reduce the irregularity, but still, it has a surface slope due to the centrifugal force. In order to quantify the variation of the substrate height, several Ecoflex substrates with a size of 20 mm × 20 mm are made, and the height variation is measured with a laser displacement sensor (The height data is measured while the laser sensor moved 17 mm with a speed of 2 mm/s with a 1 μm interval, respectively).

Figure 2.6 shows the surface slope and height of three Ecoflex substrates prepared. The Ecoflex substrate has 100 ~150 μm height difference between start and end point. According to the previous direct printing research [26] pattern stability is determined by the gap distance (h_0) and an inner diameter of dispensing needle (ID) and the flux of the EGaIn. If we consider the flux is constant, pattern stability can be described by this condition.

$$h_0/_{ID} < 0.21 \quad (2)$$

For printing narrower EGaIn pattern with the direct printing system, the inner diameter of the dispensing needle must be decreased, and it is necessary that the gap distance must be decreased to satisfy the stability of printing EGaIn pattern; however, using the previous 2-axial motorized stage direct printing system, substrate irregularity and slope of the surface cause the needle crash into the surface during the printing and also print the ununiform EGaIn pattern. To solve this technical issue, our direct printing system must need to control the gap distance with the distance feedback.

To quantify the distance feedback, we also measured the instantaneous slope. **Figure 2.7** and **table 2.2** show the surface condition of three Ecoflex substrates prepared. The Ecoflex substrate has overall tilt angles of 0.34˚ ~ 0.46˚ for the entire 17 mm movement. However, the local tilt angle that can induce a local printing defect ranges from −3.87˚ to 6.35˚. To confirm the effectiveness of the distance feedback, direct EGaIn printing with the distance feedback must be demonstrated with an intentional tilt of 10˚, that is sufficiently higher than the maximum local tilt angle measured.

2.2.3 Displacement sensor

To build up feedback system, customized direct printing system need to measure the distance between the dispensing needle and the substrate with displacement sensor. In this research, we consider that two types of displacement sensor.

One is the capacitance distance sensor, and another is the laser displacement sensor. Both of sensors are non- contact type sensor because contact type sensor may interrupt the printing sequence and can damage the substrate. As shown in **Figure 2.8(a)**, **(b)** and **Table 2.3**, capacitance sensor has an advantage in size and sensitivity. On the other hand, laser displacement sensor has narrow sensing region. In addition, unlike laser displacement sensor, capacitance sensor can measure the distance at any materials. Despite these advantages, capacitance sensor can't figure out the relative distance between the sensor and the dispensing needle. **Figure 2.8(c)** shows that the modified capacitance sensor for the direct printing system; however, EGaIn printing can be affected by the electric field. For this reason, laser displacement sensor is used for the direct printing system.

2.2.4 Hardware and software setup

Figure 2.9 and **Figure 2.10** show the custom printing designed and constructed by using a laser displacement sensor, a 3-axis motorized stage, two electronic pressure regulators, substrate and needle mounts, and a USB inspection microscope. The laser displacement sensor measures the needle-substrate distance, the two electronic pressure regulators precisely control the pneumatic pressure for dispensing EGaIn, and the USB microscope monitors the overall printing process.

Figure 2.11 shows the front panels of the control and monitoring software

written by LabVIEW. With this GUI system, the dispenser position can be controlled like end mill or drill bits in a CNC router, the dispensing needle-substrate distance can be feedback controlled, and the pneumatic pressure used for discharging EGaIn can be precisely controlled to minimize any fluctuation. **Figure 2.12** show the communication protocols and interfaces between associated hardware and LabVIEW software.

2.2.5 Direct EGaIn printing with the feedback control

In this research, we customized direct EGaIn printing system with aforementioned hardware and software. The gap distance, which is variable due to the local surface roughness or tilting, measured by the laser sensor is feedback-controlled to a set point, typically 50~100 μm, that guarantees uniform and continuous printing of EGaIn. Ecoflex substrates made with a white dye mixed (weight percentage of 0.5%) enhance the laser reflection during the distance feedback control (Experimental section). This distance feedback control ensuring uniform shear eventually contributes to EGaIn patterns with a more uniform width. For precise pressure control with minimum fluctuations, two electronic pressure regulators (ITV0010-0BL, SMC) are employed. The first regulator is directly connected to a compressed air tank regulated at ~5 bar maintains the output pressure to be 2 bar which becomes a constant regulated input to the second regulator. The second regulator, then, controls the final output pressure between 0.01 to 1 bar depending on the printing speed and the discharge rate of EGaIn.

To prevent the oxide skin that is near the free surface of EGaIn in the syringe adhering to the syringe wall, 0.5 M HCl is added in the syringe after the syringe is partially filled with EGaIn (i.e. HCl is only above EGaIn) [92]. As shown in **Figure 2.13**, the EGaIn printing demonstrated onto the tilted Ecoflex substrate with a 10-degree slope with the horizontal plane to validate the direct printing with the distance feedback control. The 10-degree slope configured is a factor of ~1.5 higher than the maximum local slope encountered in actual Ecoflex substrates resulting from fabrication uncertainties (Section 2.2.2). As shown in **Figure 2.14, Figure 2.15 and Figure 2.16**, with the distance feedback control, the dispensing needle follows the substrate slope with the gap distance maintained. If the feedback control is turned off when the needle goes downhill, the needle-substrate distance keeps increasing and eventually makes the continuous printing impossible. **Figure 2.17** show the direct EGaIn printing results on Ecoflex substrates with and without the distance feedback and the precision pressure control, respectively. A more uniform pattern is acquired when both the distance feedback and the precision pressure control is turned on.

Besides the distance feedback and precision pressure control, the adhesion of oxidized EGaIn around the stainless-steel dispenser should be mitigated to prevent accumulation of EGaIn that deteriorates the printing uniformity. Therefore, it is necessary to find proper surface treatment for the stainless steel by methods like coating. A previous research shows that paraffin waxes, known to be waterproof and electrically insulating, enhance the dewetting of ethylene glycol as well as water on polypropylene substrates [93]. Since the enhanced dewetting by the paraffin coating may work for

EGaIn on stainless steel, a paraffin wax is tested as a coating material. **Figure 2.18** I and II show that contact angles of EGaIn on a stainless-steel sheet are measured to be $132 \pm 4^{\circ}$ and $164 \pm 10^{\circ}$ before and after the paraffin coating, respectively. Indeed, the paraffin coating greatly increases the contact angle of EGaIn on stainless steel. The increased contact angle is attributed to the enhanced dewetting that prevents the oxidized EGaIn from adhering to the stainless-steel sheet.

After experimentally confirming the effectiveness of the paraffin coating on a stainless-steel sheet, the outer surface of stainless-steel dispensing needles (25G, the inner diameter of 180 μm) is coated with the paraffin wax (Experimental section). When the distance feedback control, the precision pressure control, and the paraffin coating on the dispensing needle are combined all together, the best printing quality can be expected. **Figure 2.18** III and IV show the EGaIn printing results and process with the paraffin-coated syringe needle configured in the custom printing setup with the distance feedback and the precision pressure control. Continuous and uniform EGaIn patterns are guaranteed only with the paraffin-coated needle due to the fact that the paraffin coating enhances the dewetting of the EGaIn on the stainless-steel needle. **Figure 2.19** shows optical and scanning electron micrographs of the most reliable printing results of which the pattern width is 120 μm. **Figure 2.20** also shows the printing sequence with distance and pressure feedback and paraffin coated needle. In comparison to the pattern result with **Figure 2.14** and **Figure 2.15** patterns, EGaIn patterns become more straightforward and have less roughness than that of the past.

2.2.6 Direct EGaIn printing condition and various width result

Optimizing the pattern resolution with major factors affecting the printing is crucial for direct printing [26]. However, the resolution of our proposed method is determined by the stretch and transfer process rather than by the initial direct printing. Therefore, optimization of the printing resolution is not of great importance. This is why we have tried various strains to explore the achievable minimum pattern width along with the required iteration number of stretch and transfer process (Section 3.2). It is more important to obtain uniform EGaIn patterns during the initial direct printing. To this end, the effect of nozzle inner diameter on the width of EGaIn patterns is examined while both printing velocity and pressure are fixed to 2 mm/s and 0.05 bar, respectively, both of which are experimentally found optima.

Figures 2.21 (a)-(d) show various EGaIn pattern widths ranging from 40 to 120 μm by using the direct printing with the distance feedback along with the paraffin-coated dispensing needle. For various dispensing needles (25~32G), the needle-substrate distance is tightly controlled around a set point ranging from 70 to 100 μm. **Figure 2.22** shows the EGaIn pattern width changes as the inner diameter of the dispensing needle is varied. As expected, the EGaIn pattern width increases as the inner diameter of the dispensing needle increases. Obtained results show good agreement with results previously reported [26]. However, the slope of the linear regression in the

graph is slightly less than that in the previous report while the uncertainty in the pattern width is smaller than that in the previous report. To get uniform 120 μm wide EGaIn patterns with the printing velocity of 2 mm/s and back pressure of 0.05 bar, the inner diameter of the dispensing needle should be 250 μm and the needle-substrate distance should be 70~80 μm.

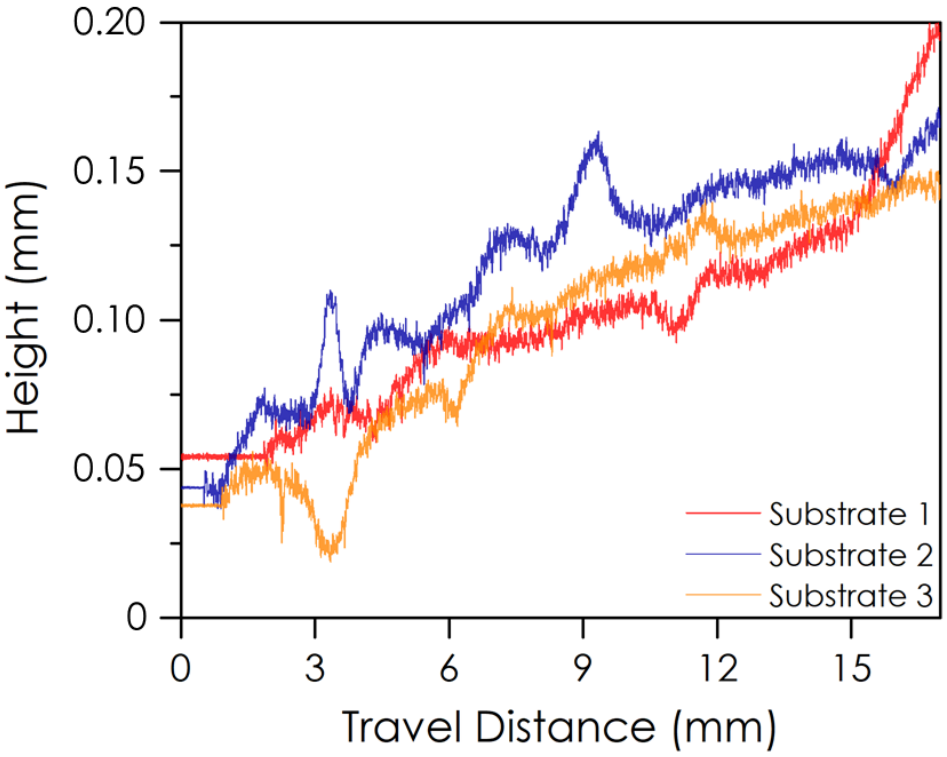

Figure 2.6. Measured height of the Ecoflex substrate by the laser sensor.

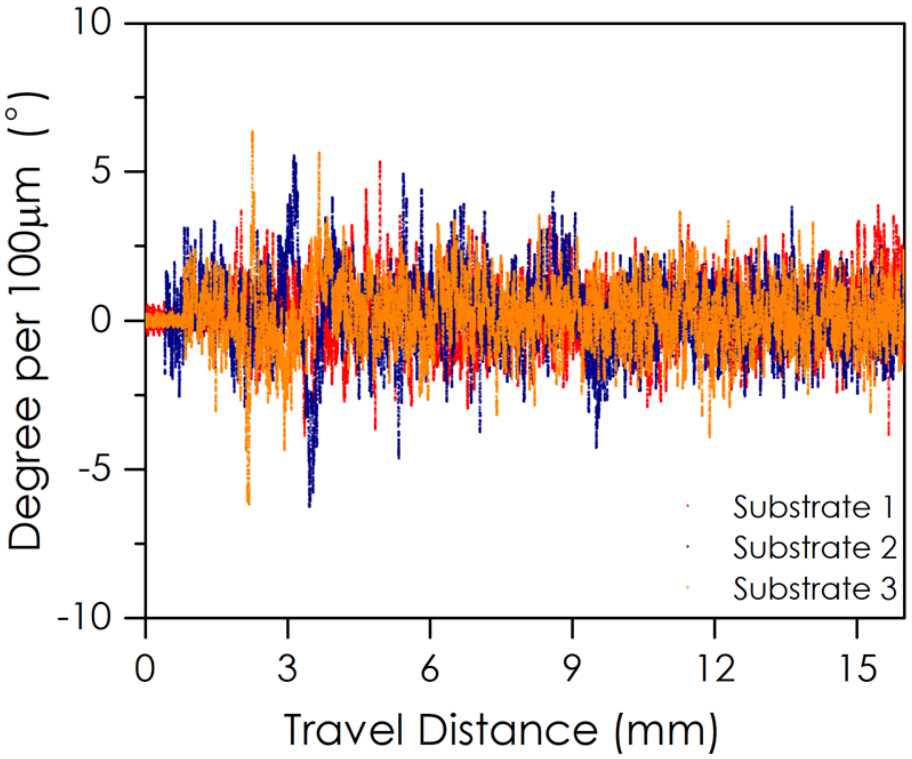

Figure 2.7. Calculated angle of the Ecoflex substrate per unit length of 100 µm.

Table 2.2. Overall, maximum, and minimum tilted angles for three Ecoflex substrates tested.

	Total	Angle changes per unit length (100 μm)	
	Overall tilt (˚)	Max. degree (˚)	Min. degree (˚)
Substrate 1	0.46	5.33	–3.87
Substrate 2	0.38	5.56	–6.26
Substrate 3	0.34	6.35	–6.17

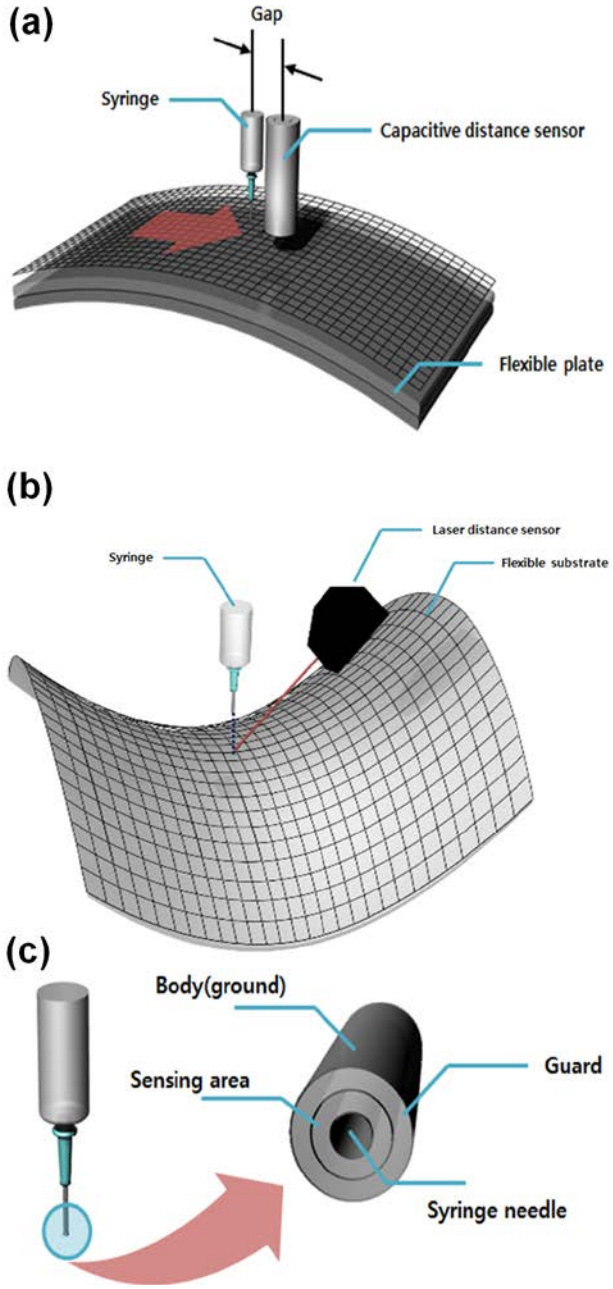

Figure 2.8 (a) Capacitance displacement sensor (b) Laser displacement sensor (c) Modified capacitance displacement sensor.

Table 2.3. Characteristics of each sensors.

	Capacitance displacement sensor	Laser displacement sensor
Size	Diameter: 10 mm Length: 32 mm	25 mm × 44 mm × 20 mm
Sensitivity	100 nm ~ 10 μm	1 ~ 10 μm
Advantage	- Can measure the distance at any materials	- Narrow sensing region - Easy to use - Cost
Disadvantage	- Large sensing region - High cost - Electrical field	- Laser cannot reflect at a transparent surface

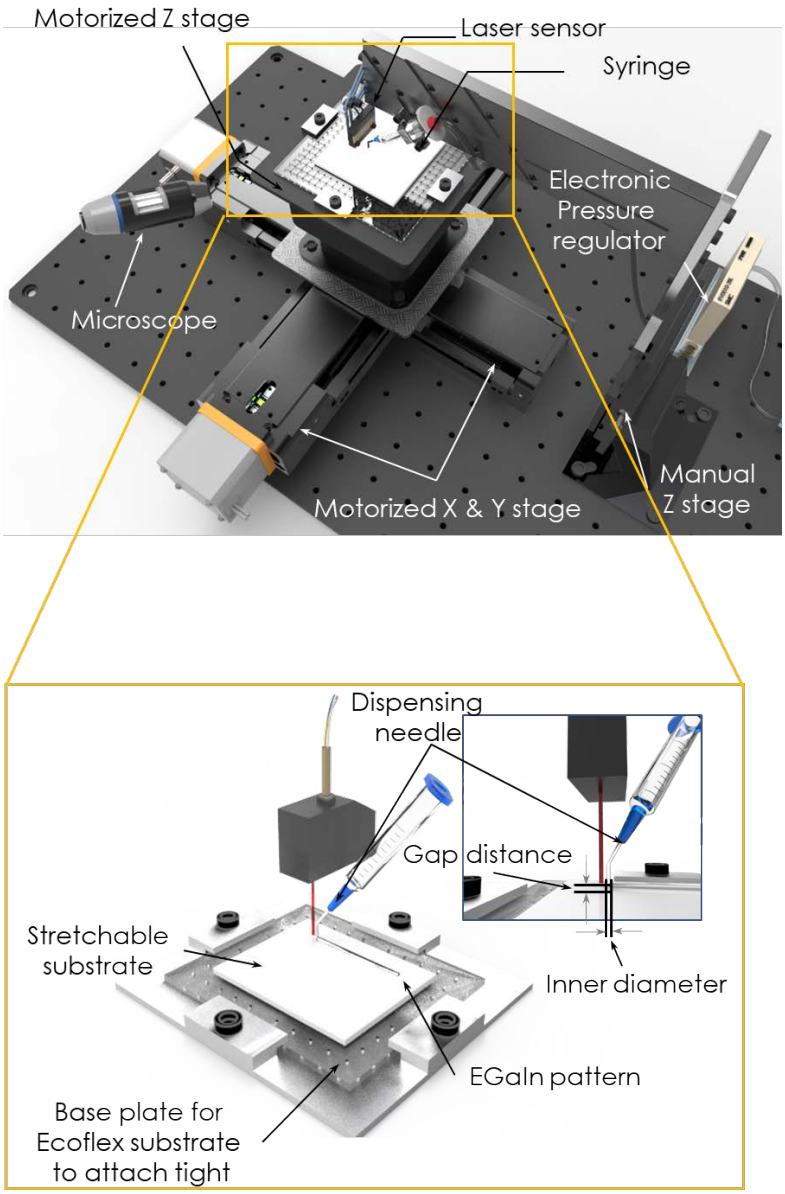

Figure 2.9. A 3D schematic of the custom direct printing setup for EGaIn with the feedback control of the dispensing needle-substrate distance by using a laser displacement sensor, a 3-axis motorized stage and electronic pressure regulators.

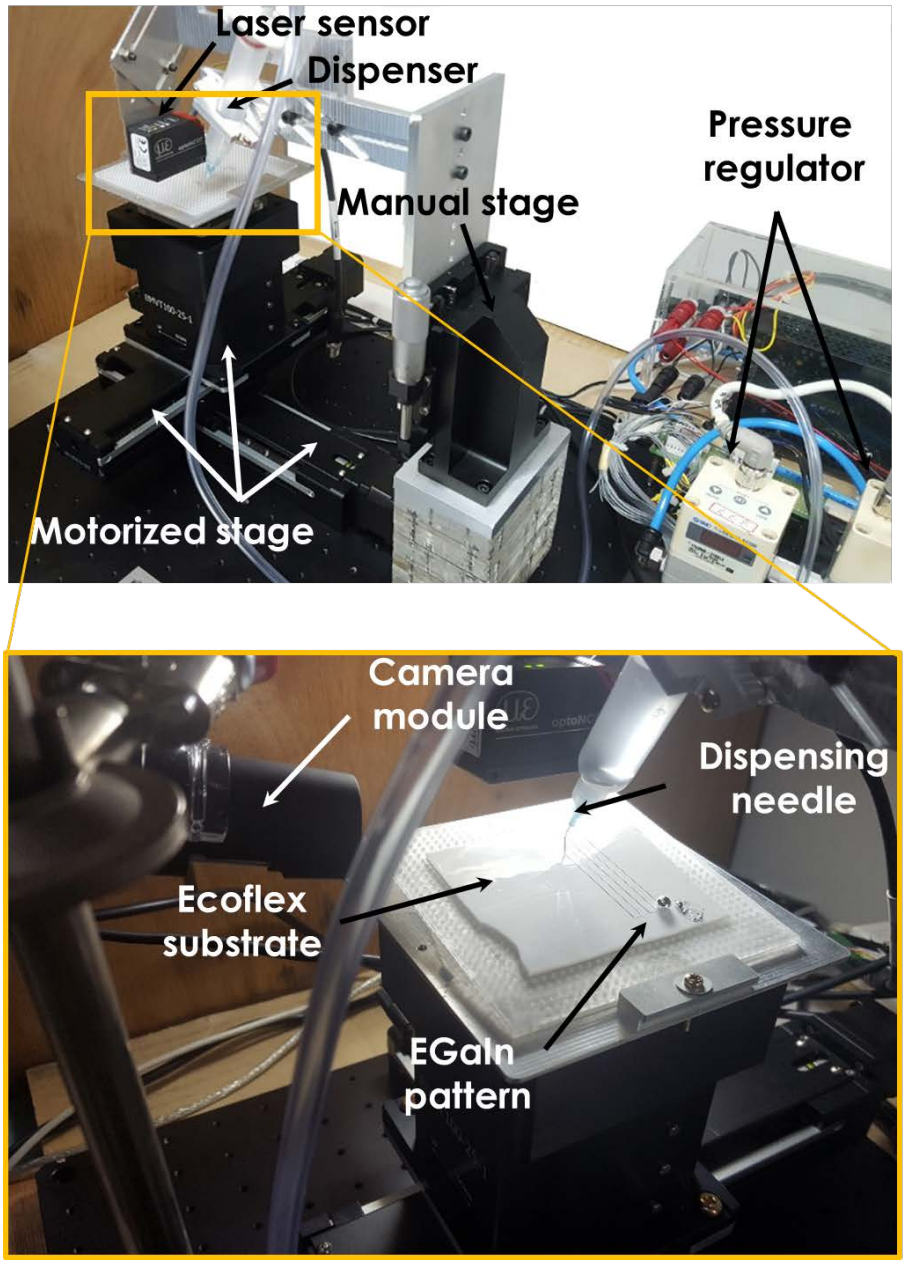

Figure 2.10. Photographs of custom direct EGaIn printing system.

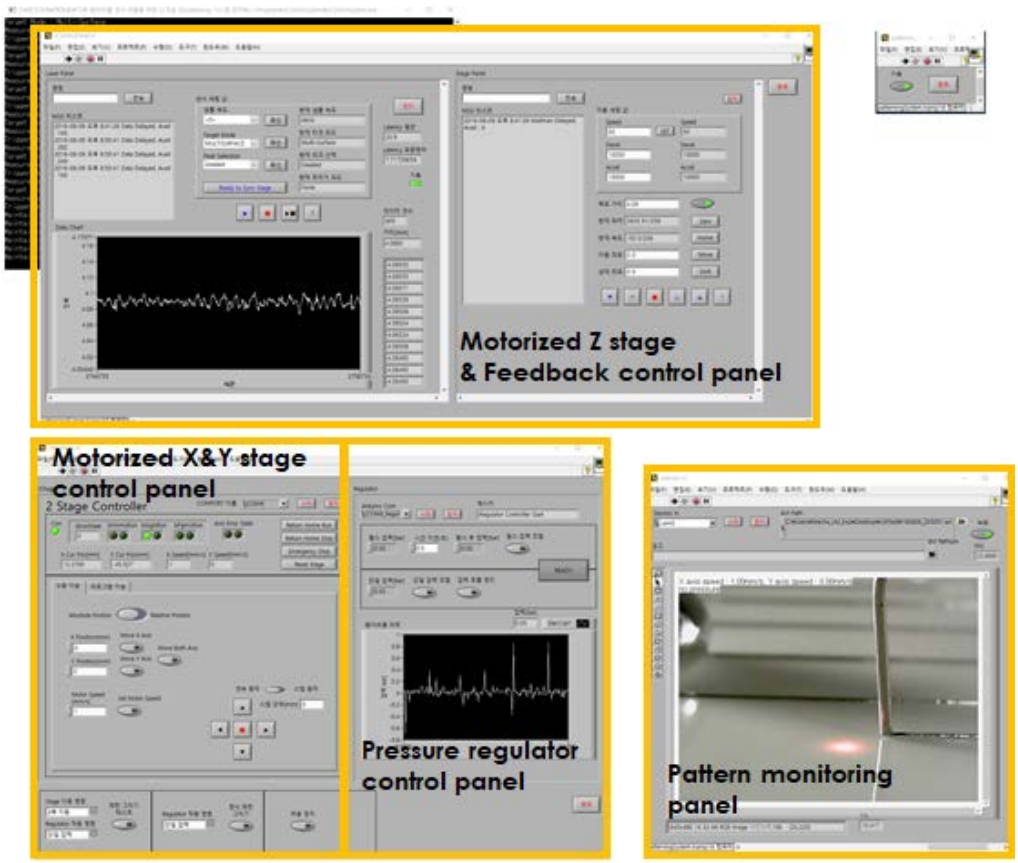

Figure 2.11. LabVIEW front panels, showing the motorized XY stage scanning, the motorized Z stage feedback control, the pressure regulator control, and the printing process monitoring.

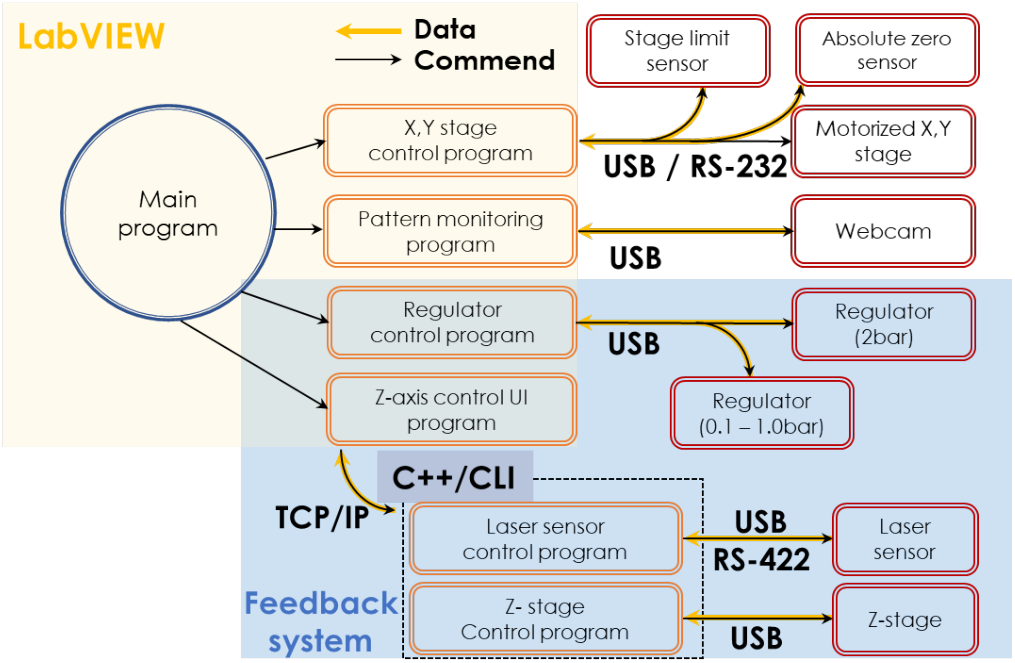

Figure 2.12. Control and process monitoring system for liquid metal printing relying on several communication protocols between hardware and the LabVIEW software.

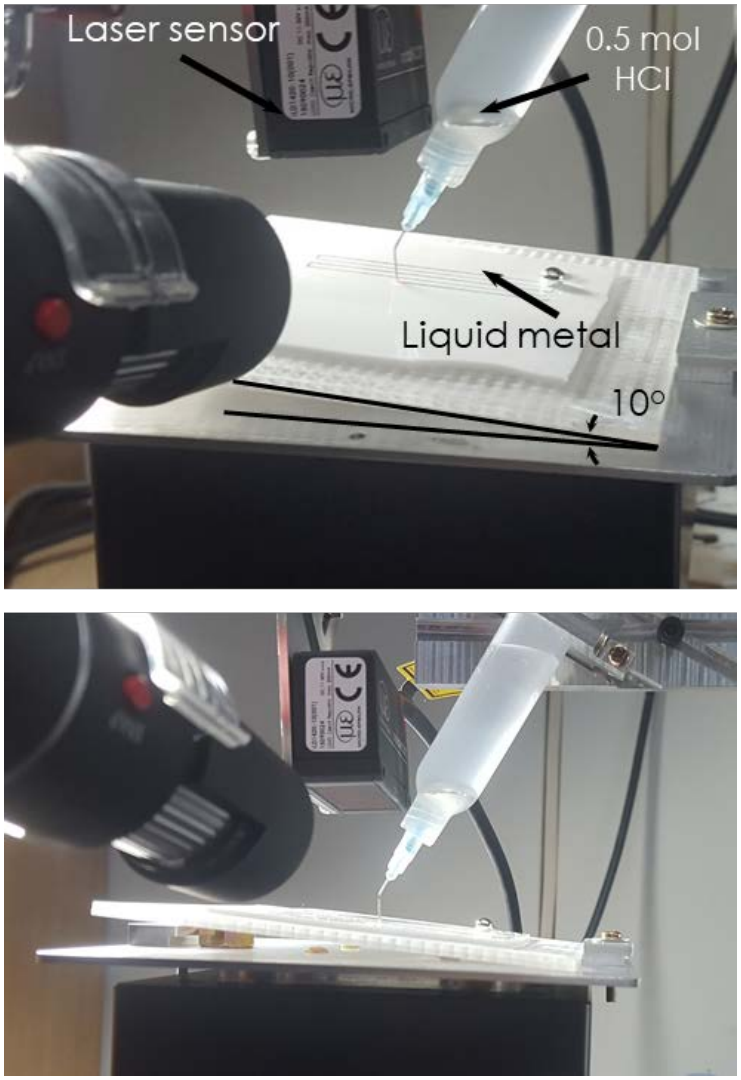

Figure 2.13. A picture showing the continuous and reliable EGaIn printing on a 10-degree tilted Ecoflex substrate.

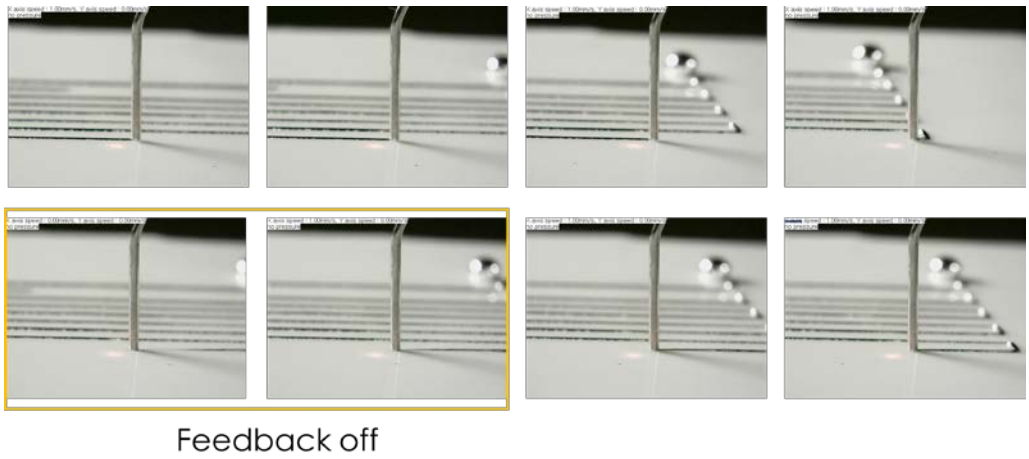

Figure 2.14. Direct printing result with Feedback on/off.

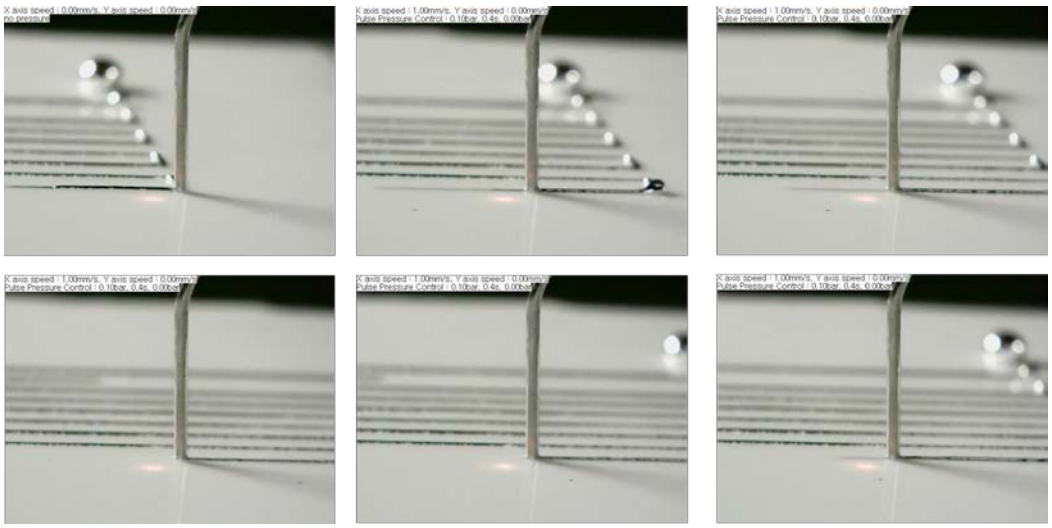

Figure 2.15. Re printing the discontinuous line with feedback on.

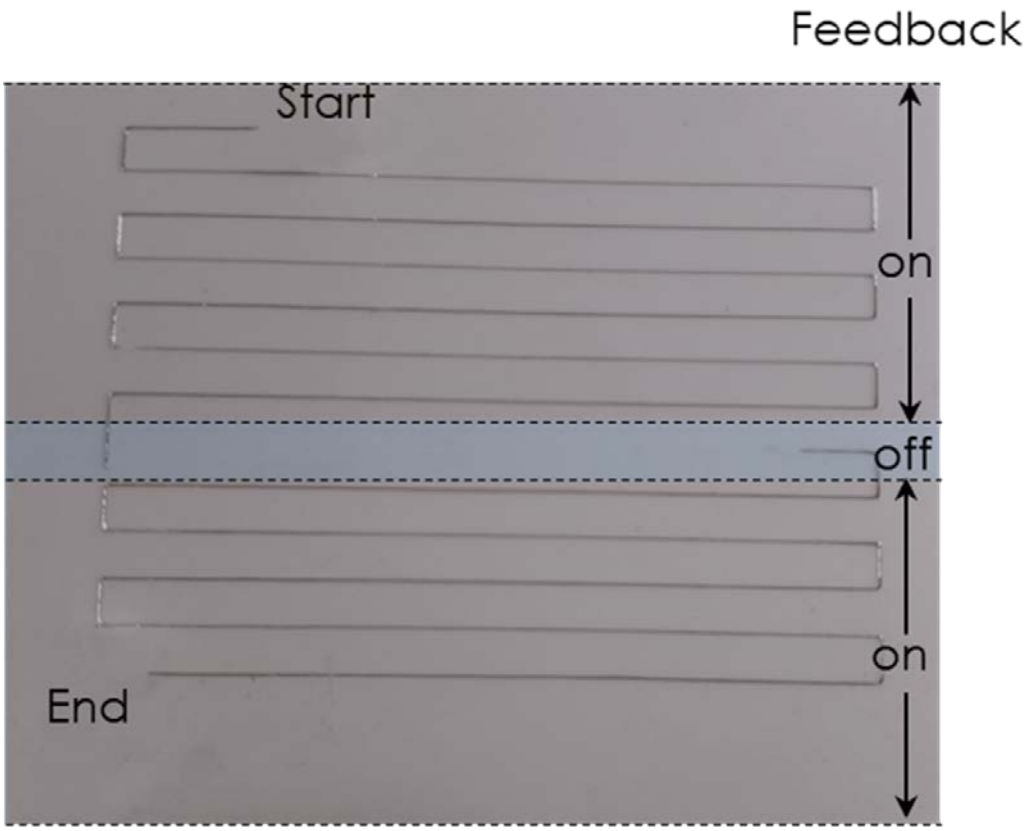

Figure 2.16. EGaIn printing result with feedback control on or off.

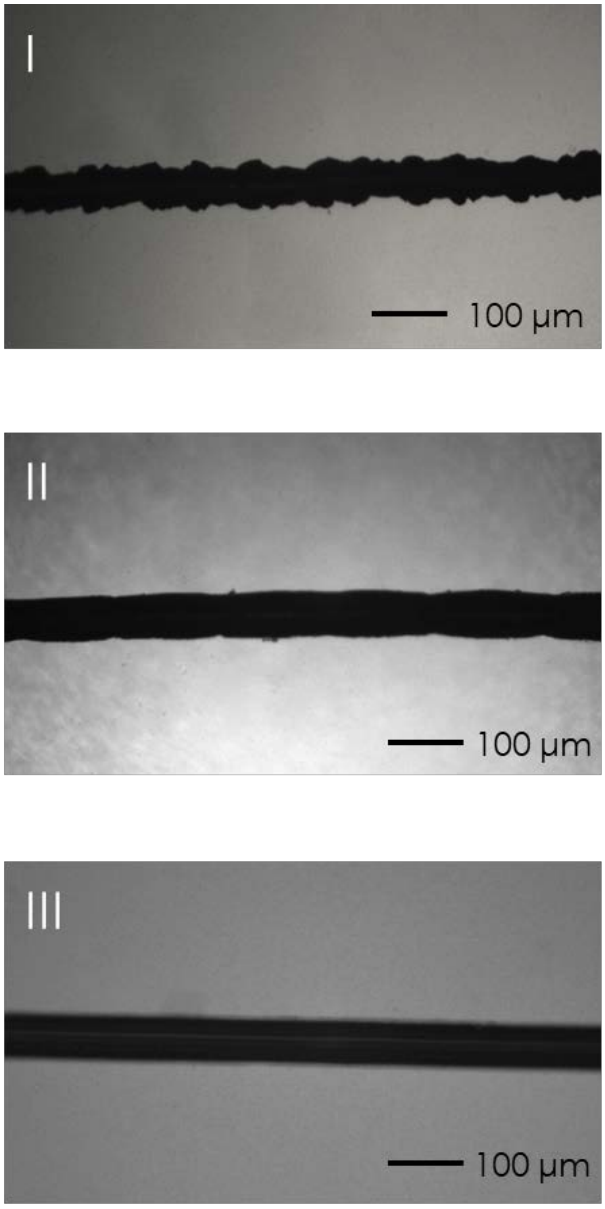

Figure 2.17. EGaIn printing results with different conditions. (I) Without the distance feedback and without the precision pressure control. (II) With the distance feedback and without the precision pressure control. (III) With the distance feedback and with the precision pressure control.

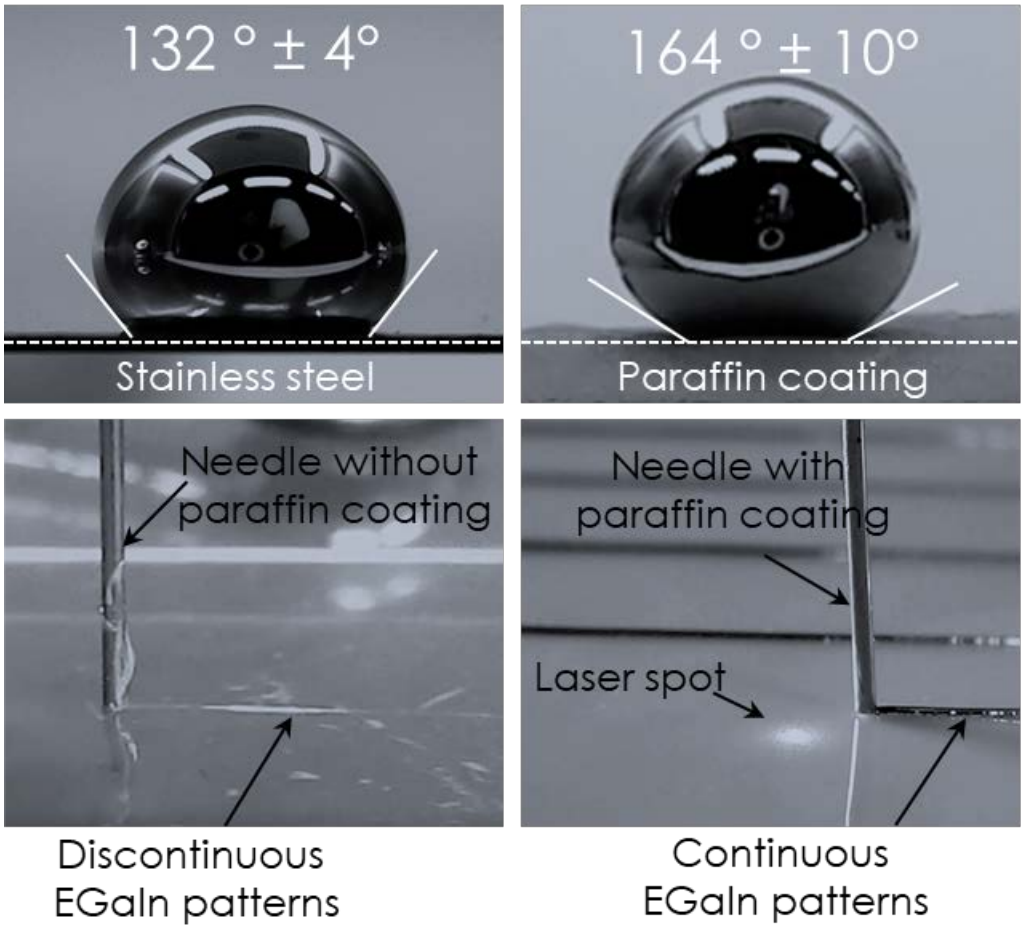

Figure 2.18. Contact angles of EGaIn on (I) bare and (II) 0.5 mm thick paraffin coated stainless steel sheets. (III) Discontinuous and (IV) continuous patterning results with bare and paraffin-coated needles, respectively.

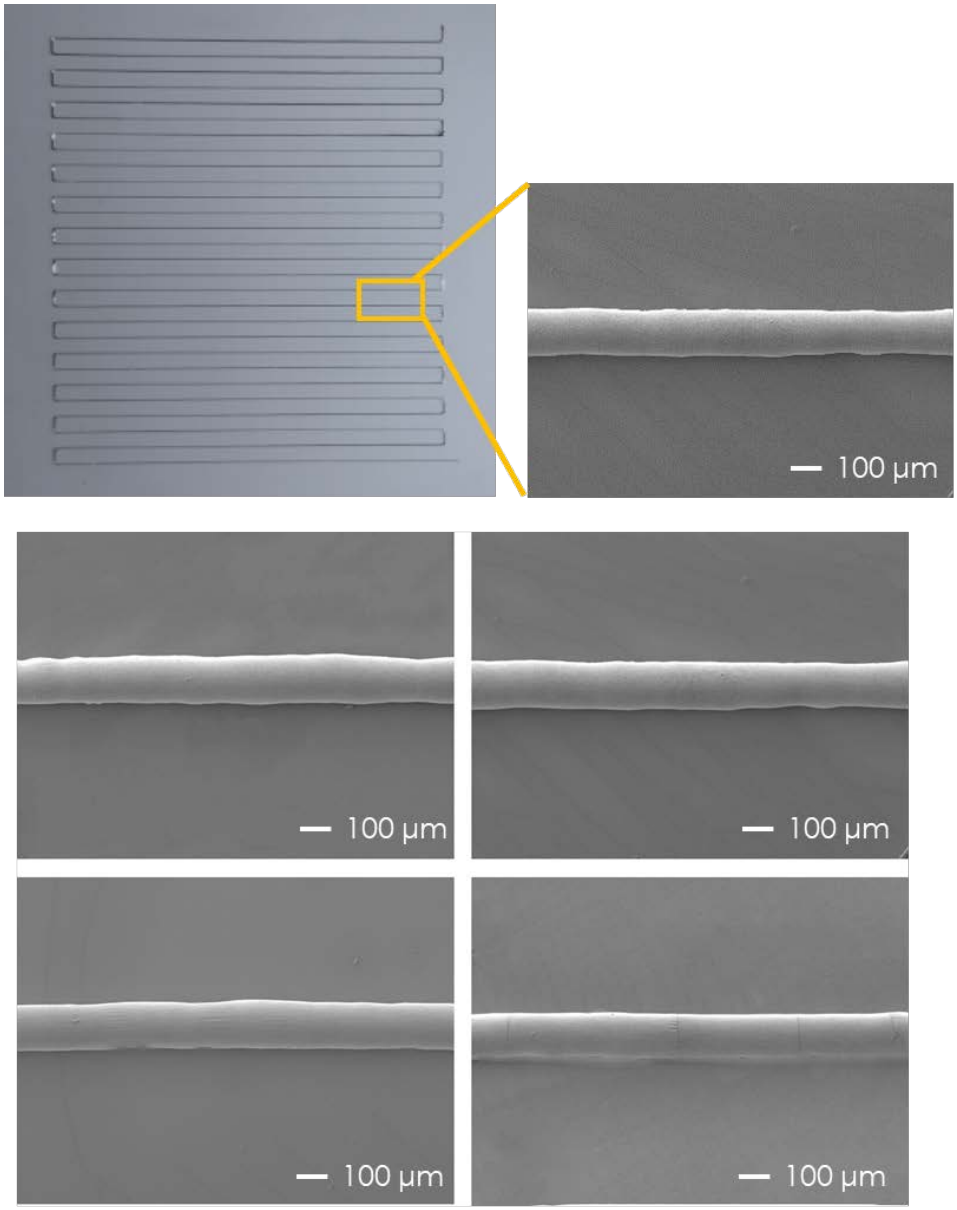

Figure 2.19. Continuous patterning result by using the paraffin-coated stainless-steel dispensing needle with the distance feedback and with the precision pressure control. The scanning electron micrograph shows a zoomed-in EGaIn pattern.

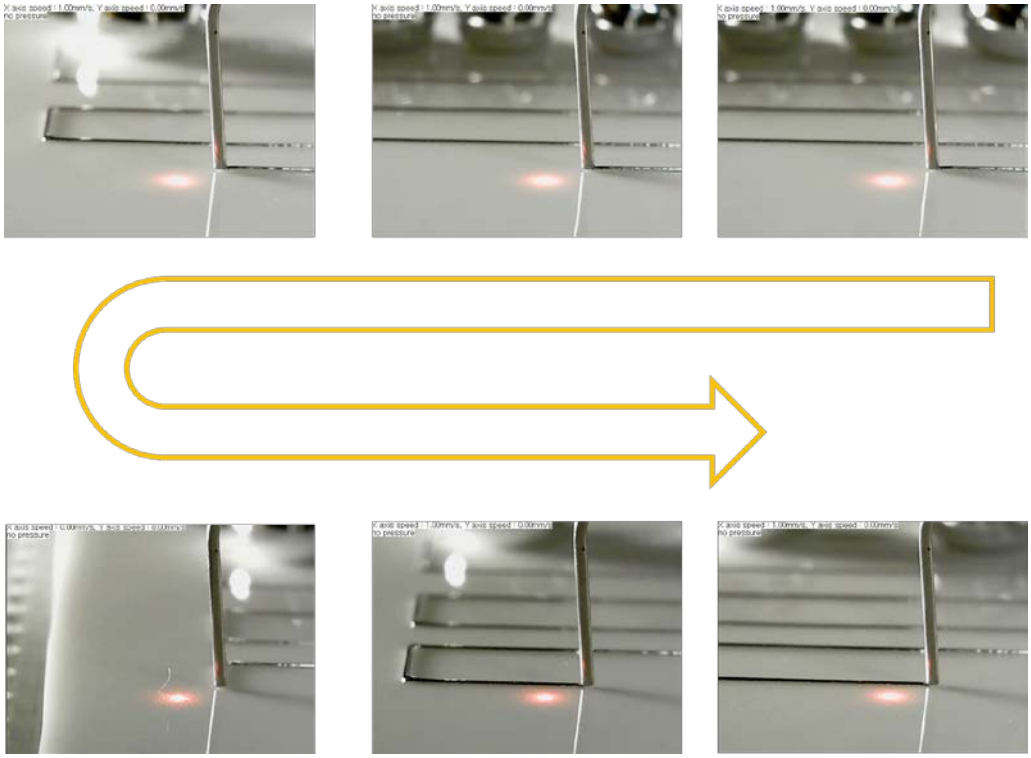

Figure 2.20. Printing EGaIn pattern with distance and pressure feedback and paraffin coated needle.

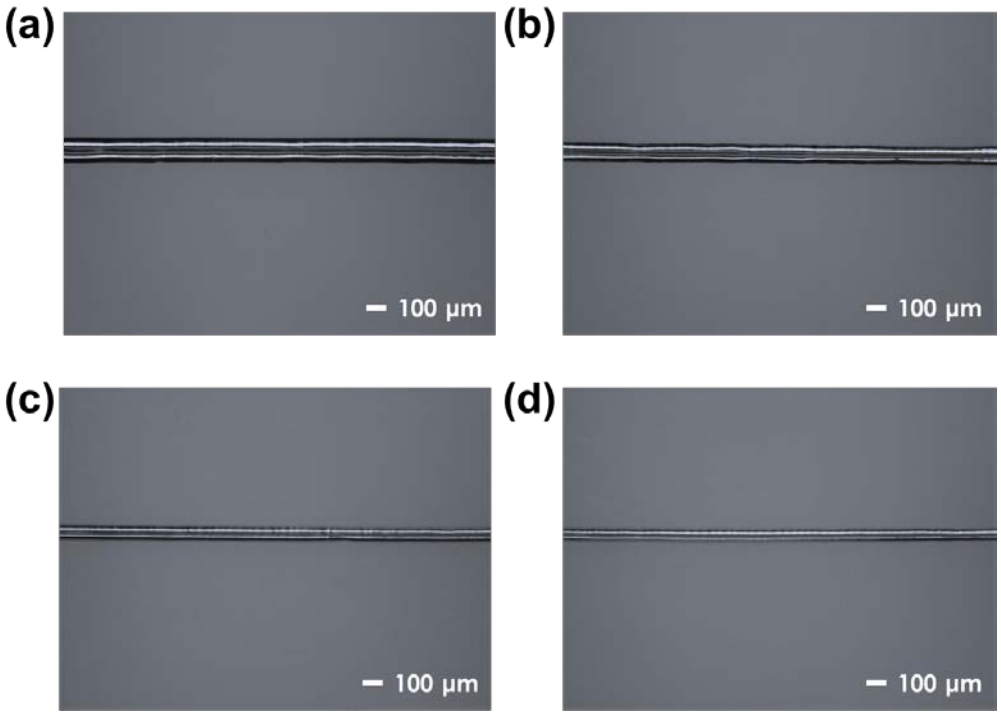

Figure 2.21. Results of the direct printing with different inner diameters of the dispensing needle or different distances between needle and substrate. (a) inner diameter: 250 µm, gap distance: 70 µm, pattern width: 120 µm. (b) inner diameter: 180 µm, gap distance: 70 µm, pattern width: 90 µm. (c) inner diameter: 120 µm, gap distance: 70 µm, pattern width: 60 µm. (d) inner diameter: 120 µm, gap distance: 80 µm, pattern width: 40 µm.

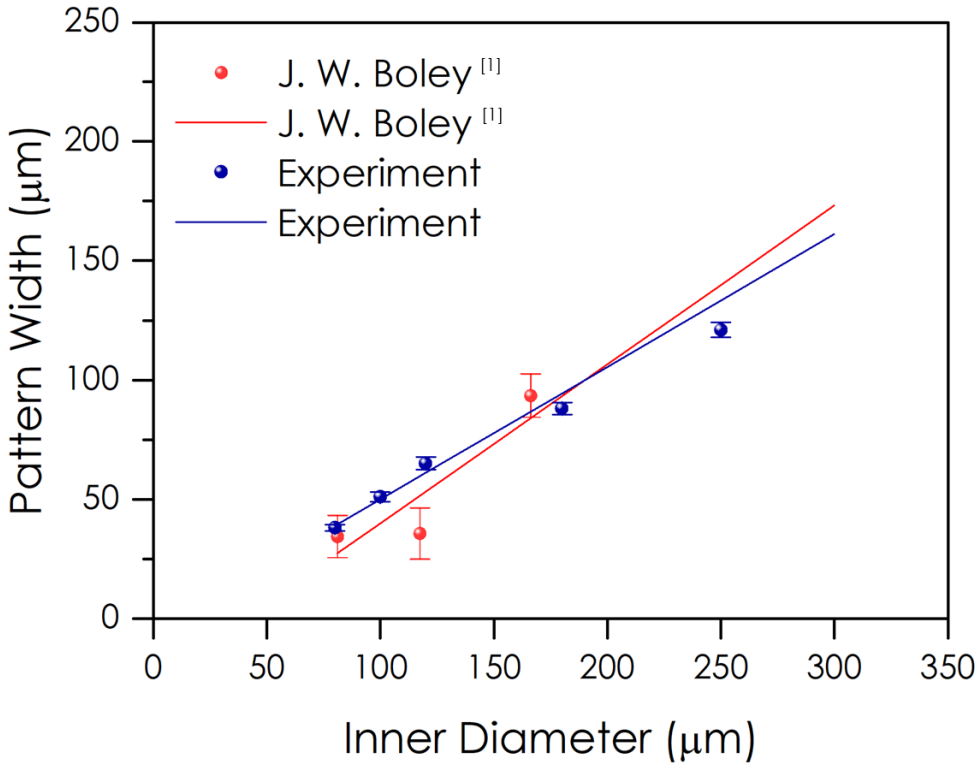

Figure 2.22. Comparison between EGaIn printing results and previously reported results.

Chapter 3. Stretch and transfer method

3.1 Stretch substrate with EGaIn

After printing liquid metal with customized the direct printing system. We reduce the liquid metal width by stretching the substrate with the motorized stage. As we mentioned in chapter 2, the pinning force between EGaIn and Ecoflex is bigger than the cohesion of EGaIn. Therefore, when we stretch the substrate, EGaIn pattern also stretched with the substrate. After stretching the substrate and the EGaIn pattern, EGaIn pattern length increased, and the EGaIn pattern width decreased because volume must be constant. In the beginning, we stretched substrate manually without using motorized stage. However, as shown in **Figure 3.1**, the gallium oxide skin can not react at the rapid stretching sequence, broken gallium oxide remains on the surface. To complement this technical issue, the motorized stage and strain supporter designed to stretch the substrate. Moreover, the motorized stage can change the stage velocity 0.1 mm/s to 10 mm/s. **Figure 3.2** shows that the SEM image of stretched EGaIn with three different stage velocities. As the velocity decrease, the stretched EGaIn form more uniform pattern.

Figure 3.3 show the strain supporter and patterned EGaIn on the Ecoflex substrate. To stretch the substrate and the EGaIn pattern smoothly, we added oil at the space between the aluminum supporter surface and the Ecoflex substrate. Next, the

Ecoflex substrate with the printed EGaIn, fixed on the strain supporter and motorized stage smoothly move the strain supporter under the stage velocity 2mm/s. After the stretch stretched EGaIn pattern with reduced width can be obtained. **Figure 3.4** shows the detail shape of the liquid metal pattern before (b) and after (a) stretching.

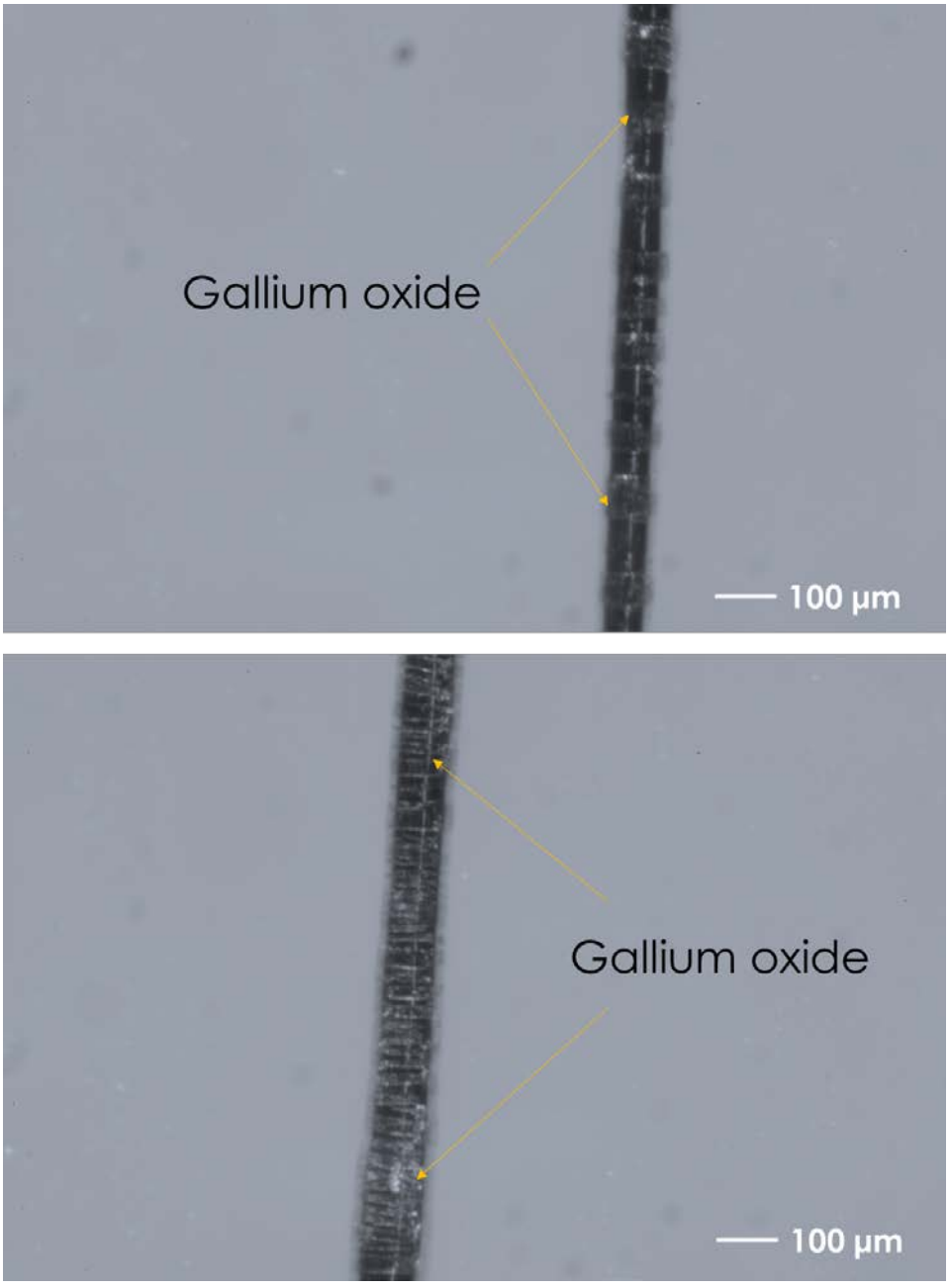

Figure 3.1. Gallium oxide film with rapid manual stretching.

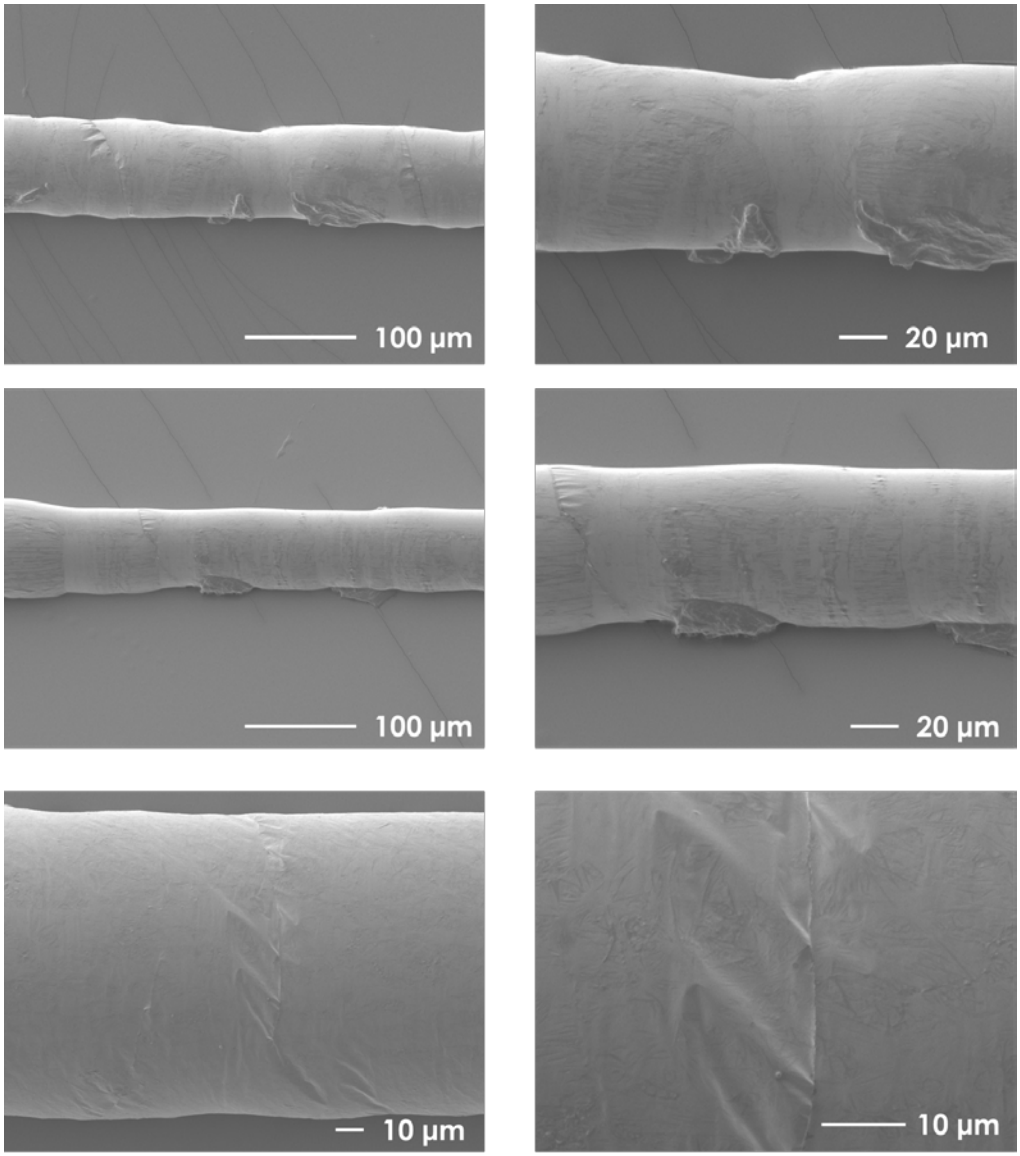

Figure 3.2. SEM image of stretched EGaIn with three different stage velocities. 5mm/s (a), 3mm/s (b), 1mm/s (c).

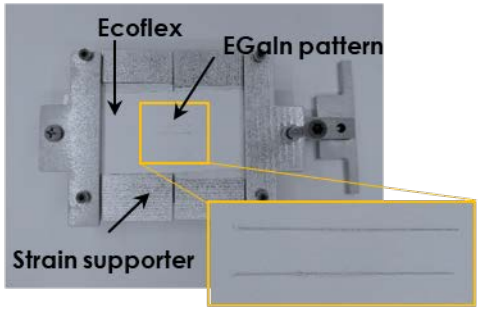

I. Initial patterning on unstretched Ecoflex

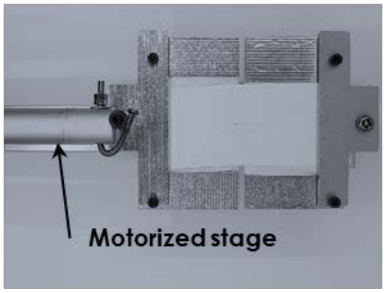

II. Setup linear motorized stage

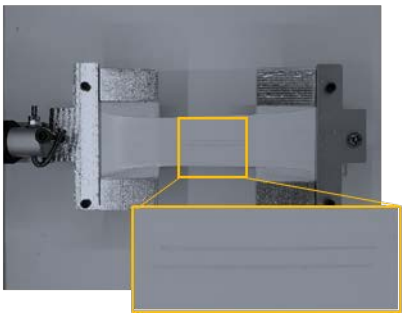

III. Stretching of Ecoflex & EGaIn with motorized stage

Figure 3.3. Sequential example pictures taken during the stretching.

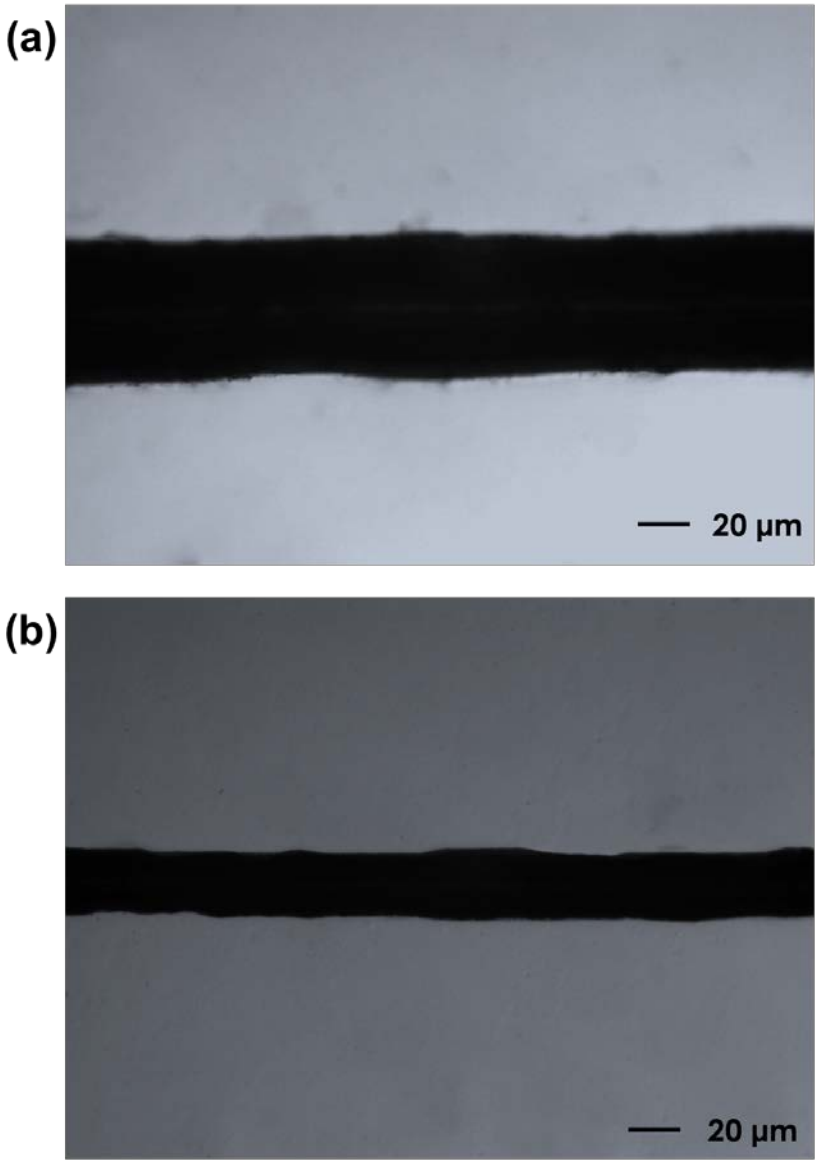

Figure 3.4. EGaIn pattern before (a) and after (b) stretching. (a) has been five times stretched and transferred from the initial direct printed pattern. (b) has been six times stretched and transferred from the initial direct printed pattern.

3.2 Strategy to transfer EGaIn pattern

After stretching EGaIn with the stretchable substrate. Stretched EGaIn pattern is phase-changed at refrigerator to transfer from pre-strained substrate to unstretched substrate. The EGaIn melting point is known for 15.3 ℃; however, because of supercool effect, the EGaIn pattern does not phase change its status into the solid state even under the zero degree. Therefore, we freeze liquid metal pattern under – 30 ℃ with refrigerator. At first, frozen EGaIn pattern can be easily pick-up with tweezer; however, this simple pick up method physically changed its pattern shape, and critically it cannot handle the small width EGaIn pattern. Therefore, we research the transfer strategy to transfer small size EGaIn pattern with no damage to the pattern. **Figure 3.5** shows the various transfer method that we tried to transfer EGaIn; however, none of the transfer can succeed to transfer small size EGaIn pattern.

3.2.1 Transfer with deionized water

As shown in **Figure 3.6**, deionized (DI) water is tested for transferring EGaIn. To verify that using DI water to transfer method is suitable for transfer, EGaIn patterns are prepared with different widths of 120, 80, and 50 μm. The 120 μm wide pattern is prepared by the direct printing (n=0) and other patterns are prepared by the phase change mediated transfer (80 μm (n=3) and 50 μm (n=5) with strain value of 0.5). As

shown in **Figure 3.7**, structural guide walls are used to confine the DI water over the Ecoflex with printed EGaIn. After freezing, the ice brick impregnating the EGaIn pattern is moved to another substrate by the pick-n-place transfer. After transfer, the EGaIn remaining on the donor Ecoflex substrate (**Figure 3.7-IV**) is compared with EGaIn transferred to the acceptor Ecoflex substrate (**Figure 3.7-III**). For a quantitative comparison, micrographs of EGaIn before and after the transfer are taken, modified to grayscale with the Adobe Photoshop, and then analyzed for the pixel's intensity by MATLAB. Using the analyzed pixel intensity, areas of remaining and transferred EGaIn can be calculated. **Figure 3.8** shows that residue EGaIn by percentage in comparison with the transferred EGaIn pattern. After the transfer, all results exhibit the residue under ~4 %. As shown in **Figure 3.9**, transfer method using DI water also performed in the stretching guide. With the experiment, we re-confirm the usability to transfer the EGaIn pattern with DI water.

3.2.2 Water effects on the oxide

When stretched EGaIn patterns are submerged in deionized water for freezing, gallium oxide surrounding EGaIn patterns may change their chemical composition or undergo thickness variation. Based on the previous paper, [94] surface elastic modulus and yield stress of the gallium oxide (Ga_2O_3) may be decreased by a factor of 10 and 5, respectively, compared to their value in air. It's seems that, as show in equation,

$$Ga_2O_3 + H_20 \rightarrow 2\ GaO(OH) \quad (3)$$

some of Gallium oxide react with deionized water and make gallium oxide hydroxide [95] and it cause the property changes of EGaIn in the water. However, gallium oxide hydroxide is also an oxide film, therefore it does not change the shape of EGaIn pattern in the water condition. In addition, we have not observed any mechanical weakening of stretched EGaIn pattern with water before or after freezing.

3.2.3 Removing ice brick from the substrate

Figure 3.10 shows the brief transfer sequence. First, making the whole stretched EGaIn solid via freezing after enclosing it with a carry-on medium (**Figure 3.10-I**). The stretched EGaIn frozen with the carry-on medium can be picked up, moved over and placed onto a new Ecoflex substrate (**Figure 3.10-II**). If the carry-on medium can be selectively removed, the width reduced and elongated EGaIn pattern will remain (**Figure 3.10-III**).

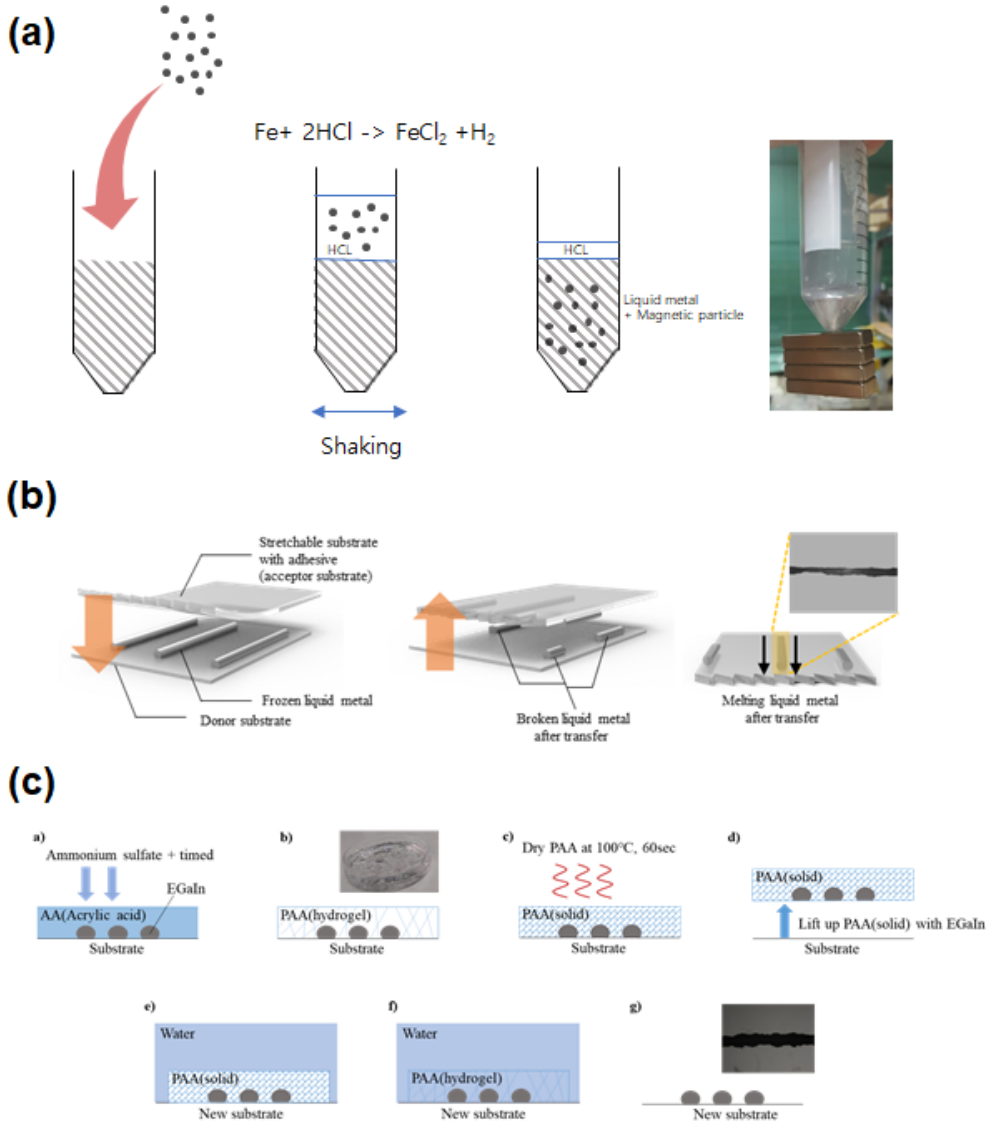

Figure 3.5. Tried methods to transfer EGaIn patterns. (a) Making a magnetic liquid metal process- magnetic liquid metal [96] (b) Tape transfer (c) PAA transfer

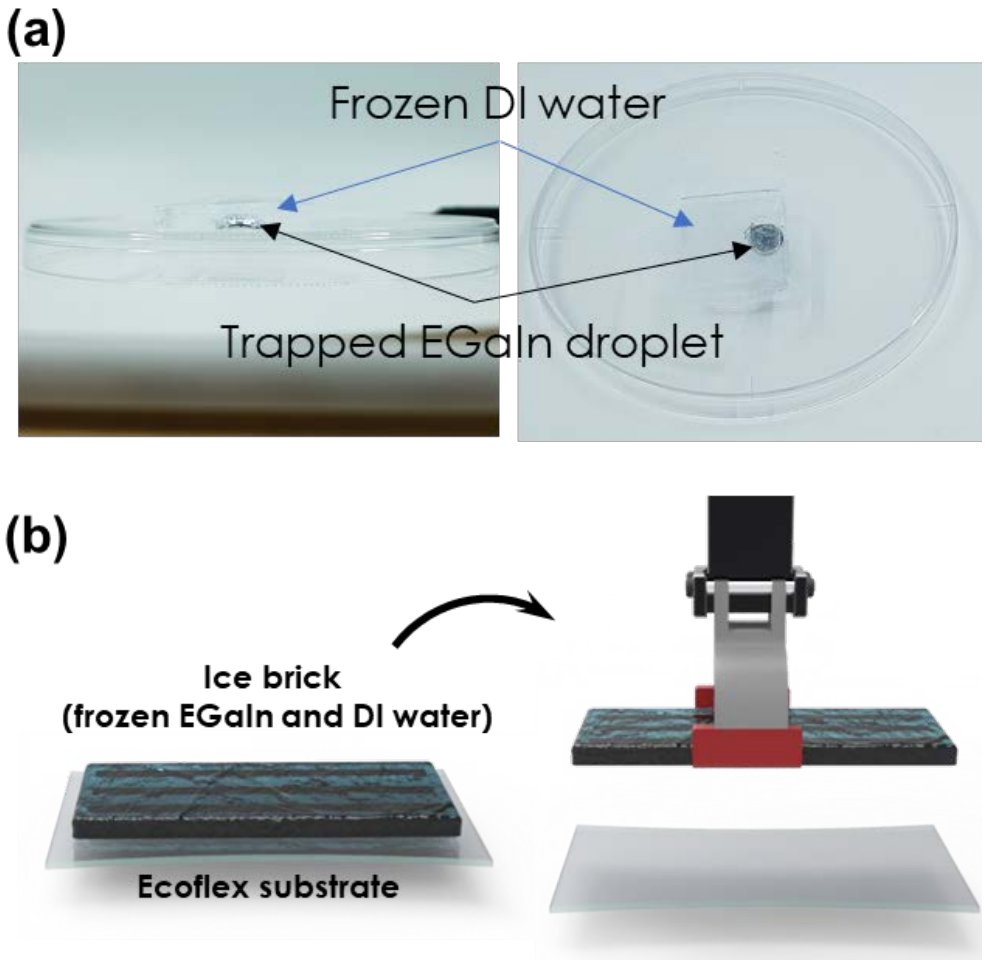

Figure 3.6. (a) Frozen ice brick with EGaIn droplet. (b) Pick-n-Place transfer of the ice brick impregnating EGaIn patterns.

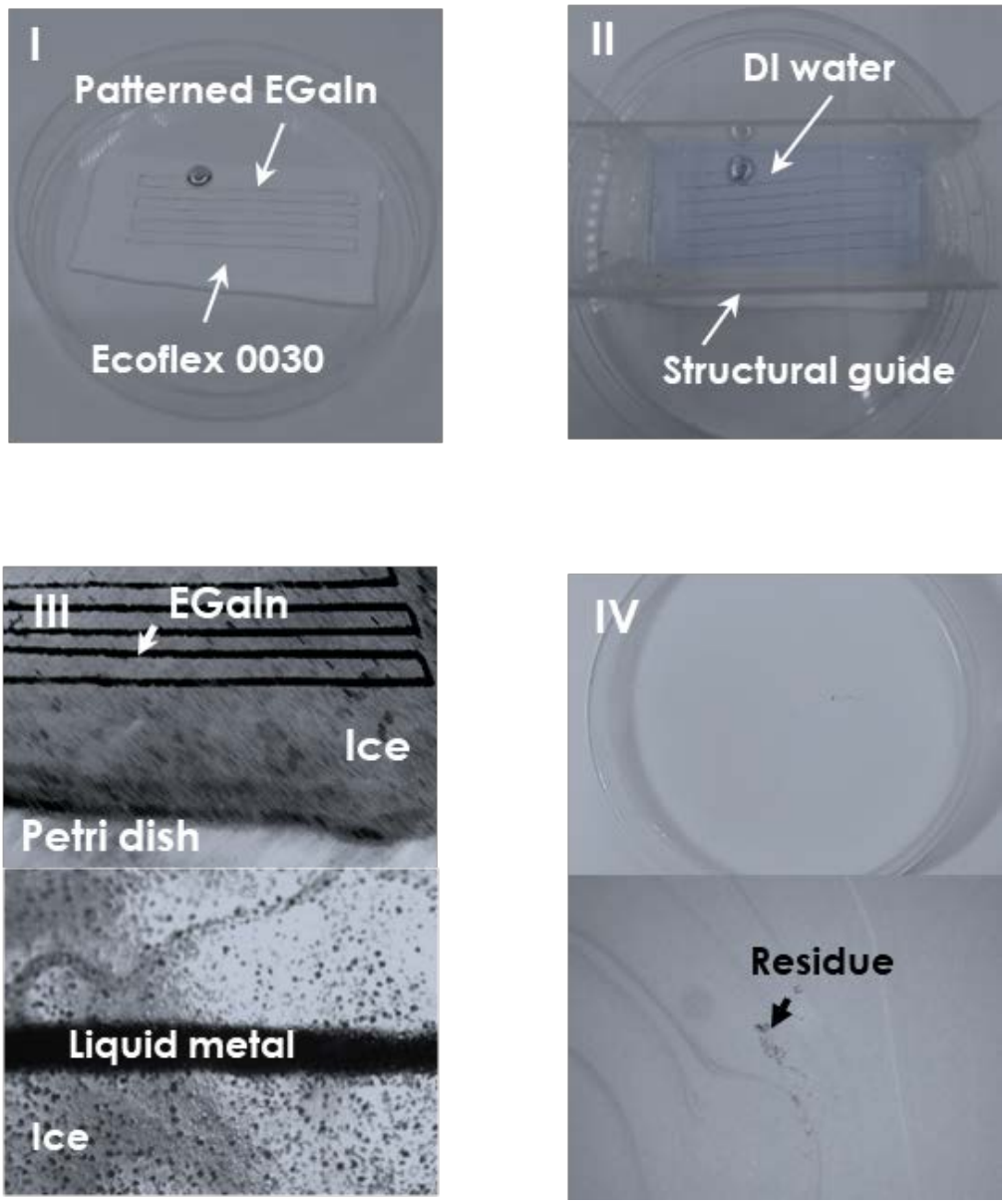

Figure 3.7. EGaIn pattern before transfer (I). EGaIn pattern with the structural guide walls and DI water (II). Frozen DI water and EGaIn pattern (III). EGaIn residue remaining on the donor substrate (IV).

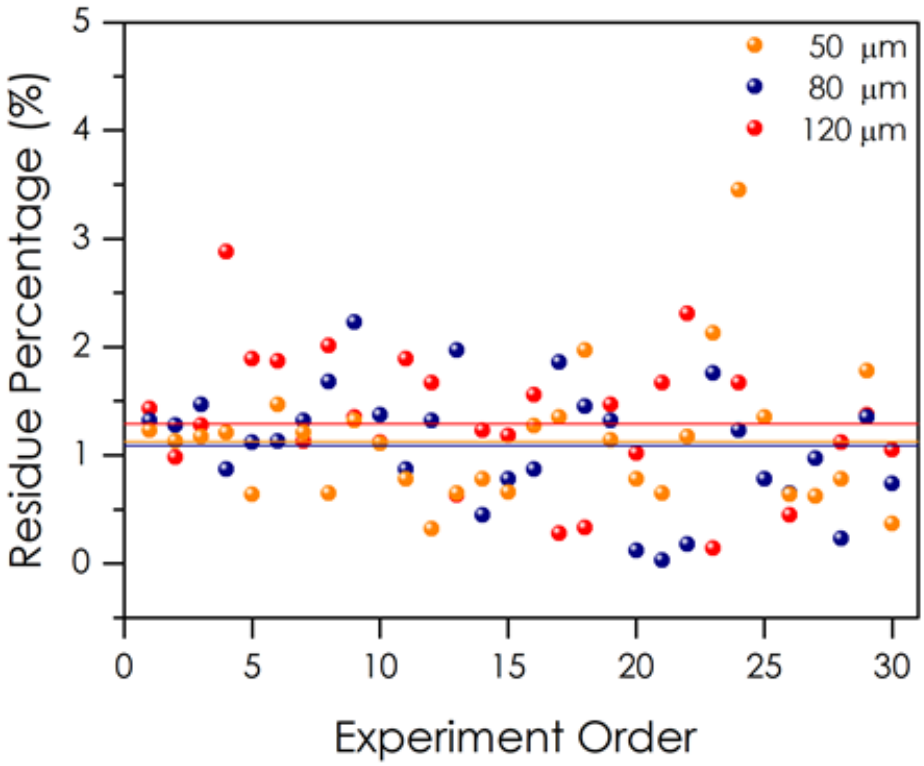

Figure 3.8. Area ratio between donor substrate's residue and transferred EGaIn pattern for EGaIn patterns with different widths (120, 80, and 50 µm).

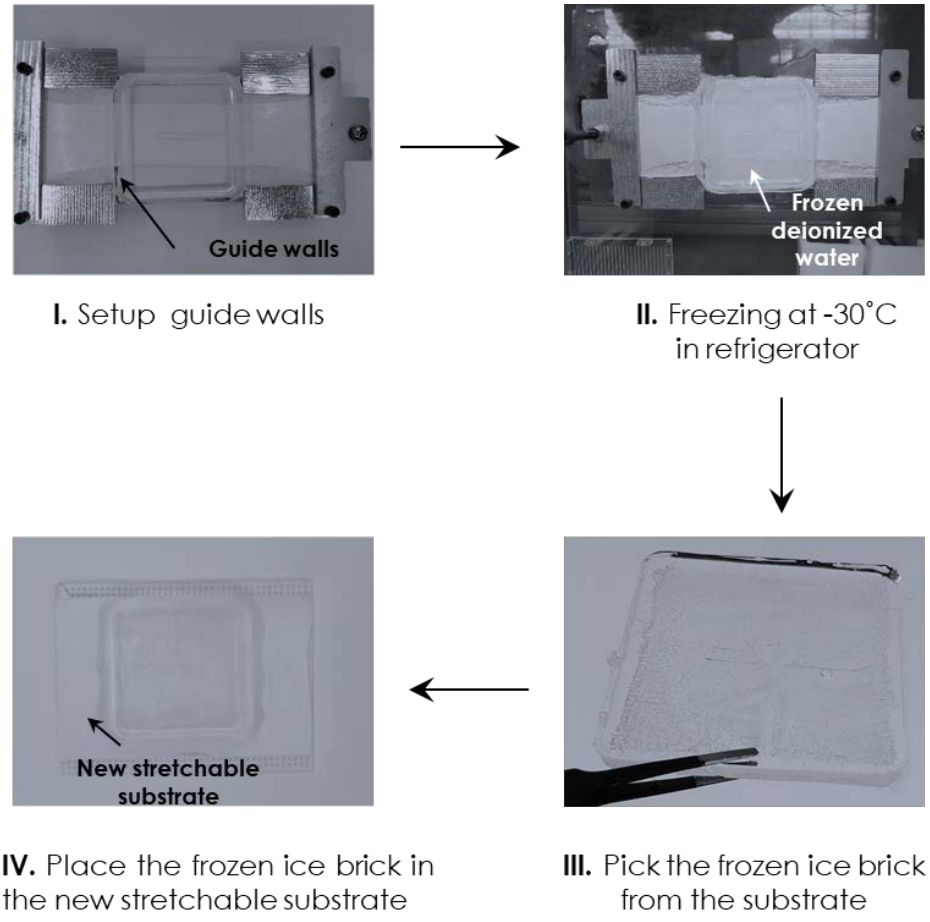

Figure 3.9. Sequential pictures taken during the phase change mediated transfer of EGaIn patterned on Ecoflex. After DI water poured onto the stretched EGaIn is frozen at -30˚C, the EGaIn embedded in the ice brick can be simply picked up and transferred onto a new unstretched Ecoflex substrate.

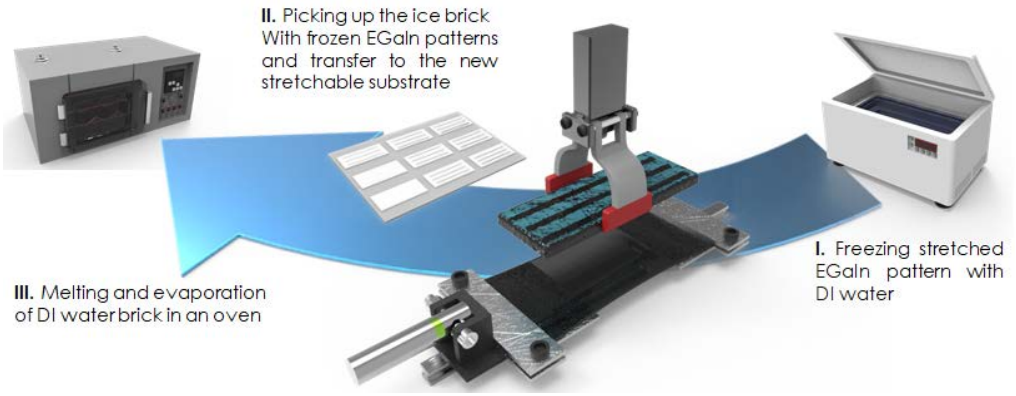

Figure 3.10. The pick-n-place transfer idea of stretched EGaIn pattern frozen with DI water onto an unstretched substrate. (I) Freezing stretched EGaIn pattern with DI water. (II) Picking up the ice brick impregnating the stretched EGaIn pattern to a new stretchable substrate. (III) Melting and evaporating DI water in an oven.

Chapter 4. Phase change mediated pick-n-place transfer

Figure 4.1 shows the process sequence for the phase change mediated transfer of the printed and stretched EGaIn on the Ecoflex substrate. The process starts with the uniform direct EGaIn printing on a stretchable Ecoflex substrate. After the EGaIn printing is completed, the EGaIn pattern on the Ecoflex substrate is moved to a strain supporter that is used to stretch the EGaIn along with the underlying Ecoflex. Then, the strain supporter is connected to a linear motorized stage. The motorized stage extends the EGaIn pattern by stretching the Ecoflex uniaxially at a constant speed of 1 mm/s. During the stretching process of the EGaIn pattern, the pattern length increases while the pattern width decreases since the volume of the printed EGaIn pattern remains constant. After the EGaIn pattern is fully stretched to a target strain, a structural guide for the carry-on medium, DI water, made with polymethylmethacrylate (PMMA) is positioned onto the stretched EGaIn wherein DI water is filled. Next, the entire experimental setup except for the linear motorized stage is moved to a freezer at −30 ˚C to freeze the EGaIn pattern and DI water together. Once the EGaIn pattern and DI water are completely frozen, a rectangular ice brick impregnating the stretched EGaIn at the bottom forms, which can be simply picked up and

placed onto a new unstretched Ecoflex substrate. Once the ice melts and water evaporate in an oven at 60 ˚C, the stretched EGaIn pattern is only left on the new Ecoflex substrate. The processes shown in **Figure 4.1-II~VII** are repeated multiple times until the target width is reached.

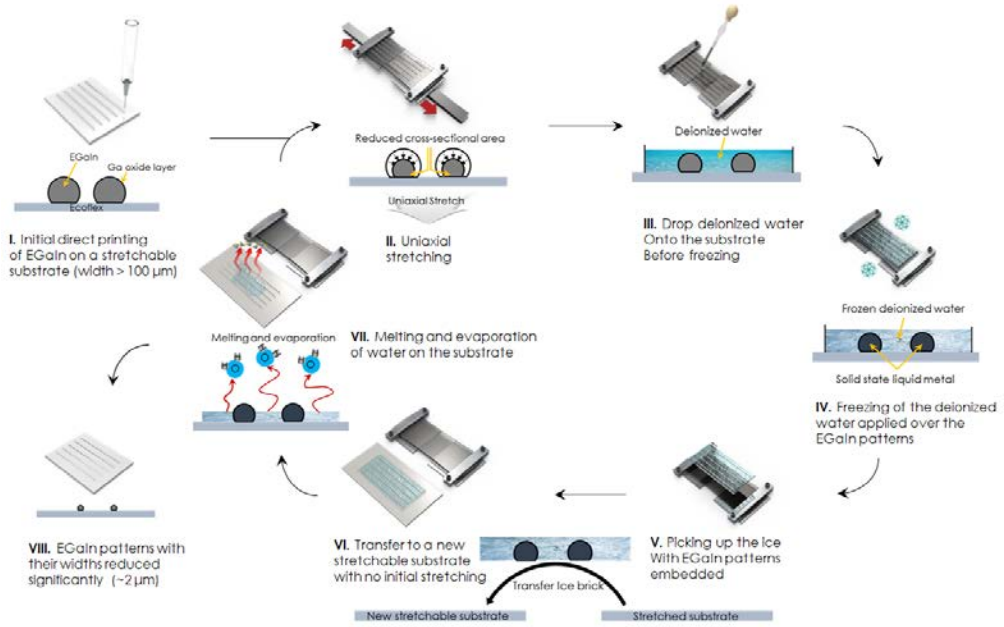

Figure 4.1. Fabrication process of the phase change mediated transfer of EGaIn patterned on a stretchable substrate.

Chapter 5. Patterning result

Figure 5.1 shows patterning results with the initial direct EGaIn printing and phase change mediated transfer of stretched EGaIn patterns. Optical and scanning electron micrographs show the change in the width of linear EGaIn patterns with the applied strain of 2.0 after the sequential transfer where n = 0 represents an as-printed pattern with customized direct printing system and n increases by 1 after every transfer process. After 7 sequential transfers (n= 7), the width of the EGaIn pattern becomes ~2 μm, which is a ~60-fold reduction from the 120-μm width of the as-printed EGaIn pattern. While scanning electron micrographs are taken only for n=0 and n=7, **Figure 5.2** shows zoomed-in optical micrographs showing the entire sequential transfer process. In contrast to the stretch mediated size reduction of EGaIn reporting ~10 μm by a single stretching process at room temperature [41], our method reduces the width of EGaIn down to ~2 μm by multiple cycles of stretching and transfer at room temperature and –30 °C, respectively. In addition, the uniformity in EGaIn patterns is improved with the aid of the motorized stage used for stretching and stretched liquid metals are easily transferred to an arbitrary substrate. These additional advantages are also in stark contrast with the previous work [41].

Figure 5.3 shows the ration between EGaIn widths before and after transfer for different uniaxial strains. For a strain value of 0.5, 1.0, 1.5, and 2.0, the averaged

ratios between EGaIn widths before and after transfer are 80.43, 70.84, 63.68, and 56.16 %, respectively. The averaged ratio between EGaIn widths before and after transfer decreases as the uniaxial strain increases. In addition, the error in the width reduction tends to increase as the strain value increases. As expected, the percent reduction for any strain condition is constant (average) along with finite uncertainty (error). **Figure 5.4** displays the actual width of EGaIn patterns as a function of the stretching (or transfer) number, n, for uniaxial strains of 0.5, 1.0, 1.5 and 2.0. As expected, the higher strain is, the fewer number of transfer cycles required to achieve a desired pattern width. For example, to reach the target width of ~2 μm, the strain of 0.5 requires 15 consecutive transfers while the strain of 2.0 requires 7 consecutive transfers, which is less than a half compared to the case with the strain of 0.5.

Figure 5.5 compares measured and calculated specific resistances, the resistance per unit length (Ω/cm), as a function of the EGaIn width where the phase change mediated transfer is performed with the strain of 1.0 and dispensing needles with various sizes. To compare the resistance between measurements and theory, cross-sectional area was analyzed. The cross-section of the transferred EGaIn pattern is examined carefully by the scanning electron microscope. As shown in **Figure 5.6**, the cross-section looks like a semicircle on top of a rectangle. Therefore, it is necessary to measure height (h) and width (w) of the EGaIn pattern precisely. Before measuring the pattern height with the laser sensor, heights of EGaIn droplets are measured with the laser sensor and compare them with the digitized information for EGaIn droplet micrographs by the pixel count as shown **Figure 5.7**. Results show good agreement

between the height information from the laser sensor and the digitized information from the image pixel count. However, the width measured by the laser sensor tends to be inaccurate due to the oblique incidence of the laser near the pattern edge. To minimize the error, the width is measured from a top-view image taken with the optical microscope. **Figure 5.8** shows the representative height measurement of the EGaIn pattern (n=1) with the laser sensor. The cross-sectional area, *S*, is given by

$$s = \frac{\pi}{2} \times \left(\frac{w}{2}\right)^2 + w \times \left(h - \frac{w}{2}\right) \quad (4)$$

, where *h* is the height measured with the laser sensor and *w* is the width measured with the optical microscope. Finally, the specific resistance of the EGaIn pattern is calculated by dividing the known resistivity of EGaIn, 29.4 $\times 10^{-6}$ Ω-cm [28] by the calculated cross-sectional area and multiplying the unit length of 1 cm.

$$R = \rho \times \frac{l}{s} \quad (5)$$

As a result, the calculated resistance and measurements show similar trends in general.

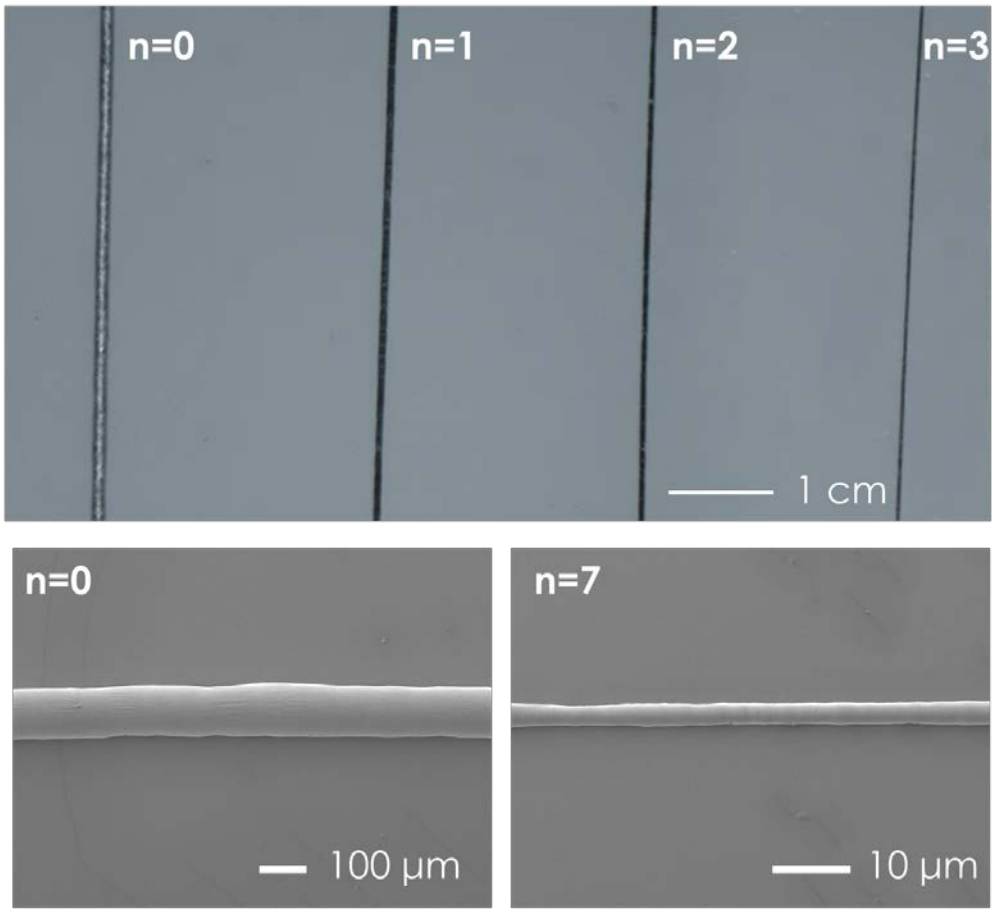

Figure 5.1. Change in width of EGaIn lines with the applied strain of 2.0 after the sequential transfer (n=0 represents as-printed line and n increases by 1 after every transfer).

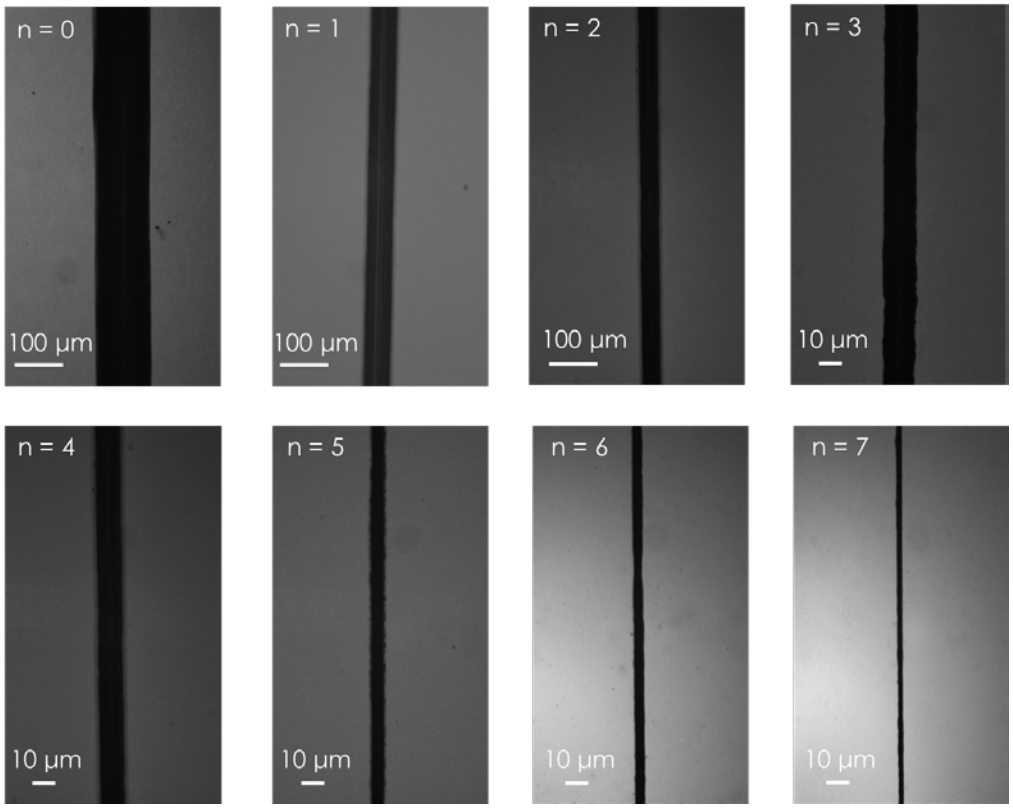

Figure 5.2. EGaIn patterns after phase change mediated transfer with the strain value of 2.0 (The process sequence is left to right and top to bottom). The EGaIn pattern width is reduced from 120 µm to ~2 µm.

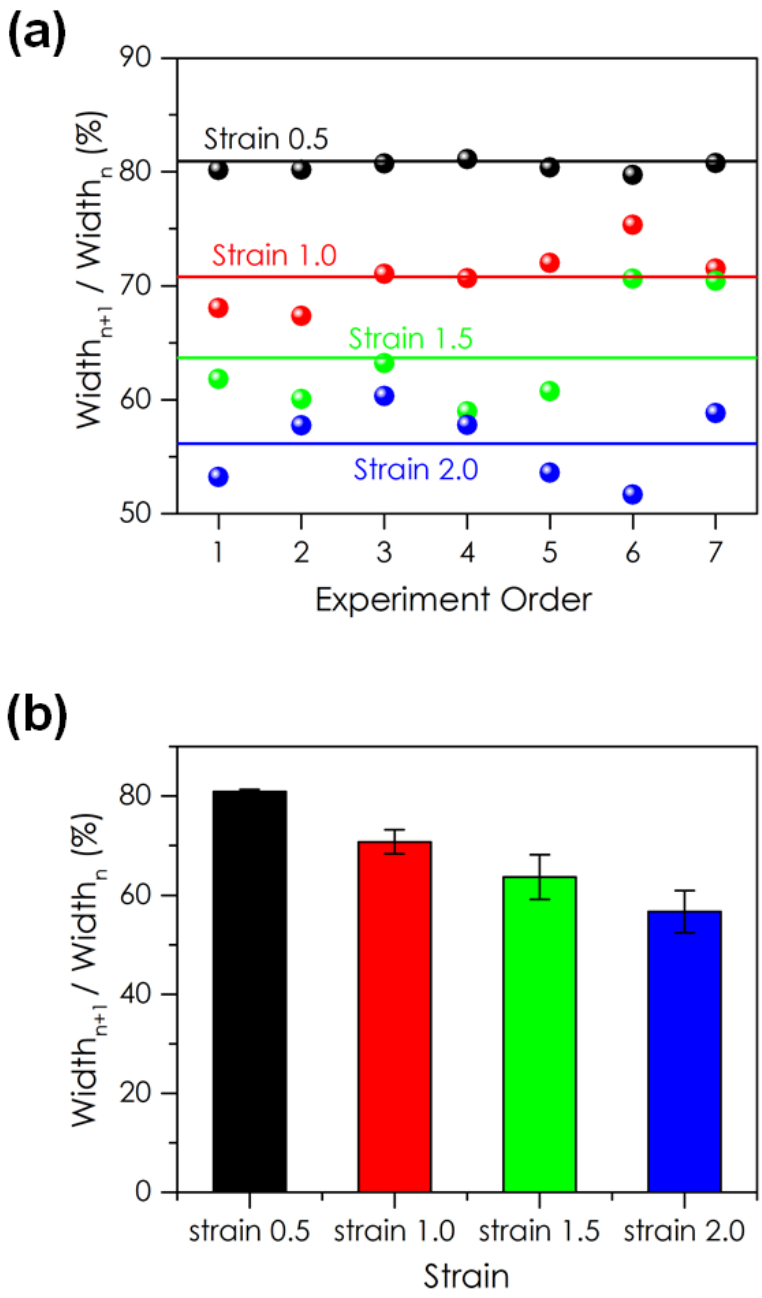

Figure 5.3. Ratio between the EGaIn widths before and after each transfer.

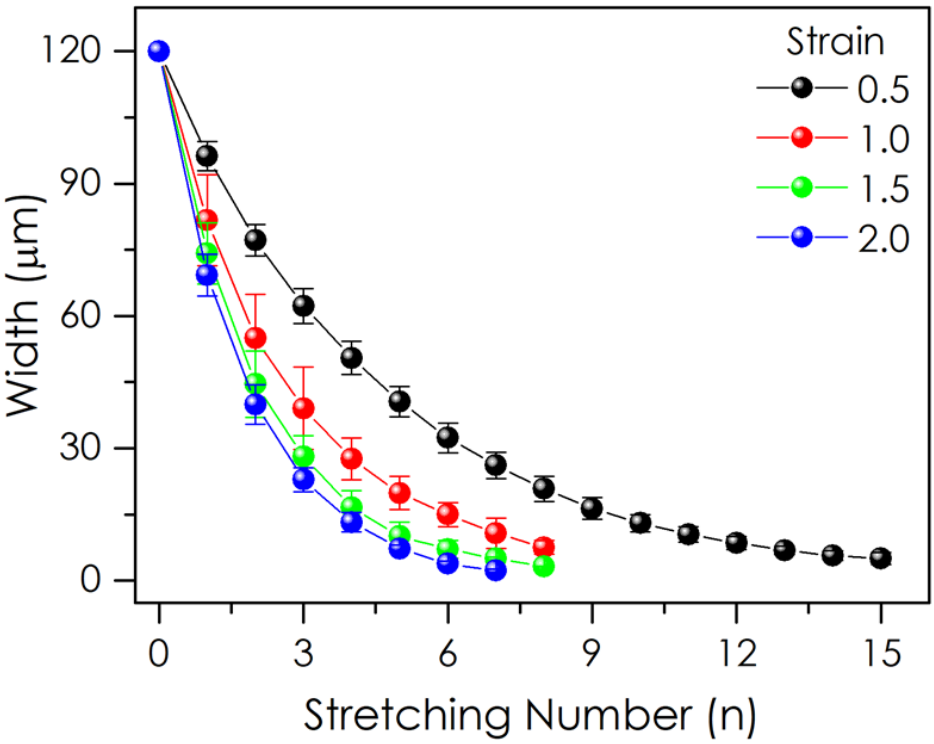

Figure 5.4. The width of the EGaIn line as a function of the stretching number, n.

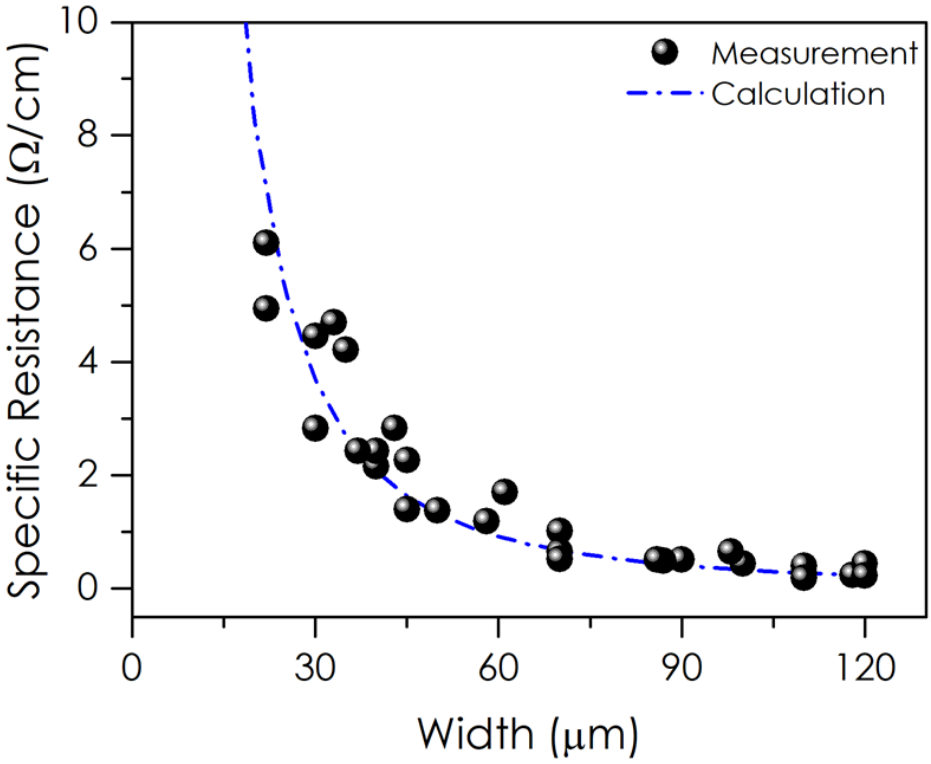

Figure 5.5. Measured and calculated specific resistances (Ω/cm) as a function of the EGaIn line width.

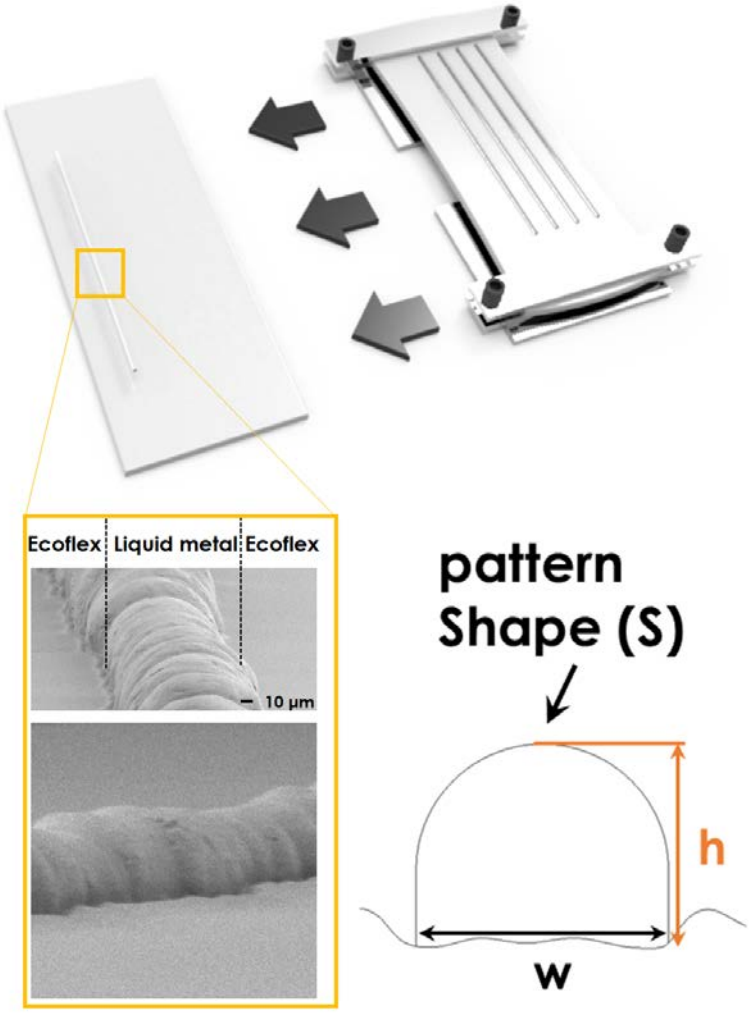

Figure 5.6. Scanning electron micrograph of the EGaIn pattern on the Ecoflex substrate and cross-section schematic of the transferred EGaIn on the Ecoflex substrate.

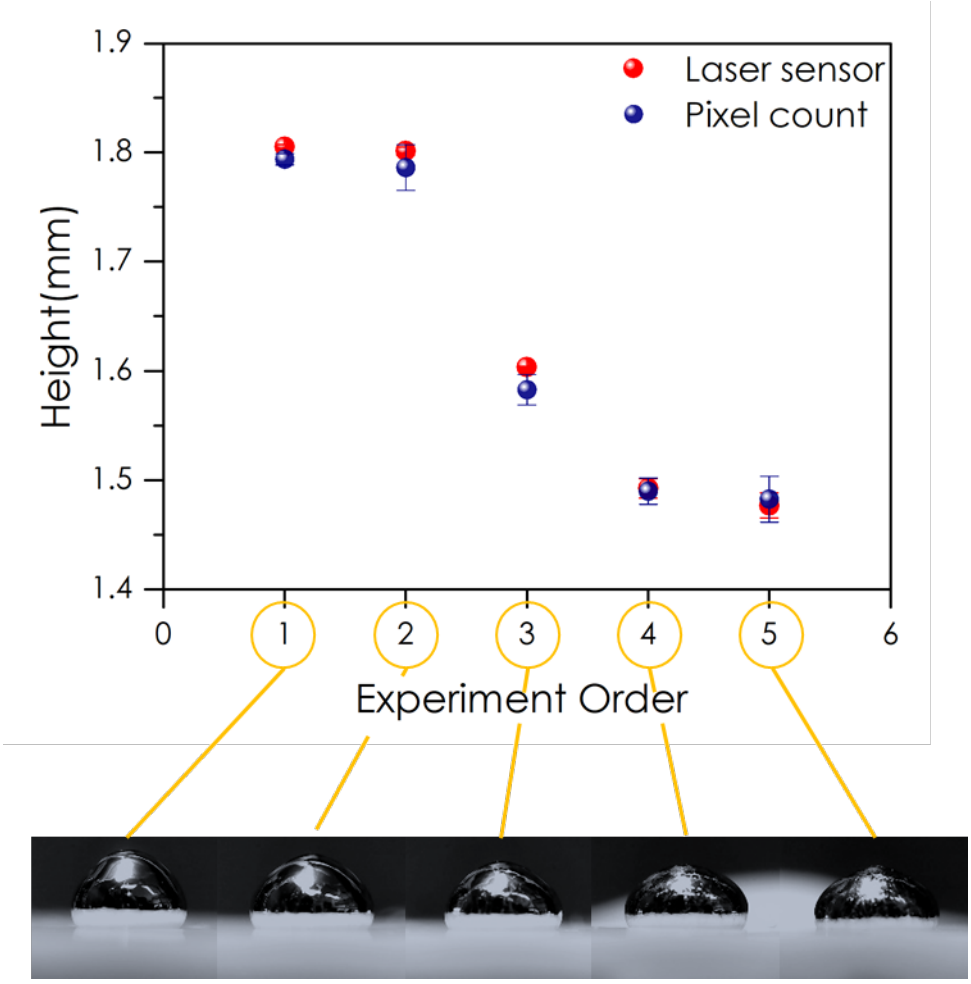

Figure 5.7. Heights of EGaIn droplet measured by the laser sensor or calculated by the pixel count in an EGaIn droplet image.

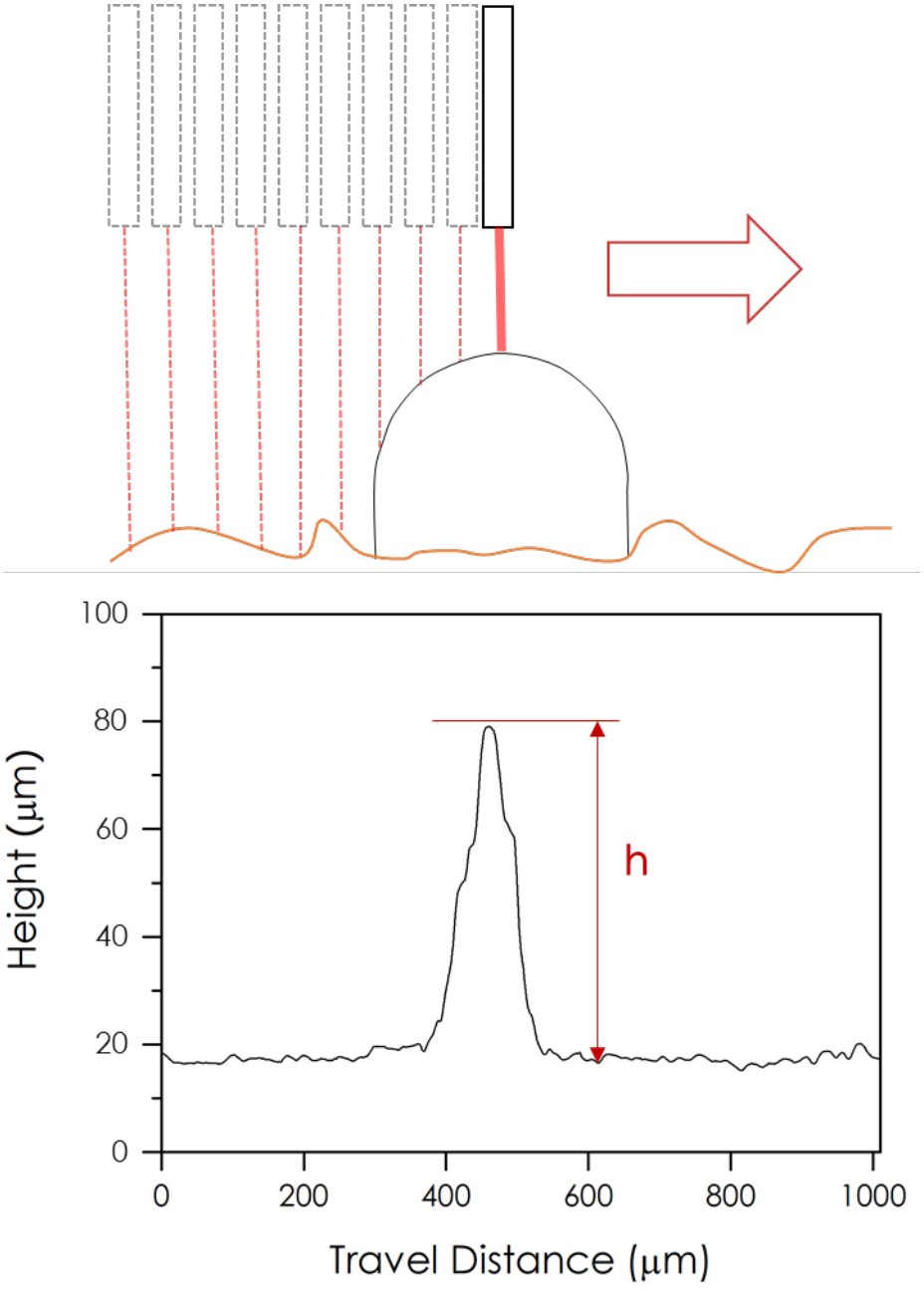

Figure 5.8. The height of EGaIn pattern measured by the laser sensor

Chapter 6. Patterning with contraction

As aforementioned method, phase change mediated transfer, the size reduction by transfer after mechanical stretching mainly works for 1D structures since longitudinal elongation accompanies transverse contraction. The transverse contraction increases the dimension of the printed EGaIn orthogonal to the longitudinal direction. This is the critical problem to reduce the complex EGaIn structure. It is sure that, we can make a complex structure by effectively combining 1D and 2D substrate deformation and transfer via freezing with ice. However, it takes a lot of time and need sophisticated transfer. Therefore, we research to reduce the complex EGaIn patterns with natural contraction.

6.1 Contraction process

Figure 6.1 shows the sequential process to reduce the patterning with the natural contraction of hydrogel. First, the initial EGaIn pattern is printed with the customized direct printing setup. Next, printed EGaIn covered with Ammonium sulfate and deionized water. After cover all printed area, TEMED (hardener) is mixed with the liquid and form a Poly Acrylic Acid (PAA), a kind of hydrogel that contains the water molecular inside. After curing the PAA, cut the liquid metal area and covered the PAA.

In this part, the most important thing is that the PAA contains the outlet channel of liquid metal shown in **Figure 6.1-III**. This channel serves as an outlet to bring the excess volume of liquid metal out while contraction. Upon gentle heating inside the oven, water inside the PAA evaporate. After heating, the volume of the PAA is reduced by the volume of the water that has evaporated, and PAA phase changes its state from the hydrogel to the solid state. In addition, EGaIn pattern inside the PAA also contracts its volume, and the excess volume caused by the contraction is exited through the outlet channel. As shown in **Figure 6.2**, contract PAA and liquid metal soak inside the water, to re-connect the water molecule and the solid state PAA. When re-connect is done, the PAA changes its phase from the solid state to the hydrogel. After phase change of the PAA, the PAA can easily remove from the substrate and just reduced EGaIn pattern remains on the substrate.

6.2 Result

Figure 6.3 shows the picture of contracted EGaIn pattern and PAA, and excess volume of the EGaIn after contraction. Rectangle area is the same area and easily can observe the PAA is contracted 40% after heating. And can easily observe the excess volume exited through the external channel.

Figure 6.4 shows the optical image of the EGaIn pattern before **(a)** and after **(b)** contraction. To visualize the reduced size of EGaIn pattern before and after contraction, EGaIn pattern is coated by Pt (Pt is the black dot in the image). After contraction, the width of EGaIn pattern becomes ~60 μm, which is a half reduction from the 120 μm width of the as-printed EGaIn pattern. **Figure 6.4 (c)** shows the optical image of the EGaIn pattern after removing the PAA from the substrate. Some broken EGaIn pattern detected after removing sequence, and it may occur because of the expansion of the PAA.

Compare to the result of phase changed mediated transfer, the reduction rate is very small, but this contraction method does not need a complex system and also have a possibility to reduce complex structure. In addition, to control the PAA water molecular percentage can reduce the EGaIn pattern more. However, our handling technique to control PAA limited 20% max.

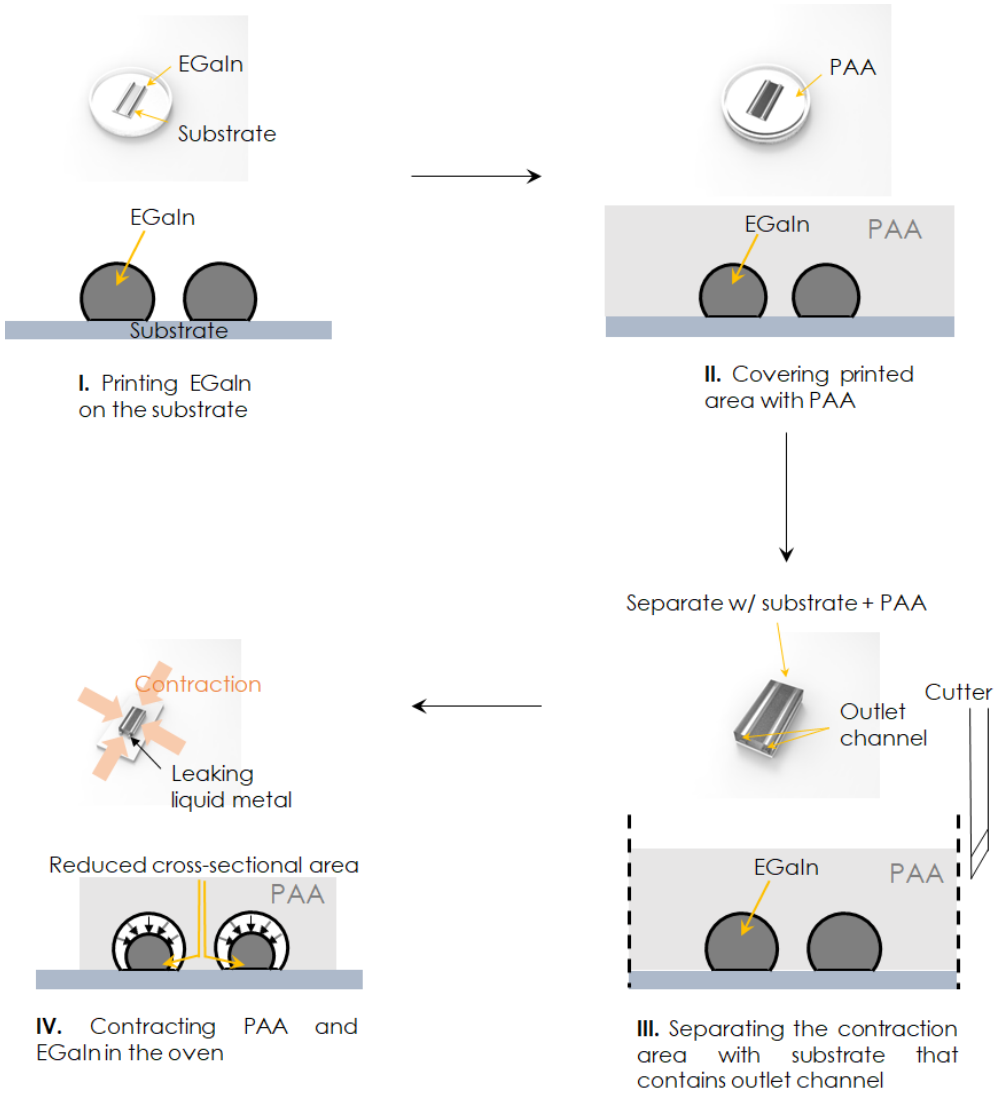

Figure 6.1. Fabrication sequence of the contraction patterning method using the PAA.

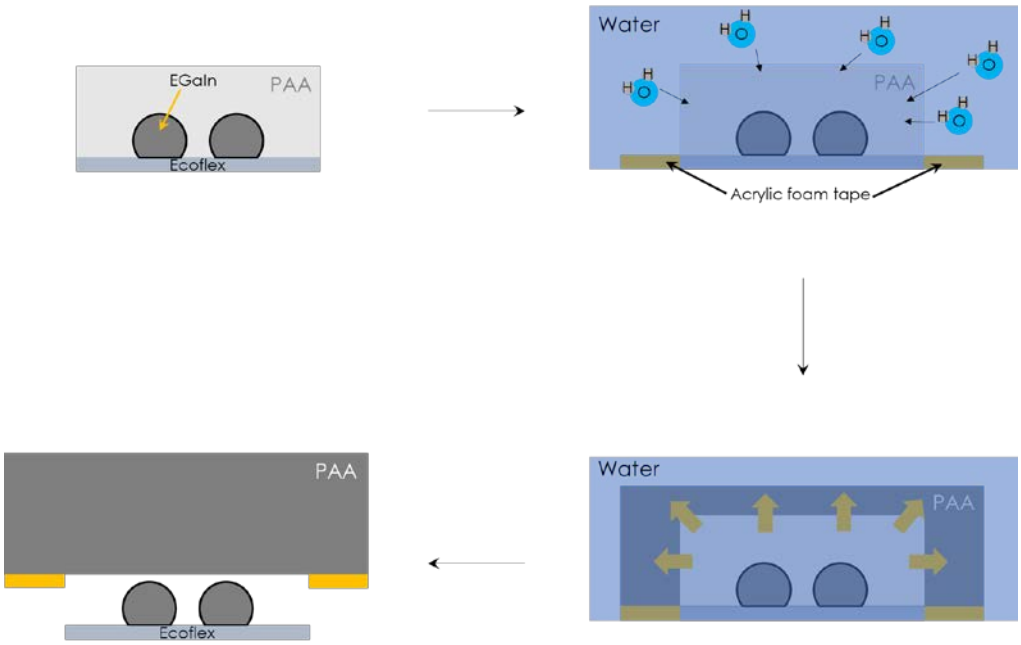

Figure 6.2. Method to remove the PAA from the substrate.

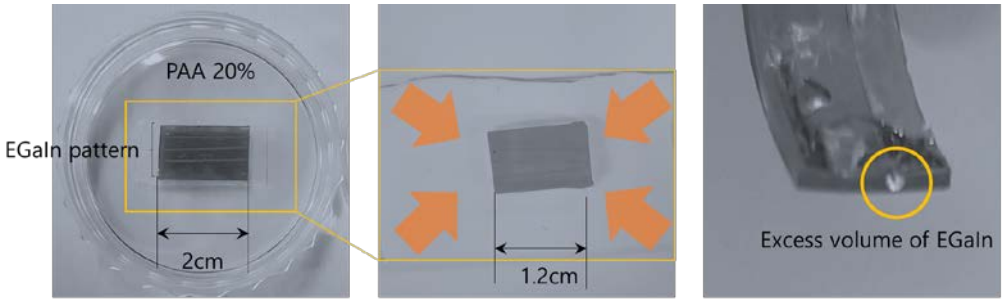

Figure 6.3. Picture of contracted PAA and EGaIn pattern (left). Picture of excess volume that exited through the outlet channel during the contraction (right).

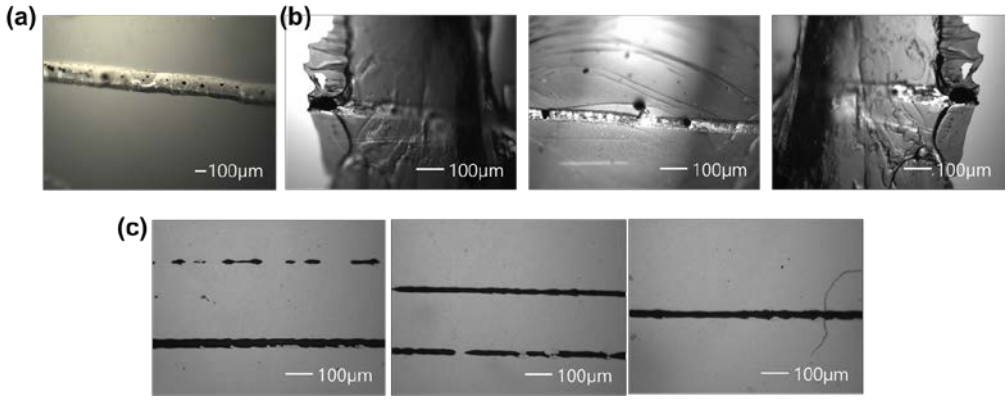

Figure 6.4. (a) PAA and EGaIn pattern before contraction (b) PAA and EGaIn pattern after contraction. Outlet channel (left, right), contracted EGaIn pattern (center) (c) EGaIn pattern after removing PAA from the substrate.

Chapter 7. Practical applications

7.1 Structure of the sensor and the method to connect EGaIn with solid electronic wire

Strain and tactile sensors are demonstrated for practical applications with transferred linear EGaIn patterns. **Figure 7.1** shows schematics of strain and tactile sensors to be fabricated. The strain sensor is comprised of a single transferred EGaIn line enclosed with Ecoflex and the tactile sensor is comprised of 8 transferred EGaIn lines, 4 horizontal and 4 vertical lines, enclosed with Ecoflex. Considering a reliable connection between EGaIn patterns and solid conductive wires, thin and flexible copper tapes on PDMS are integrated into both strain and tactile sensors. For each copper tape, one end makes direct contact with the transferred EGaIn line while the other end is soldered to a solid conductive wire. Since copper tapes are sitting on PDMS (junction region, A), far less stretchable than Ecoflex (sensing region, B), they maintain the reliable electric connection with the soldered wires.

First, copper tapes are placed in a frame and molds for the PDMS junction region (A) are positioned on top of copper tapes. Then, the PDMS pre-polymer is poured and cured in the molds. After the PDMS curing, molds for the PDMS junction region are removed and then the Ecoflex pre-polymer is poured and cured in the sensing region (B). After the Ecoflex curing, the entire substrate is flipped over to make the copper tape face up. Next, solid conductive wires are soldered at one end of copper tapes and the wire soldered substrate is placed in the freezer at –30 ˚C. A linear EGaIn pattern is placed over two separated copper tapes on the wire soldered

substrate via phase change mediated transfer. Then, the processed substrate is placed in the oven to melt the ice and evaporate the water. As the transferred frozen EGaIn line melts, it directly sticks to copper tapes. Finally, Ecoflex pre-polymer is poured over the entire processed substrate for encapsulation that provides protection for a reliable operation. The fabrication processes for the two sensors are similar except for the number of the copper tapes on PDMS (junction region) and the transferred EGaIn. As shown in **Figure 7.2**, The size of fabricated strain sensors is 2 cm × 6 cm × 0.5 cm and they consist of 4 cm long EGaIn lines with widths of 3, 5, and 10 μm. The distance between two copper tapes for strain sensors is 3.5 cm thus ~250 μm long EGaIn segments make contact with the copper tape. **Figure 7.3** shows the size of fabricated tactile sensors is 3 cm × 3 cm × 0.15 cm and they consist of 1.5 cm long EGaIn lines with widths of 20, 40, 60, and 80 μm. The distance between copper tape pairs for tactile sensors is 1.0 cm. Thus, ~250 μm long EGaIn segments make contact with the copper tape and the tactile sensing region is 1 cm × 1 cm. While strain sensors are simple 2-terminal devices, tactile sensors fabricated by orthogonally transferred 4 horizontal and 4 vertical lines exhibit 16 intersecting points as a 4 by 4 array configuration. The tactile sensors are thin enough to be directly attached to a curved and irregular surface like a 3D printed human hand model.

7.2 Strain sensor

Figure 7.4 shows the test results of three strain sensors fabricated by phase change mediated transfer of 3, 5, and 10 μm wide EGaIn lines that are 4 cm long. The distance between two copper tapes for strain sensors is 3.5 cm thus ~250 μm long EGaIn segments make contact

with the copper tape. The electrical resistance of each sensor is measured as a function of the applied strain. As the applied strain increases, the resistance monotonically increases for all three strain sensors. As expected, a higher electrical resistance is observed for the narrower EGaIn line.

7.3 Tactile sensor

To test the tactile sensor, each EGaIn pattern is connected to a reference resistor in series to adjust the output signal to ~2.5 V. A 400-gram weight is placed over one of the 16 intersecting points. The tested tactile sensor consists of 40, 20, 80, and 60 μm wide EGaIn lines for (x0, x1), (x2, x3), (y0, y1), and (y2, y3), respectively. **Figure 7.5** shows the measurement system with using Arduino due and voltage amplifier, and **Figure 7.6** shows the software GUI of the system. **Figure 7.7** shows the voltage change resulting from the normal pressure of ~20 kPa induced by the 400-gram weight placed on (x0, y0) at t=0.5 sec and on (x2, y2) at t=6 sec. When the normal pressure is applied, electrical resistances of underlying horizontal and vertical EGaIn patterns increase while voltages from reference resistors decrease. Voltage drops at (x2, y2) are greater than those at (x0, y0) and voltage drops measured from horizontal lines (x0 and x2) are greater than those from vertical lines (y0 and y2). The observed voltage differences are attributed to different widths of EGaIn lines. The signal increases as the EGaIn line becomes narrower. While the vertical EGaIn lines are placed beneath horizontal EGaIn lines, ~0.5 mm away from the tactile contact, this difference in the embedded position negligibly affects the observed signal difference.

To test tactile sensors more thoroughly, an automated setup that can apply various pressures repeatedly is constructed by using a height gauge, a motorized z-stage, and a precision scale. **Figure 7.8** shows the normalized resistance changes of the horizontal (x0) and vertical (y0) EGaIn lines at the intersecting point (x0, y0) as a function of the applied pressure. The normalized resistance changes increase monotonically as the applied pressure increases. In addition, a higher signal level is observed for the narrower horizontal line (x0) as observed in **Figure 7.7**. To test the hysteresis, the normalized resistance change of the EGaIn line is measured as the applied pressure increases or decreases between 0 and 90 kPa. **Figure 7.9** shows the hysteresis of the normalized resistance change of the horizontal line (x0) at the intersecting point (x0, y0) acquired during pressurizing (red) and depressurizing (blue) cycles. The observed hysteresis is mainly attributed to the viscoelastic nature of the Ecoflex and the flow of the liquid phase alloy into and out of the loaded portion [97]. The error in the normalized resistance change is higher in the depressurizing cycle than that in the pressurizing cycle. As shown in **Figure 7.10**, Hysteresis analyses are also performed for other horizontal and vertical lines.

Next, to investigate the long-term operation reliability of the tactile sensor, the pressurizing and depressurizing cycles are repeated up to 500 times at the motorized stage's speed of 1.5 mm/s. **Figure 7.11** shows 500 repeated cyclic operations of the tactile sensor and its zoomed-in results, respectively. The zoomed-in results show ~8 cycles where the normalized resistance change is recorded from the horizontal line (x0) at the intersecting point (x0, y0). During the 500 cycles, the tactile sensor output is repeatable without showing degradation or drift. In spite of the hysteresis, the tactile sensor is proven to be used reliably for a long term.

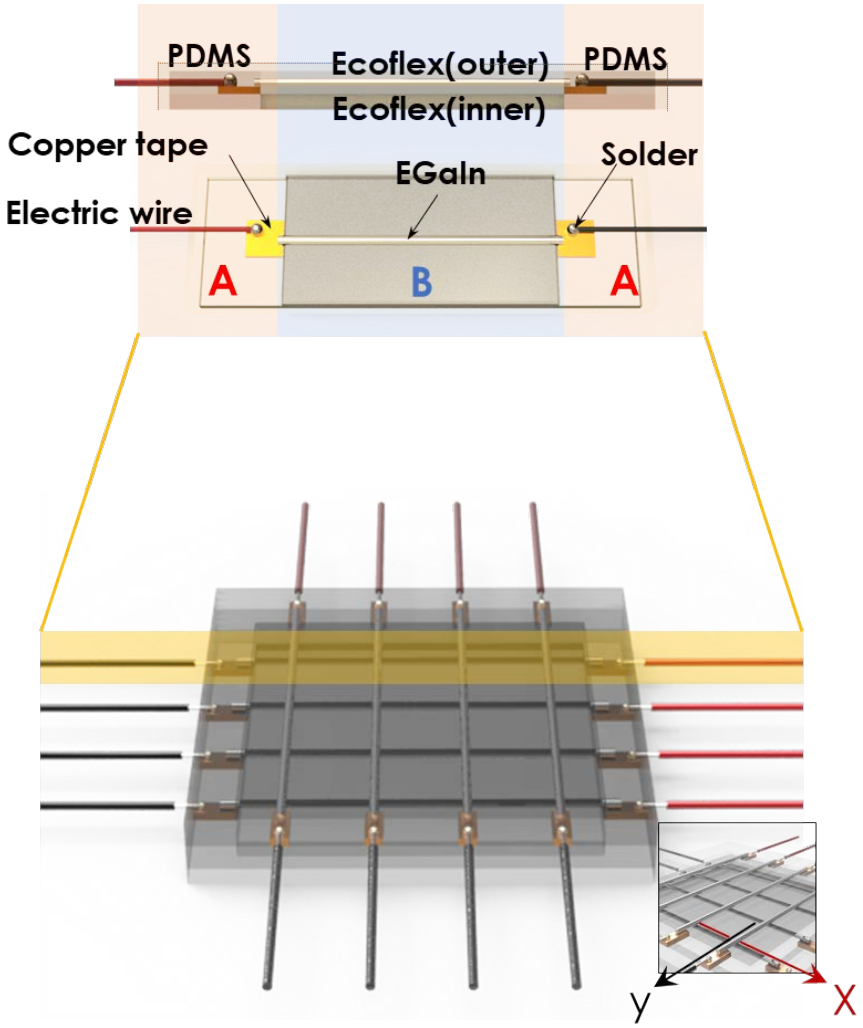

Figure 7.1. Structural schematic and pictures of the 1D stretching sensor under stretching and 2D tactile sensor exhibiting 4 horizontal and 4 vertical EGaIn lines, thus 16 intersecting points.

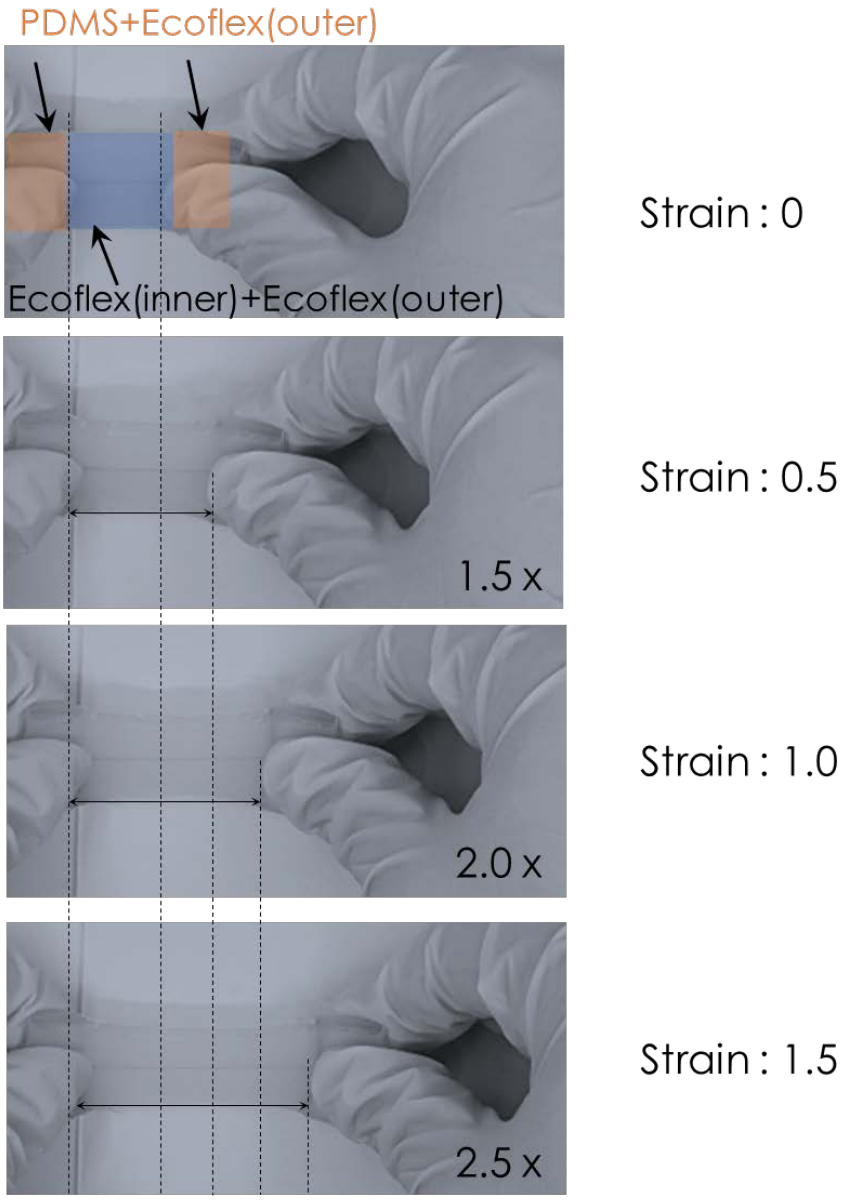

Figure 7.2. Image of the strain sensor. The strain sensor is comprised of a 4 cm long EGaIn pattern with different widths of 3, 5, and 10 μm and the overall volume is 2 cm × 6 cm × 0.5 cm.

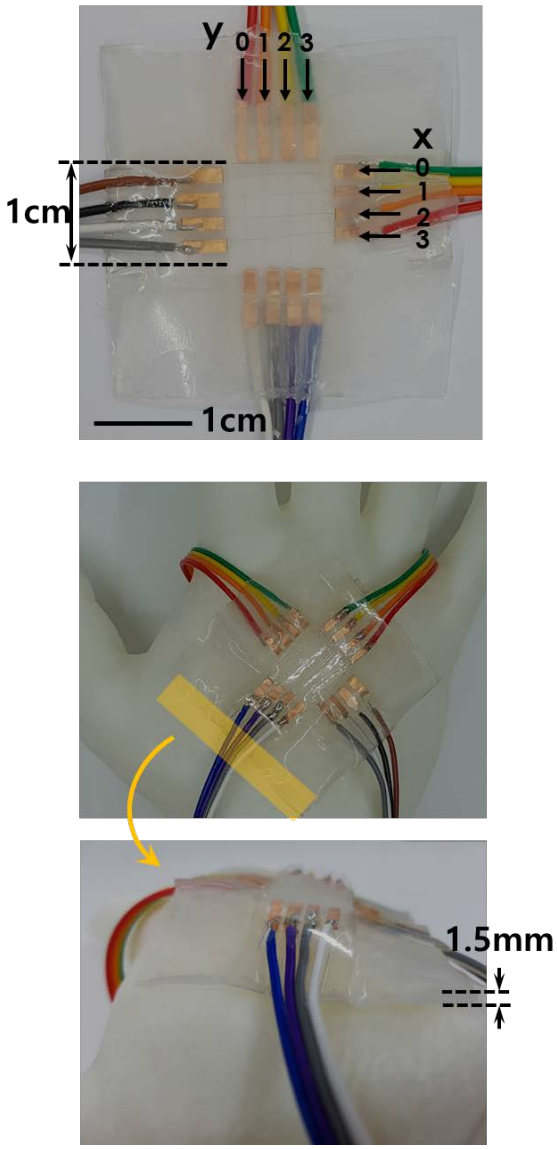

Figure 7.3. Image of the tactile sensor with 3D printed hand model. The 2D tactile sensor is comprised of 1.5 cm long EGaIn patterns with different widths of 20, 40, 60, and 80 μm and the overall volume is 3 cm × 3 cm × 0.15 cm.

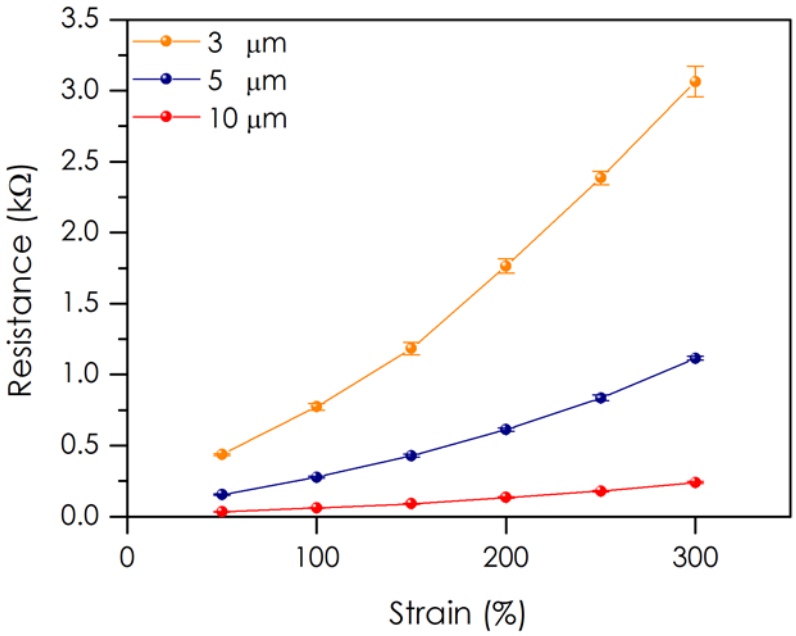

Figure 7.4. Relative resistance changes of 1D stretching sensors as a function of the applied strain.

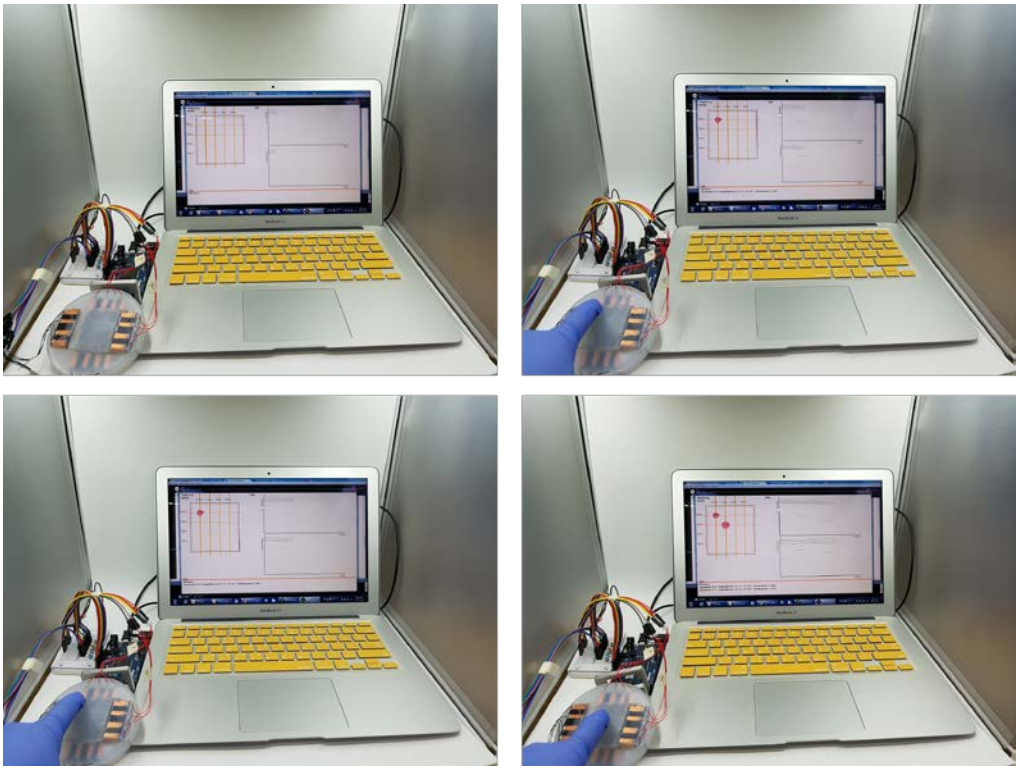

Figure 7.5. Tactile sensor with measurement hardware and software.

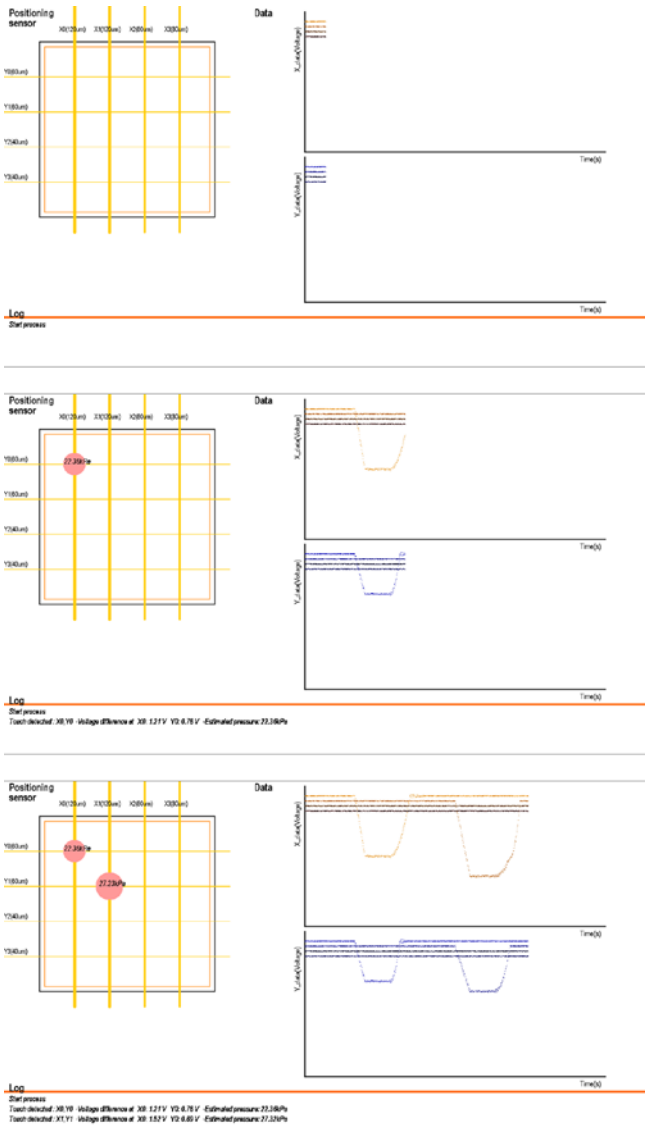

Figure 7.6. Measurement software GUI made by processing. GUI can visualize the pressurized point and can calculate the estimated pressure with the voltage data.

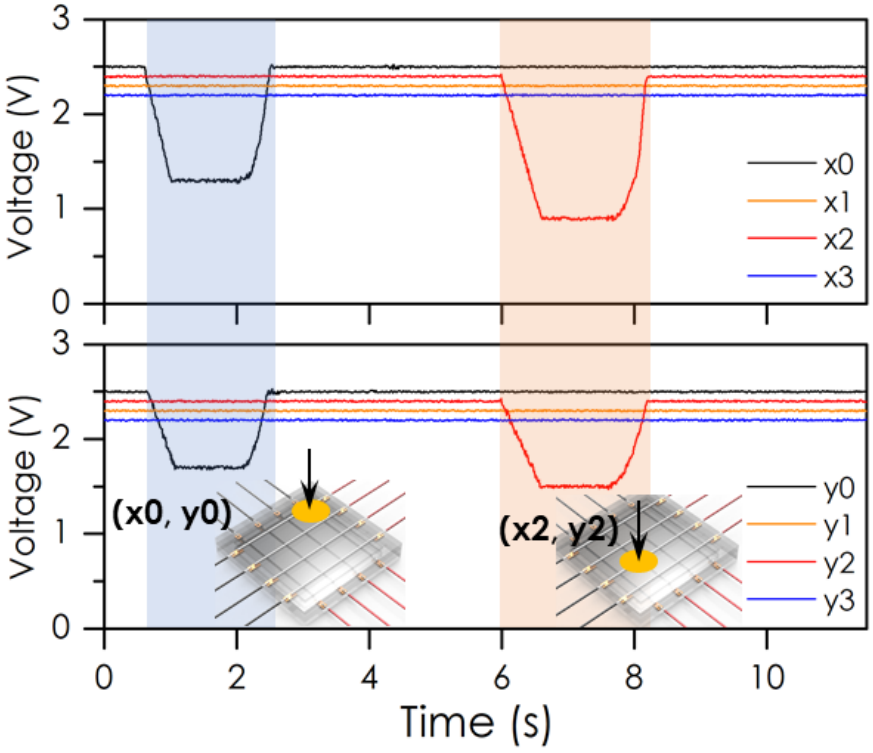

Figure 7.7. Voltage change from a half bridge circuit, two resistors with identical values in series where one is the transferred EGaIn pattern and the other is an off-chip carbon film resistor, induced by the applied pressure by a 400-gram weight (20 kPa) at two intersecting points.

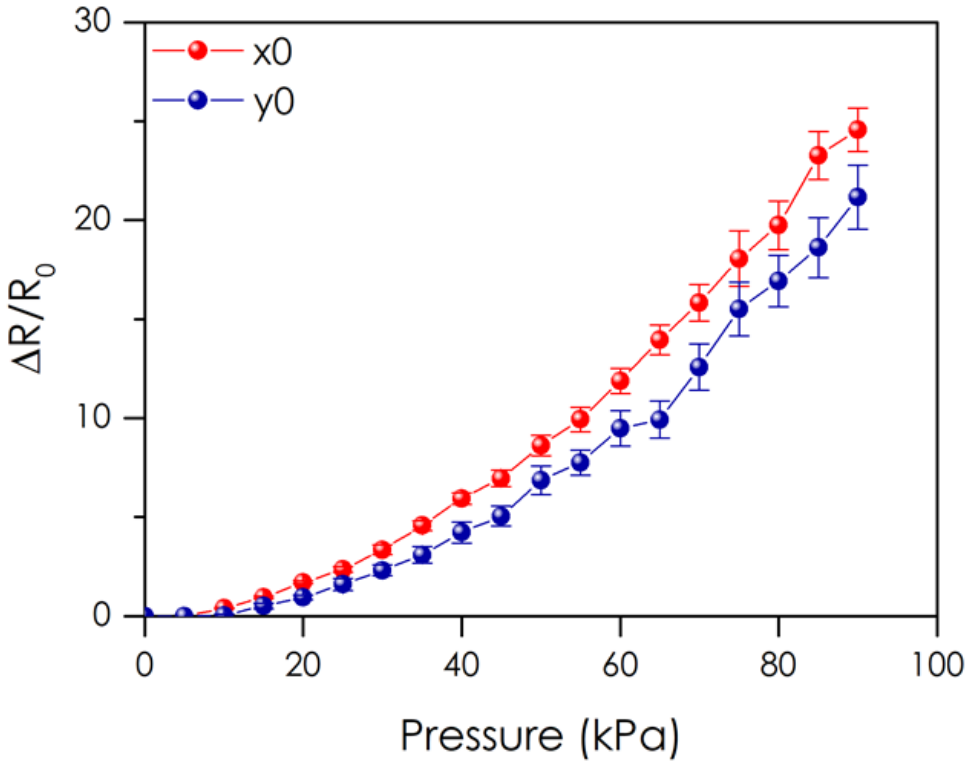

Figure 7.8. The normalized resistance changes of the horizontal and vertical EGaIn lines at the intersecting point (x0, y0) as a function of the applied pressure.

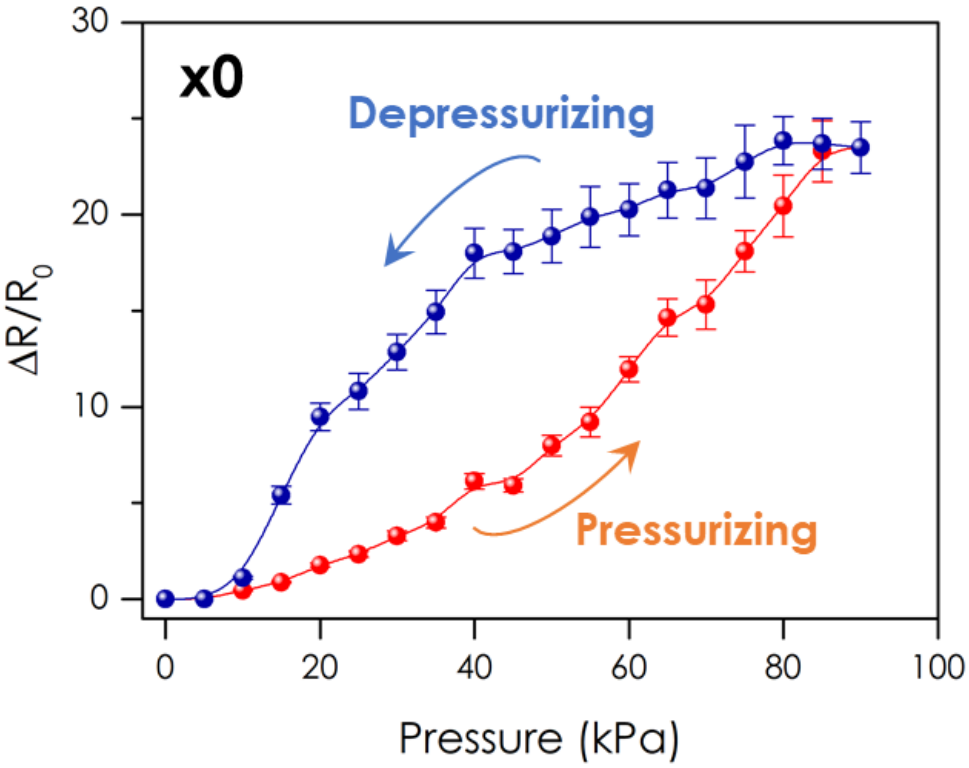

Figure 7.9. Hysteresis of the normalized resistance change of the horizontal line (x0) at the intersecting point (x0, y0) recorded during pressurizing (red) and depressurizing (blue) cycles.

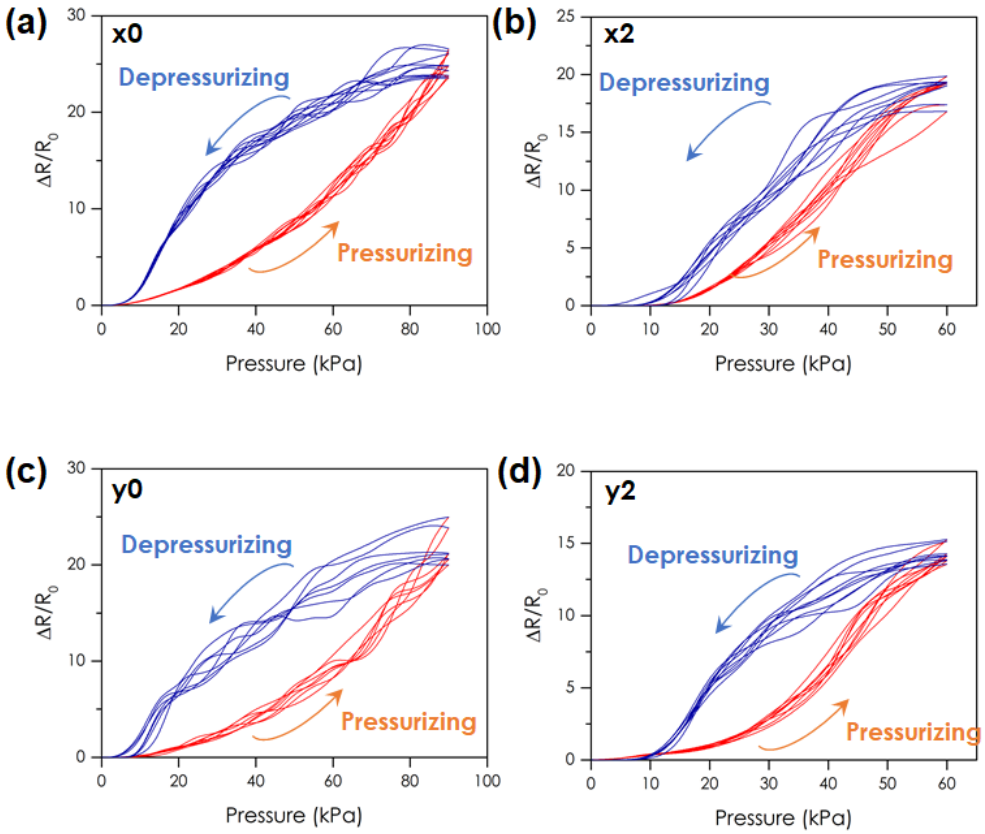

Figure 7.10. The experimental results of the resistance changes at each intersecting position. 8 repeated pressurizing and depressurizing cycles (0 to 90 kPa for x0 and y0 and 0 to 60 kPa for x2 and y2 considering relatively small widths of x2 and y2 to prevent device failures). Each graph shows a hysteresis between pressurizing and depressurizing cycles.

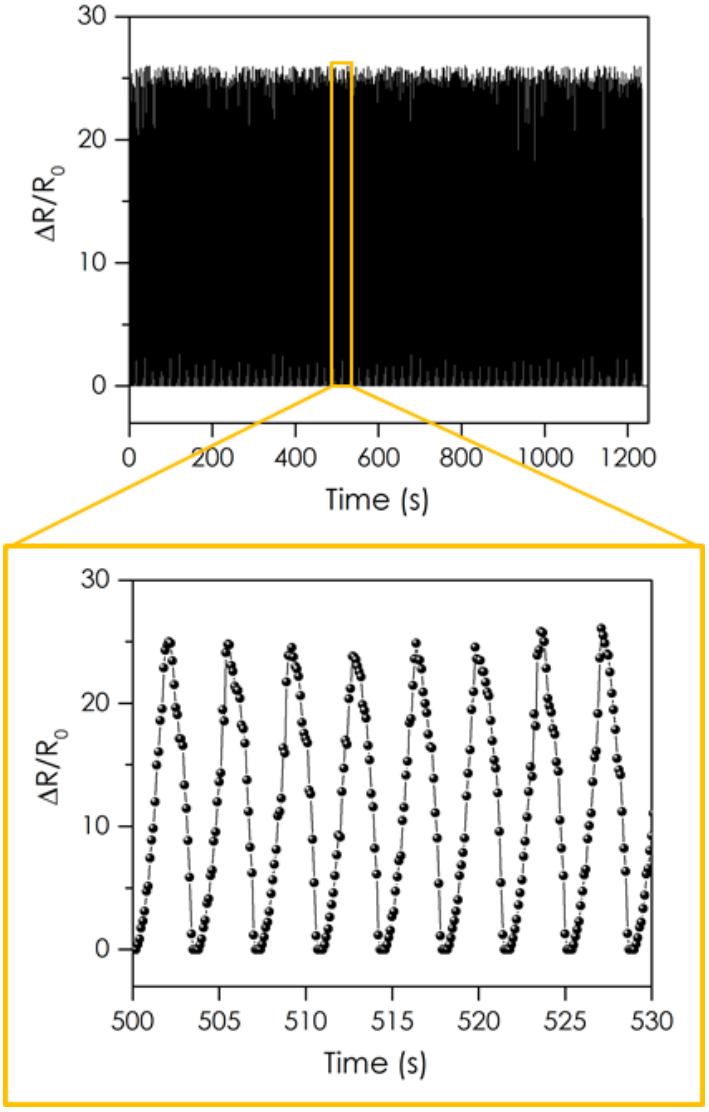

Figure 7.11. 500 repeated cyclic operations of the 2D tactile sensor and its zoomed-in results showing ~8 cycles. Data are recorded from the horizontal line (x0) at the intersecting point (x0, y0).

Chapter 8. Discussion & Experimental section

8.1 Conclusion

In this paper, a novel patterning method for liquid metal eutectic gallium indium (EGaIn) that enables reduced the size of pattern on a flat silicone elastomer is proposed and demonstrated for the first time. We prepare the linear EGaIn pattern directly printed on an Ecoflex substrate with the customized direct printing system. Next, we reduced the pattern width with two patterning methods.

In phase change mediated transfer, EGaIn patterns and the stretchable substrate are uniaxially stretched and frozen with deionized water to make ice brick impregnating stretched EGaIn patterns that are picked up and placed on a new unstretched Ecoflex. Upon heating the ice brick with the stretched EGaIn embedded, the surrounding ice melts and eventually evaporates to leave the stretched EGaIn on the unstretched Ecoflex substrate. By cascading the aforementioned stretched EGaIn transfer with the aid of liquid-solid phase change, EGaIn patterns with their initial widths of ~120 μm can be narrowed down to ~2 μm, i.e., about sixty-fold improvement in the patterning resolution is achieved. With a strain of 0.5, the stretched EGaIn transfer can be cascaded 15 times. To the best of our knowledge, the ~2 μm resolution is the record high of the EGaIn patterning on a plain substrate without exhibiting replicated groove or channel

structures that help fine patterning of EGaIn by injection or molding. The demonstrated patterning method is successfully employed for strain and tactile sensors. Once more sophisticated stretching and pick-n-place equipment along with *in-situ* process monitoring are prepared, the minimum EGaIn width can be further improved below the sub micrometer regime. In addition, the uniaxially stretched transfer may be extended to the biaxially stretched transfer realizing large scale 2D EGaIn patterns with their resolution improved. With the aid of the improved direct printing system by incorporating the distance feedback, more complicated structures can be printed. However, the size reduction by transfer after mechanical stretching mainly works for 1D structures since longitudinal elongation accompanies transverse contraction. The transverse contraction increases the dimension of the printed EGaIn orthogonal to the longitudinal direction. For 2D planar structures, we can propose two-dimensional deformation (biaxial compression or tension) to reduce or enlarge them. Upon reduction or extension of planar structures, their thicknesses also vary, and this would be useful to realize various patterns. By effectively combining 1D and 2D substrate deformation and transfer via freezing with ice, more complex EGaIn structures can be demonstrated.

In contraction method, printed EGaIn patterns are covered by hydrogel to contract. Upon gentle heating inside the oven, water evaporates from the hydrogel and hydrogel contract. With hydrogel contraction, EGaIn pattern also contracts because it trapped inside the hydrogel. By removing the hydrogel from the substrate, EGaIn patterns with their initial widths of ~120 μm can be narrowed down to the minimum

~25 μm. Although, yet this contraction method can only produce large-scale patterns than cascaded phase changes mediated transfer, it can easily reduce the pattern width and less time-consuming. In addition, this method has a possibility to reduce the complex structure. If more research on this contraction method progress, it may open the new chapter of a nanoscale liquid metal pattern.

With width reduced EGaIn lines, the overall size of strain sensors can be miniaturized, and materials and fabrication costs can be saved. In addition, optical transparency can be significantly improved when EGaIn lines on a transparent elastomeric substrate get further narrowed down by more sophisticated stretching and pick-n-place equipment along with in-situ process monitoring. Overall, our results open up a new avenue for wearable and stretchable electronics based on EGaIn.

8.2 Discussion with other similar works

To the best of our knowledge, the ~2 μm resolution equalizes the record high of the EGaIn patterning on a plain substrate done by imprinting [28]. However, imprinting always requires soft-lithographically prepared molds. As we expect, making PDMS molds takes appreciably amount of time in cleanroom and laboratory. In addition, removal of the mold after imprinting possibly induces defects by taking away some amount of EGaIn residue with the mold and distorting underlying EGaIn patterns.

Presumably due to such defects, the length of EGaIn patterns employed in a practical application (strain sensor) seems to be limited. Length-to-width ratio of the strain sensor made by imprinting EGaIn in Majidi group was 75~150. In contrast, our proposed process does not rely on molds (i.e. moldless process) so that the overall processing time may not be extremely time-consuming if the total number of transfer cycles is decreased by using a higher strain rate upon stretching. Since our process is moldless, arbitrary pattern widths can be realized without investing extra time to make molds with different widths. Most importantly, our cascaded stretch transfer can offer long and narrow EGaIn patterns with their length-to-width ratios of 5,000~7,500, at least one order of magnitude improvement over the previous report. Besides decreasing the total number of transfer cycles, the overall processing time of our method can be further improved by adopting liquid nitrogen upon freezing and heating in vacuum oven upon dethawing to sublimate ice.

The freeze casting also reported previously [98] is hard to apply small patterns down to a few micrometers since it is difficult to uniformly fill within a few micrometers wide and a few centimeter-long molds and it is also hard to handle (take out, pick up, or more) the frozen EGaIn structure that is long and narrow even though the mold is somehow completely filled. In contrast, our freeze casting with ice works well for narrow patterns down to ~2 μm and long patterns up to 1~4 cm and offers easy handling because the relative large ice impregnating narrow and long EGaIn patterns can be easily picked up.

8.3 Experimental section

Materials: Eutectic gallium indium (EGaIn, 99 %) was purchased from Sigma Aldrich. Hydrochloric acids (HCl, 0.5 mol) was purchased from DAEJUNG. Polydimethylsiloxane (PDMS, Sylgard 184 silicone elastomer) was purchased from Dow Corning. Ecoflex (Platinum catalyzed silicone elastomer, 0030) was purchased from Smooth-on. All materials were used as received without any treatment and purification.

Preparation of substrates: (i) PDMS - The base and the curing agent were mixed uniformly at the weight ratio of 10:1, degassed, poured in a petri dish and cured in a convection oven at 60 ˚C for two hours. (ii) Ecoflex for phase change mediated transfer - The base, the curing agent, and a white dye were mixed uniformly at the weight ratio of 1:1:0.01, degassed, poured in a petri dish and cured at room temperature for four hours or cured in a convection oven at 40 ˚C for two hours. (iii) Ecoflex for making strain and tactile sensors - The base and the curing agent were mixed uniformly at the weight ratio of 1:1, degassed, poured in a petri dish and cured at room temperature for four hours. All prepared elastomeric substrates are ~1 mm thick and cut to proper sizes, 75 mm × 25 mm, 100 mm × 100 mm, and 50 mm × 150 mm for contact angle measurements, direct printing, and phase change mediated transfer, respectively.

Direct printing system setup: A motorized XY stage (travel range of 100 mm, Max. velocity of 30 mm/s, resolution of 2 μm, and Max. load of 10 kg) was custom-ordered

from JAEWON. A motorized Z stage (travel range of 100 mm, Max. velocity of 5 mm/s, resolution of 0.125 μm, and Max. load of 7 kg) was purchased from Standa. The dispenser and dispensing needles (25~34G) were purchased from Banseok Jungmil and Dental store, respectively. A laser sensor (optoNCDT 1420) was purchased from Micro-Epsilon. Two pressure regulators (ITV0010-0BL) were purchased from SMC.

Paraffin coating: Paraffin wax purchased from Sigma Aldrich was melted in a 70 ˚C oven and the dispensing stainless steel needle filled with EGaIn was immersed in the molten paraffin wax for 2~3 seconds and was taken out. By removing the EGaIn in the needle, only exterior of the needle was coated with paraffin wax.

Phase change mediated transfer: The strain supporter made with aluminum and directly configured with a linear motorized stage is used to stretch Ecoflex substrates with a linear velocity ranging from 0.1 to 3.0 mm/s up to the maximum strain of 3.0. Structural guide walls to confine the DI water during the phase change mediated transfer are made with PMMA. The volume within the guide walls is 75 mm × 75 mm × 10 mm (56.25 ml).

Repeated cyclic tests for tactile sensors: A height gauge attached to a motorized z-stage enables repeated and automated application of normal pressures onto the tactile sensor mounted on a precision electronic scale. For calibration, mass measured by the precision electronic scale is converted into pressure by multiplying the gravitational acceleration and then dividing the resultant with the cross-sectional area of the height gauge. Resistance changes of horizontal and vertical EGaIn lines at the contact point

are measured by using a microcontroller (Arduino - due).

Bibliography

[1] Kang, M.-G., Kim, M.-S., Kim, J. & Guo, L. J. Organic Solar Cells Using Nanoimprinted Transparent Metal Electrodes. *Adv. Mater.* **20,** 4408–4413 (2008).

[2] Hyun, D. C. *et al.* Ordered Zigzag Stripes of Polymer Gel/Metal Nanoparticle Composites for Highly Stretchable Conductive Electrodes. *Adv. Mater.* **23,** 2946–2950 (2011).

[3] Zeng, X.-Y., Zhang, Q.-K., Yu, R.-M. & Lu, C.-Z. A New Transparent Conductor: Silver Nanowire Film Buried at the Surface of a Transparent Polymer. *Adv. Mater.* **22,** 4484–4488 (2010).

[4] Rathmell, A. R., Bergin, S. M., Hua, Y., Li, Z. & Wiley, B. J. The growth mechanism of copper nanowires and their properties in flexible, transparent conducting films. *Adv. Mater.* **22,** 3558–3563 (2010).

[5] Yu, Z., Li, L., Zhang, Q., Hu, W. & Pei, Q. Silver Nanowire-Polymer Composite Electrodes for Efficient Polymer Solar Cells. *Adv. Mater.* **23,** 4453–4457 (2011).

[6] Wang, X., Hu, H., Shen, Y., Zhou, X. & Zheng, Z. Stretchable conductors with ultrahigh tensile strain and stable metallic conductance enabled by prestrained polyelectrolyte nanoplatforms. *Adv. Mater.* **23,** 3090–3094 (2011).

[7] Rathmell, A. R. & Wiley, B. J. The synthesis and coating of long, thin copper nanowires to make flexible, transparent conducting films on plastic substrates. *Adv. Mater.* **23,** 4798–4803 (2011).

[8] Lee, P. *et al.* Highly stretchable and highly conductive metal electrode by very long metal nanowire percolation network. *Adv. Mater.* **24,** 3326–3332 (2012).

[9] Xu, F. & Zhu, Y. Highly conductive and stretchable silver nanowire conductors. *Adv. Mater.* **24,** 5117–5122 (2012).

[10] Amjadi, M., Pichitpajongkit, A., Lee, S., Ryu, S. & Park, I. Highly stretchable and sensitive strain sensor based on silver nanowire–elastomer nanocomposite. *ACS Nano* **8,** 5154–5163 (2014).

[11] Lu, N., Lu, C., Yang, S. & Rogers, J. Highly sensitive skin-mountable strain gauges based entirely on elastomers. *Adv. Funct. Mater.* **22,** 4044–4050 (2012).

[12] Muth, J. T. *et al.* Embedded 3D printing of strain sensors within highly stretchable elastomers. *Adv. Mater.* **26,** 6307–6312 (2014).

[13] Yamada, T. *et al.* A stretchable carbon nanotube strain sensor for human-motion detection. *Nat. Nanotechnol.* **6,** 296 (2011).

[14] Cohen, D. J., Mitra, D., Peterson, K. & Maharbiz, M. M. A highly elastic, capacitive strain gauge based on percolating nanotube networks. *Nano Lett.* **12,** 1821–1825 (2012).

[15] Yu, Z., Niu, X., Liu, Z. & Pei, Q. Intrinsically Stretchable Polymer Light-Emitting Devices Using Carbon Nanotube-Polymer Composite Electrodes. *Adv. Mater.* **23,** 3989–3994 (2011).

[16] Eda, G., Fanchini, G. & Chhowalla, M. Large-area ultrathin films of reduced graphene oxide as a transparent and flexible electronic material. *Nat. Nanotechnol.* **3,** 270 (2008).

[17] Kim, K. S. *et al.* Large-scale pattern growth of graphene films for stretchable transparent electrodes. *Nature* **457,** 706 (2009).

[18] Boland, C. S. *et al.* Sensitive, high-strain, high-rate bodily motion sensors based on graphene–rubber composites. *ACS Nano* **8,** 8819–8830 (2014).

[19] Mates, J. E., Bayer, I. S., Palumbo, J. M., Carroll, P. J. & Megaridis, C. M. Extremely stretchable and conductive water-repellent coatings for low-cost ultra-flexible electronics. *Nat. Commun.* **6,** 8874 (2015).

[20] Sun, Y., Choi, W. M., Jiang, H., Huang, Y. Y. & Rogers, J. A. Controlled buckling of semiconductor nanoribbons for stretchable electronics. *Nat. Nanotechnol.* **1,** 201 (2006).

[21] Khang, D.-Y., Jiang, H., Huang, Y. & Rogers, J. A. A stretchable form of single-crystal silicon for high-performance electronics on rubber substrates. *Science.* **311,** 208–212 (2006).

[22] Qi, Y. *et al.* Enhanced piezoelectricity and stretchability in energy harvesting devices fabricated from buckled PZT ribbons. *Nano Lett.* **11,** 1331–1336 (2011).

[23] Kim, D.-H. *et al.* Epidermal electronics. *Science.* **333,** 838–843 (2011).

[24] Xu, S. *et al.* Stretchable batteries with self-similar serpentine interconnects and integrated wireless recharging systems. *Nat. Commun.* **4,** 1543 (2013).

[25] Kramer, R. K., Majidi, C. & Wood, R. J. Masked Deposition of Gallium-Indium Alloys for Liquid-Embedded Elastomer Conductors. *Adv. Funct. Mater.* **23,** 5292–5296 (2013).

[26] Boley, J. W., White, E. L., Chiu, G. T. & Kramer, R. K. Direct writing of gallium-indium alloy for stretchable electronics. *Adv. Funct. Mater.* **24,** 3501–3507 (2014).

[27] Lu, T., Finkenauer, L., Wissman, J. & Majidi, C. Rapid Prototyping for Soft-Matter Electronics. *Adv. Funct. Mater.* **24,** 3351–3356 (2014).

[28] Gozen, B. A., Tabatabai, A., Ozdoganlar, O. B. & Majidi, C. High-Density Soft-Matter Electronics with Micron-Scale Line Width. *Adv. Mater.* **26,** 5211–5216 (2014).

[29] Jin, S. W. *et al.* Stretchable loudspeaker using liquid metal microchannel. *Sci. Rep.* **5,** 11695 (2015).

[30] Hirsch, A., Michaud, H. O., Gerratt, A. P., De Mulatier, S. & Lacour, S. P. Intrinsically stretchable biphasic (solid–liquid) thin metal films. *Adv. Mater.* **28,** 4507–4512 (2016).

[31] Bartlett, M. D. *et al.* Stretchable, High-k Dielectric Elastomers through Liquid-Metal Inclusions. *Adv. Mater.* **28,** 3726–3731 (2016).

[32] Mohammed, M. G. & Kramer, R. All-Printed Flexible and Stretchable Electronics. *Adv. Mater.* **29,** (2017).

[33] Dickey, M. D. Stretchable and soft electronics using liquid metals. *Adv. Mater.* **29,** (2017).

[34] Joshipura, I. D., Ayers, H. R., Majidi, C. & Dickey, M. D. Methods to pattern liquid metals. *J. Mater. Chem. C* **3,** 3834–3841 (2015).

[35] Kim, M., Alrowais, H., Pavlidis, S. & Brand, O. Size-Scalable and High-Density Liquid-Metal-Based Soft Electronic Passive Components and Circuits Using Soft Lithography. *Adv. Funct. Mater.* **27,** (2017).

[36] So, J.-H. & Dickey, M. D. Inherently aligned microfluidic electrodes composed of liquid metal. *Lab Chip* **11,** 905–911 (2011).

[37] Tabatabai, A., Fassler, A., Usiak, C. & Majidi, C. Liquid-phase gallium–indium alloy electronics with microcontact printing. *Langmuir* **29,** 6194–6200 (2013).

[38] Cavallini, M., Gentili, D., Greco, P., Valle, F. & Biscarini, F. Micro-and nanopatterning by lithographically controlled wetting. *Nat. Protoc.* **7,** 1668 (2012).

[39] Cavallini, M., Albonetti, C. & Biscarini, F. Nanopatterning soluble multifunctional materials by unconventional wet lithography. *Adv. Mater.* **21,** 1043–1053 (2009).

[40] Eryilmaz, I. H., Mohanraj, J., Dal Zilio, S. & Fraleoni-Morgera, A. Controlled self-organization of polymer nanopatterns over large areas. *Sci. Rep.* **7,** 10526 (2017).

[41] Lin, Y. *et al.* Drawing liquid metal wires at room temperature. *Extrem. Mech. Lett.* **7,** 55–63 (2016).

[42] Khoshmanesh, K. *et al.* Liquid metal enabled microfluidics. *Lab Chip* **17,** 974–993 (2017).

[43] Zrnic, D. & Swatik, D. S. On the resistivity and surface tension of the eutectic alloy of gallium and indium. *J. less common Met.* **18,** 67–68 (1969).

[44] Koster, J. N. Directional solidification and melting of eutectic GaIn. *Cryst. Res. Technol. J. Exp. Ind. Crystallogr.* **34,** 1129–1140 (1999).

[45] Regan, M. J. *et al.* Surface layering in liquid gallium: An X-ray reflectivity study. *Phys. Rev. Lett.* **75,** 2498 (1995).

[46] Lacour, S. P., Tsay, C. & Wagner, S. An elastically stretchable TFT circuit. *IEEE Electron Device Lett.* **25,** 792–794 (2004).

[47] Lacour, S. P., Wagner, S., Huang, Z. & Suo, Z. Stretchable gold conductors on elastomeric substrates. *Appl. Phys. Lett.* **82,** 2404–2406 (2003).

[48] Lacour, S. P., Jones, J., Wagner, S., Li, T. & Suo, Z. Stretchable interconnects for elastic electronic surfaces. *Proc. IEEE* **93,** 1459–1467 (2005).

[49] Minev, I. R. *et al.* Electronic dura mater for long-term multimodal neural interfaces. *Science.* **347,** 159–163 (2015).

[50] Xu, S. *et al.* Assembly of micro/nanomaterials into complex, three-dimensional architectures by compressive buckling. *Science.* **347,** 154–159 (2015).

[51] Sekitani, T. *et al.* A rubberlike stretchable active matrix using elastic conductors. *Science.* **321,** 1468–1472 (2008).

[52] Rosset, S., Niklaus, M., Dubois, P. & Shea, H. R. Metal ion implantation for the fabrication of stretchable electrodes on elastomers. *Adv. Funct. Mater.* **19,** 470–478 (2009).

[53] Sekitani, T. *et al.* Stretchable active-matrix organic light-emitting diode display using printable elastic conductors. *Nat. Mater.* **8,** 494 (2009).

[54] Park, M. *et al*. Highly stretchable electric circuits from a composite material of silver nanoparticles and elastomeric fibres. *Nat. Nanotechnol.* **7,** 803 (2012).

[55] Zhang, Y. *et al.* Polymer-embedded carbon nanotube ribbons for stretchable conductors. *Adv. Mater.* **22,** 3027–3031 (2010).

[56] Liu, K. *et al.* Cross-Stacked Superaligned Carbon Nanotube Films for Transparent and Stretchable Conductors. *Adv. Funct. Mater.* **21,** 2721–2728 (2011).

[57] Stoyanov, H., Kollosche, M., Risse, S., Waché, R. & Kofod, G. Soft conductive elastomer materials for stretchable electronics and voltage controlled artificial muscles. *Adv. Mater.* **25,** 578–583 (2013).

[58] Kim, Y. *et al.* Stretchable nanoparticle conductors with self-organized conductive pathways. *Nature* **500,** 59 (2013).

[59] Jinno, H. *et al.* Printable elastic conductors with a high conductivity for electronic textile applications. *Nat. Commun.* **6,** 7461 (2015).

[60] Morley, N. B., Burris, J., Cadwallader, L. C. & Nornberg, M. D. GaInSn usage in the research laboratory. *Rev. Sci. Instrum.* **79,** 56107 (2008).

[61] Duggin, M. J. The thermal conductivity of liquid gallium. *Phys. Lett. A* **29,** 470–471 (1969).

[62] Hayes, G. J., So, J.-H., Qusba, A., Dickey, M. D. & Lazzi, G. Flexible liquid metal alloy (EGaIn) microstrip patch antenna. *IEEE Trans. Antennas Propag.* **60,** 2151–2156 (2012).

[63] Hu, H., Shaikh, K. & Liu, C. Super flexible sensor skin using liquid metal as interconnect. in *Sensors, 2007 IEEE* 815–817 (IEEE, 2007).

[64] Kramer, R. K., Majidi, C. & Wood, R. J. Wearable tactile keypad with stretchable artificial skin. in *Robotics and Automation (ICRA), 2011 IEEE International Conference on* 1103–1107 (IEEE, 2011).

[65] Kubo, M. *et al.* Stretchable microfluidic radiofrequency antennas. *Adv. Mater.* **22,** 2749–2752 (2010).

[66] Park, Y.-L., Majidi, C., Kramer, R., Bérard, P. & Wood, R. J. Hyperelastic pressure sensing with a liquid-embedded elastomer. *J. Micromechanics Microengineering* **20,** 125029 (2010).

[67] Pekas, N., Zhang, Q. & Juncker, D. Electrostatic actuator with liquid metal–elastomer compliant electrodes used for on-chip microvalving. *J. Micromechanics Microengineering* **22,** 97001 (2012).

[68] Rashed Khan, M., Hayes, G. J., So, J.-H., Lazzi, G. & Dickey, M. D. A frequency shifting liquid metal antenna with pressure responsiveness. *Appl. Phys. Lett.* **99,** 13501 (2011).

[69] Roberts, P., Damian, D. D., Shan, W., Lu, T. & Majidi, C. Soft-matter capacitive sensor for measuring shear and pressure deformation. in *Robotics and Automation (ICRA), 2013 IEEE International Conference on* 3529–3534 (IEEE, 2013).

[70] So, J. *et al.* Reversibly deformable and mechanically tunable fluidic antennas. *Adv. Funct. Mater.* **19,** 3632–3637 (2009).

[71] Traille, A. *et al.* A wireless passive RCS-based temperature sensor using liquid metal and microfluidics technologies. in *Microwave Conference (EuMC), 2011 41st European* 45–48 (IEEE, 2011).

[72] Wang, X. & Liu, J. Recent advancements in liquid metal flexible printed electronics: Properties, technologies, and applications. *Micromachines* **7,** 206 (2016).

[73] Kramer, R. K., Majidi, C., Sahai, R. & Wood, R. J. Soft curvature sensors for joint angle proprioception. in *Intelligent Robots and Systems (IROS), 2011 IEEE/RSJ International Conference on* 1919–1926 (IEEE, 2011).

[74] Majidi, C., Kramer, R. & Wood, R. J. A non-differential elastomer curvature sensor for softer-than-skin electronics. *Smart Mater. Struct.* **20,** 105017 (2011).

[75] Mengüç, Y. *et al.* Soft wearable motion sensing suit for lower limb biomechanics measurements. in *Robotics and Automation (ICRA), 2013 IEEE International Conference on* 5309–5316 (IEEE, 2013).

[76] Mengüç, Y. *et al.* Wearable soft sensing suit for human gait measurement. *Int. J. Rob. Res.* **33,** 1748–1764 (2014).

[77] Pineda, F., Bottausci, F., Icard, B., Malaquin, L. & Fouillet, Y. Using electrofluidic devices as hyper-elastic strain sensors: Experimental and theoretical analysis. *Microelectron. Eng.* **144,** 27–31 (2015).

[78] Strukov, D. B., Snider, G. S., Stewart, D. R. & Williams, R. S. The missing memristor found. *Nature* **453,** 80 (2008).

[79] Koo, H., So, J., Dickey, M. D. & Velev, O. D. Towards All-Soft Matter Circuits: Prototypes of Quasi-Liquid Devices with Memristor Characteristics. *Adv. Mater.* **23,** 3559–3564 (2011).

[80] So, J., Koo, H., Dickey, M. D. & Velev, O. D. Ionic Current Rectification in Soft-Matter Diodes with Liquid-Metal Electrodes. *Adv. Funct. Mater.* **22,** 625–631 (2012).

[81] Liu, S., Sun, X., Hildreth, O. J. & Rykaczewski, K. Design and characterization of a single channel two-liquid capacitor and its application to hyperelastic strain sensing. *Lab Chip* **15,** 1376–1384 (2015).

[82] Fuard, D., Tzvetkova-Chevolleau, T., Decossas, S., Tracqui, P. & Schiavone, P. Optimization of poly-di-methyl-siloxane (PDMS) substrates for studying cellular adhesion and motility. *Microelectron. Eng.* **85,** 1289–1293 (2008).

[83] Johnston, I. D., McCluskey, D. K., Tan, C. K. L. & Tracey, M. C. Mechanical characterization of bulk Sylgard 184 for microfluidics and microengineering. *J. Micromechanics Microengineering* **24,** 35017 (2014).

[84] Shi, X. *et al.* Mechanics design for stretchable, high areal coverage GaAs solar module on an ultrathin substrate. *J. Appl. Mech.* **81,** 124502 (2014).

[85] Decker, E. L., Frank, B., Suo, Y. & Garoff, S. Physics of contact angle measurement. *Colloids Surfaces A Physicochem. Eng. Asp.* **156,** 177–189 (1999).

[86] Lamour, G. *et al.* Contact angle measurements using a simplified experimental setup. *J. Chem. Educ.* **87,** 1403–1407 (2010).

[87] Chau, T. T., Bruckard, W. J., Koh, P. T. L. & Nguyen, A. V. A review of factors that affect contact angle and implications for flotation practice. *Adv. Colloid Interface Sci.* **150,** 106–115 (2009).

[88] Dickey, M. D. *et al.* Eutectic gallium-indium (EGaIn): a liquid metal alloy for the formation of stable structures in microchannels at room temperature. *Adv. Funct. Mater.* **18,** 1097–1104 (2008).

[89] Xiu, Y., Zhu, L., Hess, D. W. & Wong, C. P. Relationship between work of adhesion and contact angle hysteresis on superhydrophobic surfaces. *J. Phys. Chem. C* **112,** 11403–11407 (2008).

[90] Ladd, C., So, J., Muth, J. & Dickey, M. D. 3D printing of free standing liquid metal microstructures. *Adv. Mater.* **25,** 5081–5085 (2013).

[91] Gannarapu, A. & Gozen, B. A. Freeze-Printing of Liquid Metal Alloys for Manufacturing of 3D, Conductive, and Flexible Networks. *Adv. Mater. Technol.* **1,** (2016).

[92] Xu, Q., Oudalov, N., Guo, Q., Jaeger, H. M. & Brown, E. Effect of oxidation on the mechanical properties of liquid gallium and eutectic gallium-indium. *Phys. Fluids* **24,** 63101 (2012).

[93] Kamusewitz, H., Possart, W. & Paul, D. The relation between Young's equilibrium contact angle and the hysteresis on rough paraffin wax surfaces. *Colloids Surfaces A Physicochem. Eng. Asp.* **156,** 271–279 (1999).

[94] Khan, M. R., Trlica, C., So, J.-H., Valeri, M. & Dickey, M. D. Influence of water on the interfacial behavior of gallium liquid metal alloys. *ACS Appl. Mater. Interfaces* **6,** 22467–22473 (2014).

[95] Horasawa, N., Nakajima, H., Takahashi, S. & Okabe, T. Behavior of pure gallium in water and various saline solutions. *Dent. Mater. J.* **16,** 200–208 (1997).

[96] Carle, F., Bai, K., Casara, J., Vanderlick, K. & Brown, E. Development of magnetic liquid metal suspensions for magnetohydrodynamics. *Phys. Rev. Fluids* **2,** 13301 (2017).

[97] Park, Y.-L., Tepayotl-Ramirez, D., Wood, R. J. & Majidi, C. Influence of cross-sectional geometry on the sensitivity and hysteresis of liquid-phase electronic pressure sensors. *Appl. Phys. Lett.* **101,** 191904 (2012).

[98] Fassler, A. & Majidi, C. 3D structures of liquid-phase GaIn alloy embedded in PDMS with freeze casting. *Lab Chip* **13,** 4442–4450 (2013).

요약(국문초록)

최근 입을 수 있는 전자기기 (이하 웨어러블 디바이스)의 출현으로 인하여, 유연하고 접을 수 있으며 신축성을 가지는 장치에 대한 관심이 증가하고 있다. 하지만 이러한 전자기기를 구성하며 전기 전도성을 유지하는 전자회로는 대부분 고체 도선으로 이루어져 있으며, 고체라는 한계로 인하여 휘거나 늘어나는 외부 변형 조건에서 내구성이 떨어지는 단점을 가지고 있다. 이를 해결하기 위해서 도선을 구부리거나 소형으로 조각화하여 대처하는 등 다양한 방식으로 해결하려는 연구가 진행되고 있으나, 결국 고체가 가지는 본질적인 한계를 완전히 극복하지 못하고 있다. 이에 대한 대안으로, 상온에서 액체 상태로 존재하며 전기전도도가 좋고 도한 외부 변형 조건에서도 전기 전도성을 유지할 수 있는 액체 금속이 제시되었으나 수은으로 대표되듯이 독성으로 인하여 최근까지 이를 이용한 연구가 진행되지 않았다. 하지만, 최근에는 독성이 없는 갈륨을 기반으로 한 갈륨 혼합물들이 액체 금속으로 많이 개발되면서 갈륨 베이스 액체 금속들을 이용한 웨어러블 디바이스 연구가 증가하는 추세이다. 그 중 최근 가장 주목받고 있는 EGaIn(Eutectic Gallium Indium)은 갈륨과 인듐을 혼합한 합근 액체 금속으로서, 반응성이 낮고 갈륨으로 생성된 얇은 산화막에 의하여 실리콘 계열의 기판들과 접착력이 좋아 이를 이용한 다양한 전자회로 프린팅 및 패

터닝 방식들이 개발 진행되고 있다. 다만, 액체 금속의 자체적인 높은 표면 장력으로 인하여 고체 몰드를 이용하지 않고는 수십 마이크로 이하로 생산이 불가능한 단점을 지니고 있다.

본 연구에서는 기존에 연구되었던 액체 금속 분사 시스템과 인장 가능한 기판 그리고 액체 금속의 상 변화를 이용하여 고체 몰드를 이용하지 않고도 수 마이크로의 폭을 가지는 액체 금속 패턴을 만드는 시스템에 대한 연구를 진행하였다. 먼저 피드벡 제어와 파라핀 코팅된 바늘을 이용하여 수십~수백 마이크로의 균일한 폭을 가지는 액체 금속을 인장 가능한 기판에 프린팅을 하였으며, 상기 프린팅 된 패턴과 기판을 단 방향으로 늘리거나 또는 패턴을 하이드로겔로 둘러싸 수분을 증발 과 동시에 수축시켜 기존의 액체 금속 보다 폭이 줄도록 하였다. 이 후 줄어든 액체 금속을 어는점 이하에서 얼린 후 물리적으로 기판에서 분리한 후 아직 변형이 일어나지 않은 새로운 기판에 옮겼으며 이러한 "늘리고 (또는 수축하고)- 얼리고 – 옮기는" 방식을 계속 반복 진행하였으며 결과적으로 수십~수백 마이크로의 폭을 가졌던 초기 액체 금속 패턴에서 2~3마이크로의 폭을 가지는 액체 금속 패턴을 얻을 수 있었다. 또한 이러한 패턴을 이용하여 소형 사이즈의 인장 및 압력 센서를 제작하여 테스트를 진행하였다. 이렇듯 본 연구에서는 새로운 방식의 상변화를 이용한 액체 금속 이송방식 및 패터닝 시스템을 개발하였으며, 이를 토대로 인장과 상변화를 이용한 패터닝 방식

에 대한 연구가 진행될 경우 서브 마이크로의 해상도를 가지는 액체 금속 패턴을 제작할 수 있을 것으로 기대되며, 이 연구에서 사용된 EGaIn 만이 아닌 다른 액체 금속에도 이 연구가 적용 및 활용 가능 할 것으로 기대된다.

주요어 : 갈륨 기반 액체 금속, 액체 금속 프린팅, 인장 가능한 기판, 상변화 이송 시스템, 인장 센서, 압력센서

학번 : 2011-20686

감사의 글

시간은 참 빠르게 지나가는 것 같습니다. 대학원을 들어온 시간이 얼마 지나지 않은 것 같은데, 7년이라는 시간이 지나서 벌써 졸업을 목전에 두고 있는 제 자신을 보고 있으니 감회가 새롭습니다. 대학원 생활을 뒤돌아 보면 정말 감사의 마음을 전해드릴 분들이 많은 것 같습니다. 이런 많은 분들께 우선 짧은 글로나마 감사의 글을 통해 감사의 마음을 전하려 합니다.

부족한 저를 지도해 주시고, 연구에 대하여 항상 아낌없는 조언을 주신 고상근 교수님께 진심으로 머리 숙여 감사드립니다. 연구 외에도 생활에 대한 조언 하나 하나가 저에게는 큰 가르침 이였습니다. 그리고 지금 이 논문이 있기에 많은 도움을 주신 이정철 교수님께도 감사의 말씀을 전하고 싶습니다. 또한 바쁘신 와중에도 저의 논문을 심사해 주신 고승환 교수님, 김찬중 교수님 그리고 박용래 교수님께도 감사드립니다.

하루 종일 액체 금속 만들고 프린팅 하고 어리숙한 형 도와주느라 고생했을 똑똑한 용이 그리고 열심히 하는 신명이, 연구에 대한 조언을 아끼지 않았던 듬직한 동혁이 그리고 박식한 경민이형, 항상 형 잔소리 듣느라 짜증났겠지만 웃는 얼굴로 답해주던 성격 좋은 태석이, 고된 일 마다하지 않던 착실한 교명이, 연구실 사람 모두에게 좋은 후배로서 행동하지 못하고 좋은 선배로서 있어주지 못해 미안한 마음이 앞섭니다. 모두에게 항상 좋은 일 그리고 좋은 연구 결과가 있었으면 좋겠습니다. 그리고 연구실은 다르지만 항상 연구에 대한 열정이 넘쳤던 여원이, 굳은 일 마다 하지 않고 항상 열심히 하던 보라, 연구실의 활력소인 주희, 언제나 호기심 많던 지형이, 항상 듬직했던 윤혁이, 똑똑하고 아는 게 많은 석범이, 10년 만에 다시 만난 농구 친구 재현이 마지막 박사학기를 여러분과 같이 보낼 수 있어서 정말 다행이었습니다. 덕분에 즐겁게 마지막 학기를 지낼 수 있었던 것 같습니다.

그리고 항상 웃는 모습으로 모든 짜증 받아주고 조언을 아끼지 않던 지수, 이제는 애 아빠가 되어서 많이 보긴 힘들지만 언제나 든든한 석기, 항상 잘 맞고 새로운 가정을 꾸린 이해심 많은 덕수, 근 20년 동안 옆에서 항상 힘이 되주던 한준이,

동네에서 시시콜콜 잡다한 얘기를 하며 생활에 활력소가 된 동네 친구 석우, 지금은 일본에 있지만 언제나 즐거운 얘기와 인생에 대한 조언을 아끼지 않았던 훈이, 항상 유부남으로서 공감해주고 항상 배려해주는 지웅이, 항상 티격태격하지만 힘들일 있을 때 위로해주고 항상 공감해주고 옆에서 든든하게 있어준 여준이 그리고 지인누나, 항상 새로운 것에 도전하고 누구보다도 생각이 깊은 익현이형, 먼저 배려해주고 속이 깊은 준희, 일본에서 누구보다도 열심히 연구하고 있을 성중이, 같이 대학원 진학해서 누구보다도 나를 이해해주던 상수, 항상 시시콜콜 일상 얘기하며 즐거움을 주던 서희, 누구보다도 똑똑하고 항상 아이디어가 많은 수현이, 이제 곧 새 신랑이 될 영건이, 결혼하고 요즘에는 많이 보지 못하지만 가장 오래되고 만날 때마다 즐거운 친구인 성겸이 그리고 유동이, 지금은 훈련소에서 열심히 훈련하고 있을 동규, 똑똑하고 모든 일을 열심히 하는 세현이, 얼마전에 득녀해서 벌써 두 아이의 엄마가 된 하지, 한달 동안 같이 생활하면서 누구보다도 끈끈해진 세영, 보선, 성식, 상철, 고명, 광우, 정식, 소민형, 승건형, 정오형, 제현형, 재필형 모두에게도 감사의 말을 전하고 싶습니다.

누구보다도 항상 저에게 조언 아끼시지 않고 든든한 버팀목으로 있어 주신 어머니 아버지 항상 감사드리고 존경합니다. 두 분의 사랑에 보답할 수 있는 아들이 되겠습니다. 그리고 아직 사위로서 미숙한 저를 항상 보듬어 주시고 응원해주시는 장인 장모님께 항상 감사드리며, 앞으로 더욱 더 친근하고 아들 같은 사위가 되도록 노력하겠습니다.

마지막으로 항상 저에게 든든한 버팀목 그리고 항상 제 삶의 활력을 불어넣어주고 제가 살아가는 가장 큰 의미가 되어준 아내 승아와 아들 유준이에게 고마움을 전합니다.

앞으로 더욱 더 노력해서 항상 정진하여 여러분들의 기대에 어긋나지 않고 항상 열심히 하는 사람이 되겠습니다. 감사합니다.

2018년 8월

김도윤